Norwegian University
of Life Sciences

Master's Thesis 2023 30 ECTS
Faculty of Science and Technology

A Case Study on High-rise Timber Building under Wind Load:

Numerical Analysis on Global Serviceability Response of the Different Stabilizing Systems of Mass Timber Buildings

Saaruja Rathy
Structural Engineering and Architecture
Faculty of Science and Technology (REALTEK)

A Case Study on High-Rise Timber Building under Wind Load: Numerical Analysis on Global Serviceability Response of the Different Stabilizing Systems for Mass Timber Buildings

Acknowledgments

As an engineering student at Oslomet and NMBU, this thesis marks the final work of five years of education. I want to express my deepest gratitude to my supervisor, Ebenezer Ussher, for his continuous support, patience, and immense knowledge. His guidance helped me throughout the research process and the writing of this thesis. I could not have imagined having a better supervisor for my master's thesis. I also want to thank my family, my mother, Rathy Krishnapillai, and my siblings, Sanchya Rathy and Lavanyan Rathy, for their constant support and encouragement during my studies. Their belief in me and their sacrifices for my education has continuously inspired me. I will always be grateful for their love and support.

Oslo, July 2023

Saaruja Rathy

Summary

Reducing greenhouse gas emissions is crucial in the construction industry, as it is responsible for significant emissions. Building projects alone contribute to 33% of CO_2 emissions, while transportation and material production account for up to 82-96% of total emissions. Timber, a sustainable and lightweight material, positively impacts the environment when used in construction. There is a growing trend towards incorporating more timber in building construction globally, particularly in constructing tall timber buildings to reduce emissions. However, concerns have been raised about the comfort of occupants in these structures due to the lightweight nature of timber, which causes the highest oscillation to occur at the top of the building.

Different structural systems like frames, shear walls, and diagrid systems are developed and evaluated for their capacity to endure wind loads within *all-timber* systems to examine oscillation at the highest point of a building. The goal is to identify the most productive and efficient approaches to withstand wind loads by analyzing deflection, inter-story drift, and peak acceleration.

Based on the ISO 10137 comfort level, numerical models were created, observed, and evaluated. The results indicated that the diagrid system surpassed both the frame and shear wall systems due to its ability to withstand lateral forces with a higher natural frequency and lower peak acceleration despite being lighter in weight. The diagrid system demonstrated exceptional performance during the analysis despite its low mass.

When analyzing the natural frequencies and peak accelerations of all systems, it was apparent that the diagrid system had substantially higher natural frequencies than the frame and shear wall systems. Moreover, the diagrid system's peak acceleration was lower than the frame and shear wall systems. These findings conclude that a diagrid system is a superior option compared to the current frame and shear wall systems.

One essential aspect to consider is the deflection of each system, which is influenced by the structure's stiffness. The diagrid system deflected only 13.24 mm, less than the frame and shear wall system. Regarding practical applications, engineers and architects now have an alternative option in the diagrid system for controlling overall timber building vibrational serviceability, especially during wind activities.

Contents

List of Figures

List of tables

1 Introduction

The construction industry is responsible for a significant amount of greenhouse gas emissions, making it necessary to find ways to reduce emissions in building projects. To address this issue, alternative materials and innovative construction techniques are being explored to lower the carbon footprint of buildings. One such material used today to target the issue is timber materials in construction projects. Timber is considered to be highly sustainable and has a positive impact on the environment when used in construction. There is a growing focus on incorporating more timber in building construction worldwide as tall timber buildings are now considered a crucial step towards reducing building-related emissions (Leskovar & Permrov, 2021; Smith & Frangi, 2018; Zhao et al., 2021a).

There has been a growing interest in exploring the use of timber in construction projects. This has led researchers and engineers to investigate innovative ways to expand the scope of timber used in the construction industry. However, engineers have faced significant challenges in ensuring rigidity, lateral stability, and wind resistance for mass timber buildings. Durability takes precedence when constructing a building, as it must withstand various loads, including extreme temperatures and vibrations, and support gravity, wind, and snow loads (Lin & Huang, 2016; Reddy & M.Eadukondalu, 2018).

The use of timber is limited and is not widely used as concrete and steel. Therefore, the limited studies on timber buildings under lateral loads need to be specified or clarified. Today, the highly used timber material is Cross-Laminated Timber (CLT) in the form of shear walls and slab systems. Timber materials are not expanded as concrete and steel. Materials such as concrete and steel have been used for many years. Therefore, using this kind of material is well known, and designers are comfortable in applying them for various projects.

On the other hand, timber buildings have many unknown behaviors that impact the design method. Therefore, various studies have been conducted to better understand and improve Cross Laminated Timber (CLT) as a lateral load-resisting system in mid- and high-rise buildings. One notable research project was the SOFIE project in Italy, which focused on a 7-story multi-story building with CLT panels to study the building's behavior. This project aimed to examine the structural performance of the building, where they determine the feasibility of using CLT as a viable construction material (Carrero et al., 2022). Moreover, Fragiacomo et al. (2011) have discussed design methods for CLT in mid-rise buildings. This study looked at the importance of proper detailing and connections in ensuring the structural integrity of CLT buildings. The

authors also examined the benefits of using CLT, such as its environmental sustainability and ease of construction (Fragiacomo et al., 2011; Zheng et al., 2019).

It must be underlined that timber buildings under two stories have been designed and built as residential housings (Edvardsen & Ramstad, 2014) Over the years, a global race towards the highest timber building made various questions about the comfort of the building. Due to the light weight of timber, the highest oscillation is at the top of the building. Since the behavior of timber buildings are unknown, significant problems occur when the building rises in height. The dynamic loading, represented as the wind on buildings, can cause these structures to sway or vibrate, leading to discomfort for those inside or nearby. Tall timber buildings that range from 12-14 stories and above are highly affected by dynamic loadings where the acceleration level on the top of the building will be found to govern the design of the stabilization system (Abrahamsen et al., 2020). Several FE-models that are in timber elements modeled with more than 20 stories have been checked for the comfort level calculated by the first frequency and the peak acceleration on the top of the building (Abrahamsen et al., 2020; Johansson et al., 2016; Orta et al., 2020; Zhao et al., 2021a; Zhao et al., 2021b).

Many researchers have started to test tall mass timber buildings under wind-induced forces, where Bezabeh et al. (2020) have conducted a wind tunnel test on tall timber buildings ranging from 10 to 40 stories with a high-frequency pressure. Regarding tall timber structures, the primary focus is on ensuring they are safe and functional for use (Bezabeh et al., 2018a; Bezabeh et al., 2018b; Bezabeh et al., 2018c; Bezabeh et al., 2020).

Different structural systems perform differently under lateral loads, where the amount of sway depends on the mass and stiffness of the building. In general, timber buildings are known to have good strength capacity due to Ultimate Limit State (ULS) but have to be controlled for sideway motions and vibration due to Serviceability Limit State (SLS), which is deemed the most critical aspect of their design (Standardization, 2002). Due to the light weight of timber, the dynamic excitation that occurs from wind-induced actions has started to dominate the decision towards size and shape for a modern timber building. Designing and evaluating tall mass timber buildings with good dynamic performance can be challenging. This is mainly due to the lack of data and information regarding tall timber buildings' behavior under wind-induced force, where the main concerns are due to stiffness, connection, and damping (Abrahamsen et al., 2020).

Additionally, Chan (2018) emphasizes that it is indeed feasible to construct tall timber buildings by incorporating timber cores into the design. Furthermore, several tall mass buildings are built as *all-timber*. Therefore, the primary concern is the horizontal deflection and sway during a building's service time for *all-timber* buildings. The focus on *all-timber* buildings is first to increase the use of timber buildings to improve carbon sequestration and second to assess the reliability of reducing overall building superstructure gravitational loads for situations where ground conditions may not be highly competent. For the sake of this thesis, it will be focused on wind load as a form of lateral load that acts horizontally on the structure or building.

1.1 Research questions and objectives

Structural construction timber elements and systems have been found to possess high strength and stiffness despite their lightweight. This reflects that timber buildings have systems that can overcome various deformations and forces. However, due to their lightweight, serviceability criteria often govern the design choices of timber structural systems. While much work on seismic load analyses has been conducted on timber structures, more on wind loads must be done. This thesis aims to investigate the functionality of different timber stabilizing systems and answer various research questions regarding their effectiveness. Therefore, this thesis will focus on studying the global serviceability performance of timber buildings that employ various timber lateral force resisting systems (LFRS) under wind-induced loads to enhance the understanding of the performance of such different timber LFRS. Therefore, the following research questions may be answered.

The research questions,

1) How do medium- and high-rise buildings develop with complete timber components and respond to lateral loads such as wind?
2) How reliable are the current empirical formulas provided in various codes in predicting the fundamental frequencies of timber buildings?
3) How do various lateral load-resisting systems influence the dynamic characteristics of medium- to high-rise timber buildings?

The main goal of this study is to assess the global serviceability of medium- to high-rise *all-timber* buildings under wind-induced actions. The goal is broken down as follows:

1) Assessing the global vibration serviceability of tall *all-timber* buildings under wind loads.
2) Evaluate the performance of medium- to high-rise *all-timber* buildings incorporating various timber LFRS.
3) Check the accuracy of current code provisions in estimating the fundamental frequencies of timber buildings.

2 State-of-the-art

In today's world, the impact of greenhouse gas (GHG) emissions is a significant concern that influences decision-making across various sectors. Research conducted by Sizirici et al. (2021) reveals that building constructions account for a significant 33% of CO_2 emissions, while transportation and material production contribute as much as 82-96% of the total CO_2 emissions (Sizirici et al., 2021). For many years, reinforced concrete and steel have been the primary structural materials used in multi-story buildings. However, the manufacturing processes of these materials are significant contributors to CO_2 emissions. For instance, cement production through calcination and coking coal use for steel production release emissions of up to 50% and 27%, respectively (Skullestad et al., 2016).

Numerous studies have been done to compare the sustainability of various building materials, and the results consistently indicate that timber is an eco-friendlier option than concrete and steel. One such study, carried out by Žemaitis et al. (2021), analyzed the value chains of wood-based and concrete-based materials and found that mass timber construction has a more positive impact on sustainability than site-cast and precast-reinforced concrete. Abed et al. (2022) explain the importance of choosing sustainable materials to mitigate building-related emissions. Engineering sciences and advancements in timber construction technologies have emerged timber as a promising structural material even for heavy loads. Timber is known for its ability to store carbon dioxide, its low production energy requirement, and its role in reducing building-related emissions (Abed et al., 2022; Dhiman, 2020).

Similarly, Skullestad et al. (2016) conducted a life cycle analysis (LCA) on four buildings with different structural systems, ranging from 3 to 21 stories. Their findings revealed that timber buildings have a significantly lower climate change impact (34-84%) than reinforced concrete buildings while maintaining the same load capacity (Skullestad et al., 2016).

Furthermore, an example of timber's potential as a sustainable building material can be seen in Gillies Hall, which is the largest passive house building in Australia and was completed in 2018. This building used cross-laminated timber (CLT) as a structural material, which effectively reduced carbon emissions by half, according to the 2019 Global Status Report for Buildings and Construction Towards a zero-emissions, efficient and resilient buildings, and construction sector (Abergel et al., 2019). These studies demonstrate the clear benefits of incorporating timber into our construction practices to reduce the carbon footprint and make a more sustainable future (Abergel et al., 2019).

2.1 CTBUH's definitions of structural system

It is important to note that mass timber buildings are built with different structural materials, like concrete and steel. Since timber is lightweight, it depends on other robust materials to fulfill different design criteria. Therefore, structural systems for tall mass timber buildings are divided into four main categories. These categories consist of *all-timber*, *concrete-steel-timber* hybrid, *concrete-timber* hybrid, and *steel-timber* hybrid, as shown in Figure 2.1 provided below,

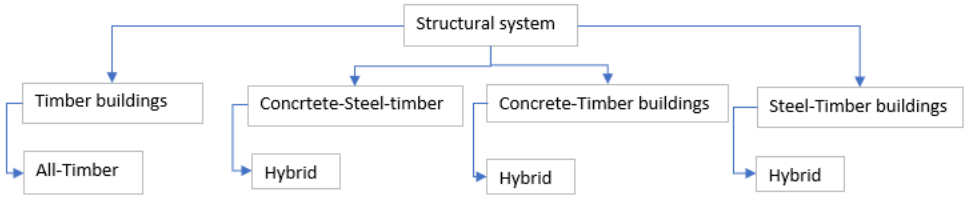

Figure 2.1 The four classifications of structural systems in timber

CTBUH, which stands for The Council on Tall Buildings and Urban Habitat, has classified timber structural systems into *All-timber, concrete-steel-timber*, *concrete-timber*, and *steel-timber hybrid buildings* (Safarik et al., 2022). An *all-timber* structure identifies timber as the primary vertical and horizontal bearing element. This type of structural system can use non-timber elements such as concrete and steel as floors and slabs, as long as those elements are not a part of the primary structure. For example, Mjøstårnet is considered an *all-timber* structural system, but it has concrete floors on the top apartment levels due to comfort criteria (Abrahamsen, 2017).

Hybrid buildings have two or more materials in the primary structural system that takes the loadings. Here the core system can be designed in concrete with beams and columns in glulam. If the core is constructed to take lateral loads, then the core is a part of the primary structural system. For example, Ascent and 25 King, where Ascent has concrete cores, and 25 King have floors and cores in concrete. Since the cores and floors resist lateral and vertical loads, those will be *concrete-timber* hybrid buildings. 25 King has a diagonal glulam bracing system to resist the lateral load. Since the basement and the ground floor are in concrete, the building is categorized as a *concrete-timber* hybrid building (archello, 2018; Architizer, 2023; Safarik et al., 2022).

2.2 Timber buildings all over the world

The comprehensive State of Tall Timber 2022 report presents findings on 139 mass timber buildings with eight or more stories. CTBUH recently updated the list, providing data on 84 impressive structures as of February 2022 (Safarik et al., 2022). In Table A.1, which can be found in Appendix A, 84 buildings are collected from the CTBUH list published in February 2022 with updated information and include 19 other timber mass buildings worldwide that also contain information from the CTBUH database. In total, 103 mass timber buildings were collected from the State of Tall Timber 2022 report and have been used to write this chapter in this thesis (Safarik et al., 2022; *State of tall buildings*, 2022). For the 103 buildings, information such as the official name of the building, where its located, height and floor count, what type of structural system it has, the function of the building, status, and completion year is collected.

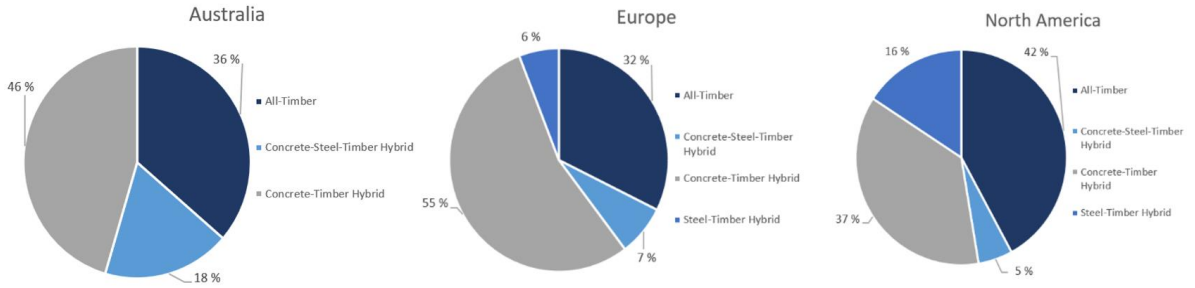

Figure 2.2 The governing structural system in a) Australia, b) Europe, and c) North America. Figure inspired by (Safarik et al., 2022)

The three diagrams represent the structural system that dominates in a) Australia, b) Europe, and c) North America. The governing structural system is the *Concrete-timber Hybrid* system in Australia and Europe, but it is the *All-timber* system in North America.

Most of the mass timber buildings are found in Australia, Europe, and North America, as sown in Figure 2.2 above. The dominating structural system is in *all-timber* and *concrete-timber* hybrid systems. Today, the tallest mass buildings are in North America and Europe. Mjøstårnet in Brumunddal, placed in Norway, is currently the tallest *all-timber* building with timber as the primary lateral structural element. Ascent, located in Milwaukee, United States, is the tallest *concrete-timber* hybrid building; Sara Kulturhus, placed in Skellefteå, Sweden, is the tallest *steel-timber* hybrid building; and De Karel Doorman in Rotterdam, Netherlands, is the tallest

concrete-steel-timber hybrid building. Figure 2.3 shows Acsent, Mjøstårnet, Sara Kulturhus, and De Karel Doorman in order and placed beside each other (Safarik et al., 2022).

Table A.1 also notes that mass timber buildings are found in Northeast and Southeast Asia, South America, and West Africa. Eunoia Junior College in Singapore was completed in 2019 with a concrete and timber structural system. Abebe Court Tower in Nigeria, the AMATA building in Brazil, W350 Tower in Japan, and the Rainbow Tree in the Philippines are all design/proposed constructions that are aimed to be built in the future. If the proposed constructions are to be constructed soon, they will be one of the region's tallest buildings in the world (*State of tall buildings*, 2022).

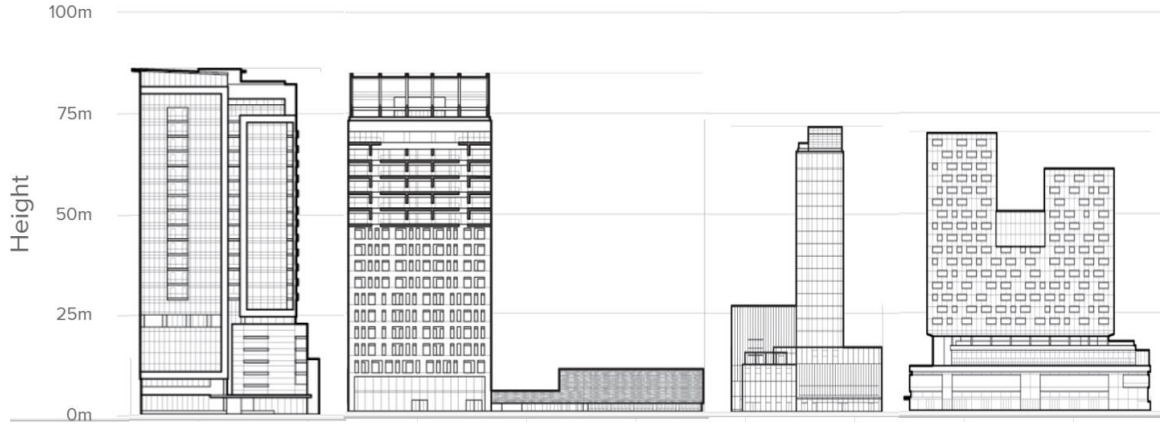

Figure 2.3 a) Acsent, b)Mjøstårnet, c) Sara Kulturhus, d) De Karel Doorman. (inspired by (State of tall buildings, 2022))

Figure 2.3 a), b), c), and d) represent; a) Acsent, *Concrete-timber* building, 86,6m in height, b) Mjøstårnet, *All-timber* building, 85,4m, c) Sara Kulturhus, *Steel-timber* building, 72,8m, d) De Karel Doorman, *Concrete-steel-timber* building, 70,5m (*State of tall buildings*, 2022).

Figure 2.4 shows the number of building with a different structural system built as tall that is either constructed, under construction or designed/proposed over the years. Shows mass-timber buildings that are eight stories or higher from Table A.1. The diagram shows the sum of different mass timber building types built from 2009 to 2041 due to collecting information from Table A.1 (Safarik et al., 2022). The dark blue color shows the number of buildings constructed with structural systems in *all-timber*. The light blue color shows the number of buildings in a *concrete-steel-timber hybrid* system. The gray color shows the amount of *concrete-timber hybrid* buildings, and the blue one shows the number of *steel-timber hybrid* buildings. It noted

that *all-timber* and *concrete-timber* hybrid buildings are the most selected structural system over the years.

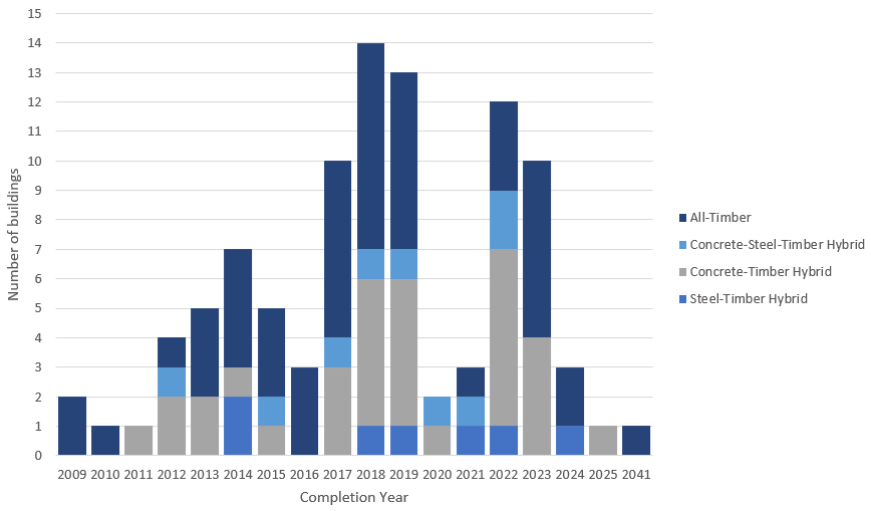

Figure 2.4 The diagram shows the sum of different mass timber building types built from 2009 to 2041. Figure inspired by (Safarik et al., 2022)

The buildings are built for different purposes. From Table A.1, the function of the building is categorized as residential, office, and mixed-use. As Figure 2.5 shows from the collected data, 62% of the mass timber buildings are residential, 18% are office buildings, and the remaining 20%is mixed-use of residential, office, or other purposes. The buildings are again divided into the structural system in Figure 2.5. Most buildings have been built for residential use, with a dominating structural system in concrete and timber. In the second lead, the structural system in timber has been selected.

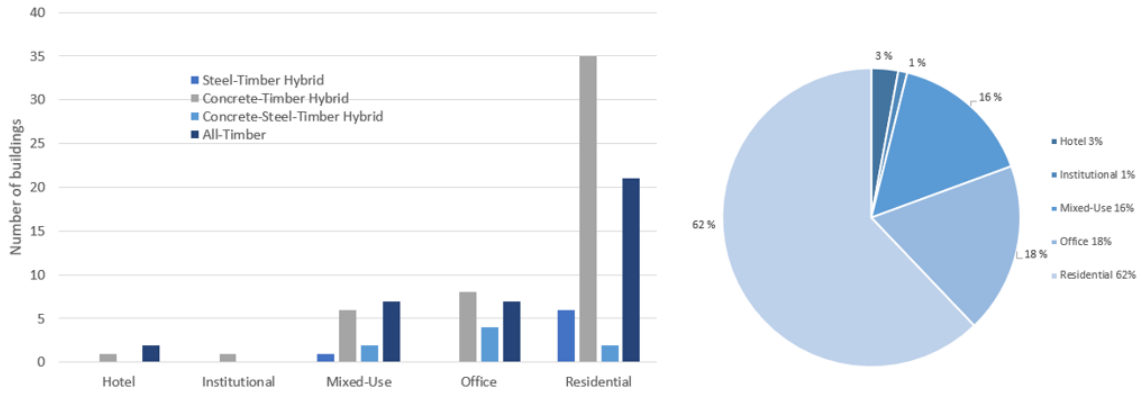

Figure 2.5 Buildings built in steel-timber, concrete-timber, concrete-steel-timber hybrid, and all-timber systems. Figure inspired by (Safarik et al., 2022)

The recently built and ranked holder for the tallest timber building is Ascent. Ascent is a *concrete-timber* hybrid building and has 25 floors. The first five stories, the elevator and stair shaft, are in concrete. In addition, the floors above are in CLT panels and glulam post and beam construction. Ascent's two cores, the elevator and stair shaft, are in concrete. The two cores provide lateral stability (architectureanddesign, 2022; Gonchar, 2022).

25 King can be found in Australia, Brisbane, and reach up to 46,8 meters with ten stories. This building was made out of good engineering choices that made this construction to be the tallest timber building with the largest floorplate in the world (Architizer, 2023). King was built with glulam timber columns and beams, where the floor and core walls are in CLT panels. Due to dampness and termites (natural causes), the basement and ground floor structures were in concrete. For the lateral resistance, diagonal glulam bracings were provided (archello, 2018).

The wood innovation design center is an office building built with glulam columns, beams, and CLT panels. It is an *all-timber* building in North America and was completed in 2014. The wood innovation design center was the tallest modern timber building then. The elevator and stair core walls in CLT were the primer lateral load-resisting system (*Wood Innovation and Design Centre*).

The mass-timber building Mjøstårnet in Norway, Brumunddal, is today's tallest *all-timber* building. Mjøstårnet is built with CLT walls and glulam beams and columns. The primary load-bearing system is the internal glulam columns and beams, along with the glulam trusses system that takes global forces in the horizontal and vertical directions. The CLT core for the elevator and staircase is the secondary load-bearing system. Those walls do not take horizontal forces (Abrahamsen, 2017). To give the necessary weight for the building and to ensure the comfort criteria for the apartments, the floors in levels 12 to 18 are made of concrete. Every floor in Mjøstårnet acts as a diaphragm. From the design combinations, wind load was the dominant load applied as statical load. Abrahamsen (2017) also points out that the 81m height building has a maximum horizontal deflection on the top of 140mm. This indicates that the deflection is within the limits of the code. The peak acceleration on the top floor was slightly above the limit (Abrahamsen, 2017).

Treet is also located in Norway, in Bergen. It has been designed with prefabricated residential CLT modules and covered with glulam truss systems inspired by modern timber bridges. Each module was stacked together on-site, where every fourth module was covered in the framework. The truss system ashore the structural stability as the primary load-bearing system, and the CLT

modules are not contributing to horizontal stability. Under wind load exposure, the diagonal bracing and columns tend to experience tensile forces (Abrahamsen & Malo, 2014).

With the characteristic height of the building, the maximum horizontal deflection on the top was calculated to be 71mm. The limitations are L/500, and the deflection is within limits. The wind-induced peak acceleration for the building was calculated based on CEN 1991-1-5 and was determined to be 0,048 m/s^2 and 0,051 m/s^2. The acceleration should not be higher than 0,04m/s^2, since it is not affecting the comfort that much, it was accepted (Abrahamsen & Malo, 2014).

2.3 Strategies against horizontal lateral loads

Various stabilizing systems are used to resist horizontal loads. Implementing timber materials in every part of a structure can be difficult due to its relatively lightweight nature, which requires sturdier materials to withstand lateral loads. Concrete and steel have been utilized as the primary lateral force-resisting systems in buildings, according to a recent study by Carrero et al. (2022). Incorporating these materials has allowed for greater structural stability and the ability to construct taller and more complex timber buildings (Carrero et al., 2022). As per the research conducted by Zheng et al. (2019), utilizing a combination of timber and concrete in the construction of tall buildings has opened new possibilities regarding height and structural integrity. The two materials perfectly withstand the various lateral loads that tall buildings are subjected to. While concrete cores are responsible for handling lateral loads, timber will handle other types of loads like gravity and diaphragm loads (Zhang et al., 2022). Foster et al. (2016) have pointed out that hybrid structural elements have several benefits and make it possible to construct tall timber buildings. The studies suggest that incorporating steel or concrete is necessary to design tall timber structures. Although the use of timber as a lateral load-resisting system is not yet fully understood, the concrete core provides a viable solution for tall timber buildings where lateral loads are significant.

As Orta et al. (2020) point out, three main strategies are used for lateral load resistance in mass timber buildings. This is reflected in the core, bracing, and shear wall systems. Usually, the core system is placed at the center of the building and helps the building stand against lateral loads. Most tall timber buildings have either concrete cores or cores in cross-laminated timber (CLT). This provides overall lateral stiffness for the building (Angelucci et al., 2022).

In Eurocode 1-4, only damping values regarded as timber bridges are found. However, there is currently no regulated value that can be used as damping when calculating peak acceleration. This makes the damping value a “guessing value” used as the modal damping for tall timber buildings (Abrahamsen et al., 2020).

However, the process of doing the on-site measurement on timber buildings and in the laboratory has started, but it is time-consuming and costly (Feldmann et al., 2016; Vilguts et al., 2020). There are different test methods to measure the dynamic properties of timber buildings. One of the testing methods can measure the dynamic response without knowing the acting load. This type of testing is called Operational Modal Analysis (OMA), also known as Ambient Vibration Testing (AVT). This method gives a reliable value in natural frequencies and mode shapes but a less reliable value due to damping. In the study by Feldmann et al. (2016), dynamic properties, such as natural frequency, mode shape, and damping, were measured by time and frequency domain method that, in this case, was with ambient vibrational testing. Here timber buildings and towers with heights ranging from 20 to 100 meters had a frequency ranging from 0,3 Hz to 3 Hz and a damping ratio of 0,5% to 3% (Feldmann et al., 2016).

On the other hand, Forced Vibration Testing (FVT), measuring over the range of frequencies, makes it possible to control the load level and determine the frequency response function. The frequency response function given by the FVT makes it possible to calibrate FE-models. However, it must be noted that a Full-scale FE-model of tall timber buildings has significant doubts regarding stiffness and damping values (Abrahamsen et al., 2020; Feldmann et al., 2016).

3 Theory

3.1 Load-bearing system

In earlier days of construction, the primary focus was on gravity loads rather than lateral loads. As buildings became taller and incorporated lighter materials, concerns for the stability and rigidity of the structure increased. Back in 1969, researcher Fazlur Khan made a groundbreaking discovery concerning the structural systems of tall buildings. He was the first to realize that a building's height significantly impacts its structural design. Khan explained that lateral loads cause the structure to sway, a critical issue requiring progressively larger column sizes downwards as gravity and lateral loads are transmitted from the upper floors to the ground. However, this increase in material size can significantly increase the building budget, which is a concern for any construction project. Therefore, Khan highlighted that a structure must be solid and stiff enough to resist side-to-side motions without incurring additional expenses. He also categorized different structural systems based on these principles, which have since become widely used in architecture (Ali, 2007; Ali & Al-Kodmany, 2022).

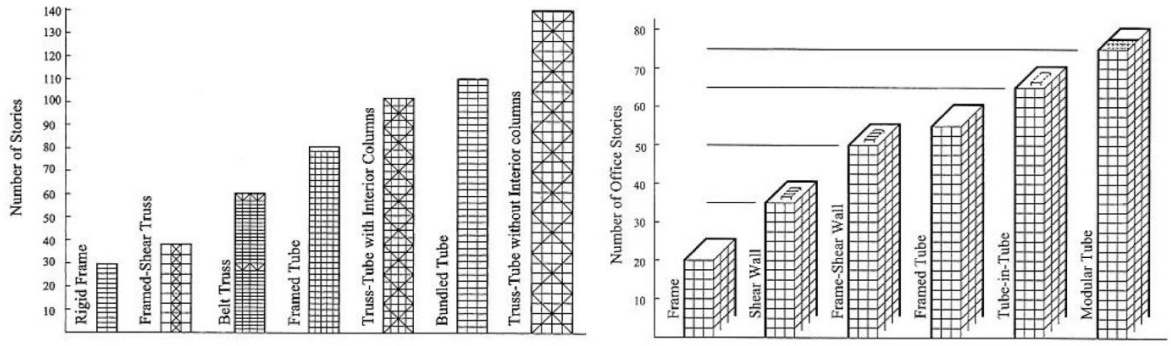

Figure 3.1 The categorized structural system based on how well the system resists lateral load for steel and concrete buildings up to 20-30 stories (Ali, 2007)

Figure 3.1 illustrates how the structural system is categorized, making it easier for architects and engineers to understand and select the most appropriate system for their project (Ali, 2007). When it comes to designing a structure, several factors need to be taken into consideration. These include the load case, the shape of the structure, where it will be located geographically, and the type of material used. Figure 3.1 can be used to determine the most suitable structural system for a particular project. Khan's reasoning behind the characterized system can also be helpful (Ali & Al-Kodmany, 2022).

Eurocode considers two types of limits state; Ultimate Limit State (ULS) and Serviceability Limit State (SLS) (Standardization, 2002). Ultimate Limit State is associated with the structures' loss of stability, structural collapse, and other structural failures. Serviceability Limited State considers the user's comfort and the ability to withstand plastic deformation under (extreme) external loads. The external loads can be dead, live, snow, wind, or earthquake. The Eurocode must satisfy maximum along-wind horizontal displacements and acceleration at the top of the building (Edskär, 2018; Lin & Huang, 2016).

How wind acts on structures or buildings is influenced by the structural shape. The frequency and the magnitude of the wind impact the structure. The environment of the building, such as the terrain and other buildings around it, also affects the wind performance. The cause of the load leads to the overall structural design and decisions (Edskär, 2018).

Method to find the equivalent static wind force and the standard deviation of the characteristic along-wind acceleration of the structure are defined in the European standard Eurocode 1: Actions on structures Part 1-4: General actions Wind load (Standardization, 2009). This thesis's equations, formulas, and methods are from Eurocode 1-4 and IOS 10137 (Standardization, 2007; Standardization, 2009). From the Eurocode and the Norwegian National Annex, two methods for determining the wind forces, where various equations are used to determine the external wind pressure, the overall wind forces, and the standard deviation, are specified.

3.2 Wind load

There are two main types of loads impacting a building. These are gravity loads and lateral loads. Gravity loads are vertically directed and perpendicular to the roof and floor systems. These types of loads can either be classified as dead or live loads. Permanent building materials, including walls, floors, and roofs, contribute to dead loads (Larsen, 2008).

In contrast, live loads are contributed by people, furniture, and other temporary items. Snow loads do belong in the live load category. However, this will vary depending on the geographical location of the building and the weight of accumulated snow on the roof (Larsen, 2008).

Lateral loads, which are horizontal forces acting on a structure, can be caused by various factors such as seismic activity, water pressure, and wind load. These mentioned loads are repeated live loads that perform in a direction parallel to the x-axis. Buildings can be affected by horizontal

or lateral loads, especially from seismic activity or wind. Seismic activity (horizontal loads) can challenge the structure and vary depending on the location and frequency of earthquakes. Wind loads become the primary concern in areas without seismic activity, especially during extreme weather conditions such as hurricane-force winds. Therefore, it is crucial to fully understand the different types of loads that can affect a building and ensure that the structure is designed to withstand them (Lin & Huang, 2016).

The force of the wind is an unpredictable and ever-changing natural occurrence that has the potential to wreak facades on structures and buildings. Researchers in the 19th century recognized this and have studied how wind interacts with surfaces and structures to create various flow situations, resulting in unique wind loads with differing sizes and characteristics. Due to its unpredictable nature, it is difficult to determine how the wind load will impact a structure, making the design process more complex (Mendis et al., 2007). It is why traditional design methods consider the potential for repeated exposure to wind loading, which can cause damage to steel structures, foundation settlement, deflections, and motion in tall buildings. The design approach ensures that the structure can withstand repeated wind loads without significant damage (Davenport, 1967).

The study conducted by Abu-Zidan et al. (2022) reveals the significant impact that wind pressures can have on a building's façade, resulting in substantial aerodynamic loads. While previous research has explored the performance of timber buildings under dynamic responses, the focus has been on seismic performance in tall timber structures.

3.3 Calculation on wind load

The focus will be on the serviceability assessment on the top of the building. Section 6.3.2 of Eurocode 1-4 will use the wind pressure on the external surfaces to assess the building's serviceability by multiplying the peak velocity pressure by the pressure coefficient for external pressure. The standard deviation calculation is at the top of the building, specifically at the height of z (Standardization, 2009).

Basic wind velocity, v_b, is defined as a function of wind direction and time of the year. The value is calculated by multiplying the fundamental value of the basic wind velocity, $v_{b,0}$, along with the factors provided in Eurocode 1-4 (Standardization,2009). Where the characteristic 10-minute mean wind velocity is above 10 meters over the ground level. The value of $v_{b,0}$ is found

in the Norwegian National Annexes and is a statical analysis of measurements at meteorological stations (Standardization, 2009). Expression (3.1) expresses the basic wind velocity,

$$v_b = C_{dir} \cdot C_{season} \cdot v_{b,0} \tag{3.1}$$

where,

v_b Basic wind velocity

$v_{b,0}$ The fundamental value of the basic wind velocity

C_{dir} Directional factor

C_{season} Season factor

As the standards and Eurocode points out, Expression (3.1) is for a 50 years return period (Johansson et al., 2016). Johansson et al. (2016) present an expression used to calculate wind velocity for shorter times, v_{bT}. In this case, T stands for the specified year. The Expression (3.2) gives the wind velocity for a shorter time as,

$$v_{bT} = v_b \cdot 0{,}75 \cdot \sqrt{1 - 0{,}2 \cdot \ln\left(-\ln\left(1 - \frac{1}{T}\right)\right)} \tag{3.2}$$

Basic wind velocity is needed to calculate the mean wind velocity. Mean wind velocity, $v_m(z)$, estimates the wind flow speed from high to low pressure on a structure. The basic wind velocity, v_b, used to calculate the mean wind velocity depends on the return period, T. Either v_b or v_{bT} is used to calculate the mean wind velocity. In Expression (3.3), the wind velocity for a shorter time , v_{bT}, is used.

$$v_m(z) = C_r(z) \cdot C_o(z) * v_{bT} \tag{3.3}$$

where,

$v_m(z)$ Mean wind velocity

$C_r(z)$ The roughness factor, taken as 1,0

$C_o(z)$ The orography factor

The terrain roughness depends on the terrain category and the terrain parameters and is calculated as shown in Expression (3.4),

$$C_r(z) = \begin{cases} k_r \cdot \ln\left(\frac{z}{z_0}\right), & z_{min} \leq z \leq z_{max} \\ C_r(z_{min}), & z \leq z_{min} \end{cases} \quad (3.4)$$

k_r Terrain factor depending on the roughness length z_0 (Expression 3.5)

$$k_r = 0{,}19 \cdot \left(\frac{z_0}{z_{0,II}}\right)^{0,07} \quad (3.5)$$

where,

z Height of the building

z_0 Roughness length

$z_{0,II}$ Terrain category 2 = 0,05 meters

z_{max} Taken as 200 meters

z_{min} Minimum height defined in Eurocode 1-4 table

The peak velocity pressure is calculated to specify the wind activities on the structure. The peak velocity pressure, $q_p(z)$, can be found with the effect of the mean wind velocity, $v_m(z)$, and turbulence intensity, $I_v(z)$, as shown in Expression (3.6) (Standardization, 2009).

$$q_p(z) = [1 + 7 \cdot I_v(z)] \cdot \frac{1}{2} \cdot \rho \cdot {v^2}_m(z) \quad (3.6)$$

where,

$q_p(z)$	Basic velocity pressure
ρ	Air density = 1,25 kg/m^3
$I_v(z)$	Turbulence intensity
$v_m(z)$	Mean wind velocity

Calculations for wind load dynamics involve determining the peak velocity pressure, which takes into account the turbulence intensity, $I_v(z)$. To calculate intensity, the standard deviation, σ_v, is divided by the basic mean wind velocity, $v_m(z)$. The expression (3.7) is simplified with the terrain and turbulence factors, k_r and k_l. The turbulence intensity is found as Expression (3.7), as specified in (Standardization, 2009).

$$I_v(z) = \begin{cases} \dfrac{\sigma_v}{v_m(z)} = \dfrac{k_l}{C_0(z) \cdot \ln\left(\dfrac{z}{z_0}\right)}, & z_{min} \leq z \leq z_{max} \\ I_v(z_{min}), & z \leq z_{min} \end{cases} \tag{3.7}$$

where,

k_l	The turbulence factor, given as 1,0 in the National annex, Eurocode 1-4
$C_0(z)$	The orography factor

3.4 Peak acceleration

The acceleration limits depend on the frequency of the vibration. How people respond to different vibration levels depends on the comfort of each one of them. Table 3.1, made by Mendis et al. (2007); Vilguts et al. (2020), points out a table describing the human perception level for different peak accelerations. Table 3.1 contains different human responses due to different peak accelerations ranging from 0,05 m/s^2 to 0,85 m/s^2. Table 3.1 below is from (Mendis et al., 2007; Vilguts et al., 2020)

Table 3.1 Human perception levels (Mendis et al., 2007)

Level	Acceleration [m/s^2]	Effect
1	< 0,05	Humans cannot perceive motion
2	0,05 - 0.1	a) Sensitive people can perceive motion b) Hanging objects may move slightly
3	0,1 - 0,25	a) Majority of people will perceive motion b) Level of motion may affect desk work c) Long-term exposure may produce motion sickness
4	0,25 - 0,4	a) Desk work becomes difficult or almost impossible b) Ambulation is still possible
5	0,4 - 0,5	a) People strongly perceive motion b) Difficult to walk naturally c) Standing people may lose balance
6	0,5 - 0,6	Most people cannot tolerate motion and are unable to walk naturally
7	0,6 - 0,7	People cannot walk or tolerate motion
8	>0,85	Objects begin to fall, and people may be injured

3.4.1 Calculation of peak acceleration

To calculate the horizontal peak acceleration, $a(z)$, at the top of the building, the standard deviation of the characteristic along-wind acceleration, $\sigma_{a,x}(z)$, will be multiplied by the peak factor, K_p, as shown in Expression (3.8) (Standardization, 2009).

$$a(z) = \sigma_{a,x}(z) \cdot K_p \tag{3.8}$$

where,

$\sigma_{a,x}(z)$ Standard deviation

K_p Peak factor

From the Eurocode 1991-1-4, two methods exist to find the standard deviation $\sigma_{a,x}(z)$. The acceleration for serviceability assessments can be found in Expression (3.9) from the National Annex B and Expression (3.10) from the National Annex C Eurocode 1991-1-4 (Standardization, 2009).

$$\sigma_{a,x(z)} = \frac{c_f \cdot \rho \cdot b \cdot I_v(z) \cdot v^2{}_m(z)}{m_1, x} \cdot R \cdot K_x \cdot \Phi_{1,x}(z) \quad (3.9)$$

$$\sigma_{a,x(y,z)} = c_f \cdot \rho \cdot I_v(z) \cdot v^2{}_m(z) \cdot R \cdot \frac{K_y \cdot Kz \cdot \Phi_{(y,z)}}{\mu_{ref} \cdot \Phi_{max}} \quad (3.10)$$

where,

c_f	Force coefficient
ρ	air density
b	Width of the structure
$I_v(z)$	Turbulence intensity at the height z=zs above the ground
$v_m(z)$	the mean wind velocity for z = zs
z	the reference height
R	the square root of resonant response
K_x	The non-dimensional coefficient
K_y and Kz	Constants
m_1, x	the along wind fundamental equivalent mass
$\Phi_{1,x}(z)$	fundamental along wind modal shape
$\Phi_{(y,z)}$	mode shape
Φ_{max}	mode shape value at the point with maximum amplitude
μ_{ref}	the reference mass per unit area

The two expressions are used to calculate a structure's standard deviation, each referencing different points. Expression (3.9) calculates the standard deviation at the top of the building, while Expression (3.10) calculates for structural points with x and y coordinates (x,y). National Annex B's Expression (3.9) determines the maximum along-wind displacement to calculate the acceleration on the top of the building at a given height z (Standardization, 2009).

Wind-induced motion with a frequency less than 1 Hz can lead to discomfort for the people that live in the building. The first mode shape of the building is represented in bending and rotating motion, where the bending happens in the x- or y-axis.

3.5 Dynamic structural properties

The dynamic structural properties are provided in National Annex F in Eurocode 1-4 by natural frequencies, modal shapes, equivalent masses, and logarithmic decrements of damping (Standardization, 2009).

The fundamental dynamic properties may be estimated and evaluated from the structural systems' behavior or properties using simplified equations based on the analytical or a combination of the theory and observations (Standardization, 2009).

3.5.1 Fundamental frequency

The lowest natural frequency from the swaying motion, dependent on the mass and stiffness of the building, in tall timber buildings aligns with the same frequency range as the wind spectra (Abrahamsen et al., 2020). From NS-EN 1991-1-4 Expression (F.2) is shown as Expression (3.11) below, natural frequency gives the fundamental frequency of multi-story buildings with heights higher than 50 meters (Standardization, 2009).

$$n_1 = \frac{46}{h}\ [Hz] \tag{3.11}$$

The equation states that the natural frequency depends on the height of the building, where h is the total height of the building. This expression is based on experience from steel and concrete buildings and, therefore, is inappropriate for wooden constructions (Johansson et al., 2016). A study from testing several buildings and towers in timber ranging from 20 to 45 meters in height found the natural frequency to be between 1-3 Hz. Plotting all the frequencies found under the test resulted in a curve defined by $n_1 = 55/h$, which indicates that timber buildings are designed for higher frequency levels than the codes (Feldmann et al., 2016).

Eurocode provides the fundamental flexural building mode by the Expression (3.12).

$$\Phi_1(z) = \left(\frac{z}{h}\right)^{\zeta} \tag{3.12}$$

where,

z is the reference height

h is the height of the building

ζ is a parameter decided due to the structural system

In the Eurocode, the parameters (ζ) are defined to different structural systems. Parameter 0,6 is for slender frame structures with no load-shearing walling or cladding, 1,0 is for buildings with s central core including outlying or large columns with or without shear bracings, 1,5 is for slender cantilever buildings supported by central reinforced concrete cores. The parameter 2,0 and 0,5 is for towers and chimneys and lattice steel towers (Standardization, 2009).

3.5.2 Equivalent masses

The equivalent mass per unit length, m_e, of the fundamental mode is given in Expression (F.14) in Eurocode 1-4 and shown as Expression (3.13) below (Standardization, 2009).

$$m_e = \frac{\int_0^l m(s) * \Phi_1^2(s) ds}{\int_0^l \Phi_1^2(s) ds} \tag{3.13}$$

where,

m_e is the mass per unit length

l is the height or span of the structure

The Eurocode also mentions that the equivalent mass per unit length for cantilever structures and structures supported at both ends of the span, with varying mass distribution, may be approximated by the average value of m. The average mass over 1/3 of the height of the structure is used to calculate m_e for cantilevered structures. For structures supported at both ends, the average mass is considered over a length of l/3 centered at the point in the structure in which the modal shape is maximum (Standardization, 2009).

3.5.3 Logarithmic decrements of damping

Material and structural damping are the two main properties considered in building design. The difference between material and structural damping is that material damping considers the internal friction within the material, while structural damping is friction and energy dissipation in the select connections (Abrahamsen et al., 2020)

The logarithmic decrement of damping is only considered for the fundamental bending mode and is given by Expression (F.15) in Eurocode 1-4, shown as Expression (3.14) below.

$$\delta = \delta_s + \delta_a + \delta_d \tag{3.14}$$

where,

δ_s The logarithmic decrement of structural damping

δ_a the logarithmic decrement of aerodynamic damping for the fundamental mode

δ_d The logarithmic decrement of damping due to special devices

The logarithmic decrement of damping due to special devices is only considered when special dissipative devices are added to the structure. Table F.2 in Eurocode 1-4 shows the logarithmic decrement of structural damping. The table in Eurocode contains values for reinforced concrete buildings, steel buildings, hybrid structures of concrete and steel, and other structures. However, values for timber buildings are not provided in the table. The table also contains bridge values and timber bridge is among them. For timber bridges, the logarithmic decrement of structural damping is between 0,06 and 0,12. Therefore, this value for the logarithmic decrement of structural damping in timber bridge structures often is used in timber buildings (Zhao et al.,

2021b). In Edskär (2018), an expression shows how to calculate the logarithmic decrement of structural damping. It is also defined by Expression (3.15),

$$\delta_s = \frac{2\pi\xi}{\sqrt{1-\xi^2}} \tag{3.15}$$

where,

ξ damping ratio

For cross-laminated timber as the main load-bearing structures, the damping ratio is between 1,3 – 9,1 % for post and beam systems and 1,4-2,4% for hybrid buildings (Edskär, 2018)

The estimation of logarithmic decrement of aerodynamic damping for bending mode along wind vibrations is expressed in Expression (F.16) National Annex in Eurocode 1-4 (Standardization, 2009). For most cases, where the modal deflections are constant for each height, the determination of logarithmic decrement of aerodynamic damping for along wind vibrations are expressed in a different equation, as represented by Expression (F.18) in the Eurocode is shown as Expression (3.16) below,

$$\delta_a = \frac{c_f * \rho * b * vm(z)}{2 * n1 * m_e} \tag{3.16}$$

3.6 Wind turbulence and Structural factor

The resonance response factor R^2 allowing for turbulence in resonance with the considered vibration mode of the structure, is determined by using the expression from NS-EN 1991-1-4 (B.6) and is shown as Expression (3.17).

$$R^2 = \frac{\pi^2}{2 \cdot \delta} \cdot S_L\left(zs, n_{1,x}\right) \cdot R_h(\eta_h) \cdot R_b(\eta_b) \tag{3.17}$$

where,

δ Is the total logarithmic decrement of damping

$S_L(zs, n_{1,x})$ Is the non-dimensional power spectral density

$R_h(\eta_h)$, $R_b(\eta_b)$ Is the aerodynamic admittance functions

3.7 Lateral displacement/ horizontal displacement

For this thesis, the external load will only be considered wind load for the structure. Large wind load exposed on buildings makes the building displace horizontally.

The horizontal displacement and acceleration limits are in the national annexes and ISO standards, ISO 68977 and 101378 (Standardization, 2007). Each standard contains limitations for a specific range of frequencies. ISO 10137 is used for a frequency range of 0,063 to 5 Hz with a one-year return period (Howarth, 2015). To provide comfort, the international standard ISO 10137 gives an evaluation curve for acceptable horizontal motions with a one-year return period, see Figure 4.7. IOS 10137 gives limitations for frequencies ranging from 0,063 to 5 Hz. The value of the first natural frequency of the building, together with the calculated peak acceleration, it is possible to evaluate human comfort (Edskär, 2018; Howarth, 2015).

To maintain comfort and to avoid non-structural elements being damaged, lateral wind induces deformations are limited within acceptable limits. The acceptable limits of global horizontal displacements of a building are not presented in Eurocodes, but limits for beam deflection are provided. Eurocode 0 and 5, EN 1990 and EN 1995, shows the provided maximum recommended deflection of a beam. For beams subjected to load combinations under the serviceability limited state, have $\frac{H}{300}$ to $\frac{H}{500}$ for simply-supported beams and $\frac{H}{1500}$to $\frac{H}{250}$for cantilever beams, where H is the height of the building. According to Edskär (2018); Malo og Stamatopoulos (2016); Vilguts et al. (2020), the maximum displacement for a building was suggested to be limited to the value $\frac{H}{300}$. However, other limits are also used, as $\frac{H}{500}$ (Zhao et al., 2021b).

3.7.1 Inter-story drift

Inter-story drift is defined as the measured story displacement about the story below. The cladding and non-structural walls and partitions are highly dependent on the story drift caused

by wind loads, as this effect can cause damage to those structural and non-structural elements. The deflection in different stories must be found and controlled to minimize the damage. Therefore, the inter-story drift in the stories is calculated and compared with the limits provided by the Eurocode. In other words, the limits are not a measurement for comfort but to estimate the displacement of a story in relation to the story below to predict the damages lateral loads can cause under their actions (Arum & Akinkunmi, 2011; Edskär, 2018).

The typical drift limits used under wind loads are between $\frac{H}{400}$to $\frac{H}{500}$. Vilguts et. Al. (2020) points out that for characteristic load combination according to Eurocode 0, the inter-story drift should not exceed 0,33% of the story height, represented by Expression (3.18),

$$\delta \leq \frac{h}{300} \tag{3.18}$$

Other researchers have used the $\delta \leq \frac{h}{500}$, where h equals story height (Zhao et al., 2021b).

Here the δ is defined as the relative displacement for the story in relation to the story below. h is the height of the story that is analyzed.

The Expression (3.19) below is used to calculate the δ,

$$\delta = \frac{\delta_{total} - \delta_{(n-1)}}{h_i} \tag{3.19}$$

Table 3.2 shows the limiting values for deflections of the beams. The deflection limiting values are discussed in the National Annex to NS-EN 1991. Some indicative values for useable deflections are given in the table below (Standardization, 2009).

Table 3.2 - Limiting values for deflections of beams. Table made inspired by Eurocode 1-4.

	W_{inst}	$W_{net,\ fin}$	W_{fin}
Beam on two supports	$\frac{l}{300}$ to $\frac{l}{500}$	$\frac{l}{250}$ to $\frac{l}{350}$	$\frac{l}{150}$ to $\frac{l}{300}$
Cantilevering beams	$\frac{l}{150}$ to $\frac{l}{250}$	$\frac{l}{125}$ to $\frac{l}{175}$	$\frac{l}{75}$ to $\frac{l}{150}$

3.8 Finite Element Method and SAP2000

The Finite Element Method has become widely used for addressing various engineering problems. This numerical analysis approach offers a highly effective way of approximating solutions for various issues encountered in the field. Nevertheless, it is important to note that the method can be challenging in cases where the problem's geometry or other features are irregular or arbitrary. Despite this limitation, the Finite Element Method remains an exceedingly valuable tool for solving complex problems in engineering (Huebner et al., 2001).

When faced with irregular problems, it can be helpful to make some simple assumptions. However, it is important to be cautious when making assumptions, as they can lead to inaccuracies and incorrect values or answers. While assumptions can sometimes be effective in reducing the complexity of a problem, they should be made carefully and with due consideration (Huebner et al., 2001). Approximating complex systems' behavior with the finite element method provides many steps. The bullet points below showed in a short form how the finite element method works (Huebner et al., 2001).

- **Discretization:** The analyzed system will be divided into smaller elements, where all the elements will be connected through nodes. When the elements and nodes are collected to be analyzed, the process is called mesh.
- **The interpolation function:** The interpolation functions are selected to define the unknown field variables. This is a default function.
- **Boundary conditions:** Boundary conditions are selected to constrain the system for analysis.
- **Appropriate geometry**: Finite element simulation involves appropriate geometry, assigning material cross-section and properties in addition to boundary conditions.
- **The accuracy of FE models:** depends on mesh size, the choice of interpolation function and boundary conditions, and the representation of the actual structure.
- **Solving the equation:** Each node contains degrees of freedom. The system will end up with a large equation. By solving the equation, it will obtain the nodal solutions.

There are many software programs available, each with its unique features. One such program is SAP2000, a Structural Analysis Program specifically designed for modeling, designing, and analyzing structures. Its library of elements, including beams, columns, and shells, allows for analyzing structures such as buildings, bridges, and even individual components within a larger

structure. This program enables users to create, modify, analyze, and design structural systems in both 2D and 3D views (Computers & structures, 2013).

It also offers the ability to create various load case scenarios, which can be analyzed through linear static and dynamic or non-linear static and dynamic methods. The dynamic analyzing techniques include modal, response spectrum, and time history analysis, providing parameters and diagrams for each response. The design process is more efficient and streamlined, with built-in features conforming to standards and codes. This program makes comparing and verifying design process results easier, ensuring that the final product meets the necessary standards and is of the highest quality possible (Computers & structures, 2013).

3.8.1 Modeling timber structures in SAP2000

In SAP2000, all the timber materials are assigned as orthotropic materials. Timber materials behave like orthotropic materials, where the behavior will differ in the three local coordinates of the material. The suitable material properties are assigned from the given Tables 4.1 and 4.1. The stress-strain relationship calculates the strain to stress for the orthotropic mechanical and thermal properties (Computers & structures, 2013).

With SAP2000 modal analysis, it is possible to determine the vibrational modes for the structure, where the structure's behavior in terms of fundamental mode can be understood and will always be a linear analysis. Different load scenarios can be made and assigned. Two types of modal analysis are done in SAP2000 from the assigned modal load case. 1) Eigenvector analysis and 2) Ritz-vector analysis. The Eigenvector analysis is done to determine the systems' undamped free-vibration mode shapes and frequencies. The connection between eigenvalue and frequency is that the eigenvalue is the square root of the circular frequency, as shown in the relationship below (Computers & structures, 2013). Expression (3.20) shows the relationship between period and frequency.

$$T_n = \frac{2\pi}{\omega_n} \qquad f_n = \frac{1}{T_n} \tag{3.20}$$

For the dynamic analysis, the mass is found by the element density and the volume. In SAP2000, it is always used lumped mass, where the mass is not coupling between degrees of freedom at a joint or between different joints (Computers & structures, 2013).

4 Methodology

Several systems have been developed to ensure structural safety and withstand lateral loads for timber mid- and high-rise buildings. Three models with different structural systems will be developed and analyzed for the global serviceability limit state. It is important to note that the ultimate limit state is not studied and investigated as much as the serviceability limit state and will not be prioritized. To ensure structural stability, critical beams, and columns are checked for flexure, compression, and buckling. Additionally, the models are analyzed for the structural behavior under lateral loads, explicitly focusing on static wind load.

This thesis focuses on modeling the frame, shear wall, and diagrid systems as an *all-timber* system to evaluate their potential under wind load conditions. The goal is to evaluate the effectiveness and efficiency of different systems in resisting lateral loads, such as wind loads, where the main concern is the deflection, inter-story drift, and peak acceleration on the top of the building. The methodology used in this study is illustrated in Figure 4.1.

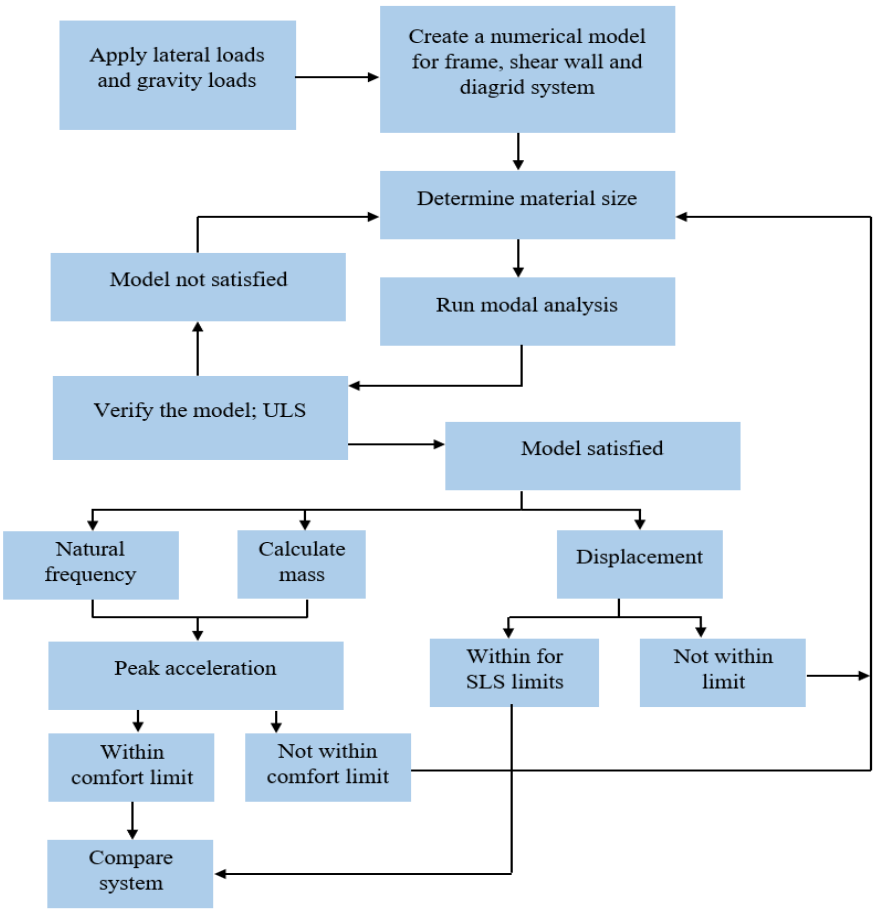

Figure 4.1 Workflow

Several frame, shear wall, and diagrid system models were developed to assess the serviceability limit state. These models underwent numerical analyses using SAP2000 to determine the natural frequency of the building and displacement caused by the applied wind loads. It is crucial to note that the choice of structural material significantly influences how a building responds to wind forces based on its mass, stiffness, and damping. Thus, the use of materials must be thoroughly considered to ensure the safety of tall structures. All models had identical lateral and gravity load applications. The gravity load was added to the slabs, and the lateral load was applied in both directions of the building at 0 and 90 degrees. The choice and calculations were made using Eurocodes, mainly Eurocode 1-4, to calculate the peak acceleration, where the Norwegian National Annex was used. Before comparing the models, ISO 10137 Annex D for comfort and Eurocode 1-4 limitations for building displacement were used. If the models failed to meet these requirements, adjustments were made to the size of the glulam beams, columns in the frame and diagrid system, and the CLT walls in the shear wall system, as shown in Figure 4.1.

4.1 Reference building

To investigate the behavior of a tall timber mass building, a CLT paneled timber building located in Ås, Norway, was used as a reference building for this thesis. The building has a rectangular shape with a length of 22,8 meters and a width of 14,74 meters. It is a student residential building that consists of eight stories, with each floor having 16 rooms and a height of approximately 3 meters. Thus, the building has a total height of 24 meters.

The structure is made of CLT panels for the walls, slabs, and roof, with the horizontal slabs and roof acting as a diaphragm. The roof is 200mm thick, considering the snow load, while the remaining slabs are 180mm thick, considering only the live load. The eight-story building was divided into three, 1-3 stories, 4-6 stories, and lastly, 7-8 stories, as shown in Figure 4.2 (Ussher et al., 2022). The walls inside and outside the building vary in thickness from top to bottom, as shown in Figure 4.2.

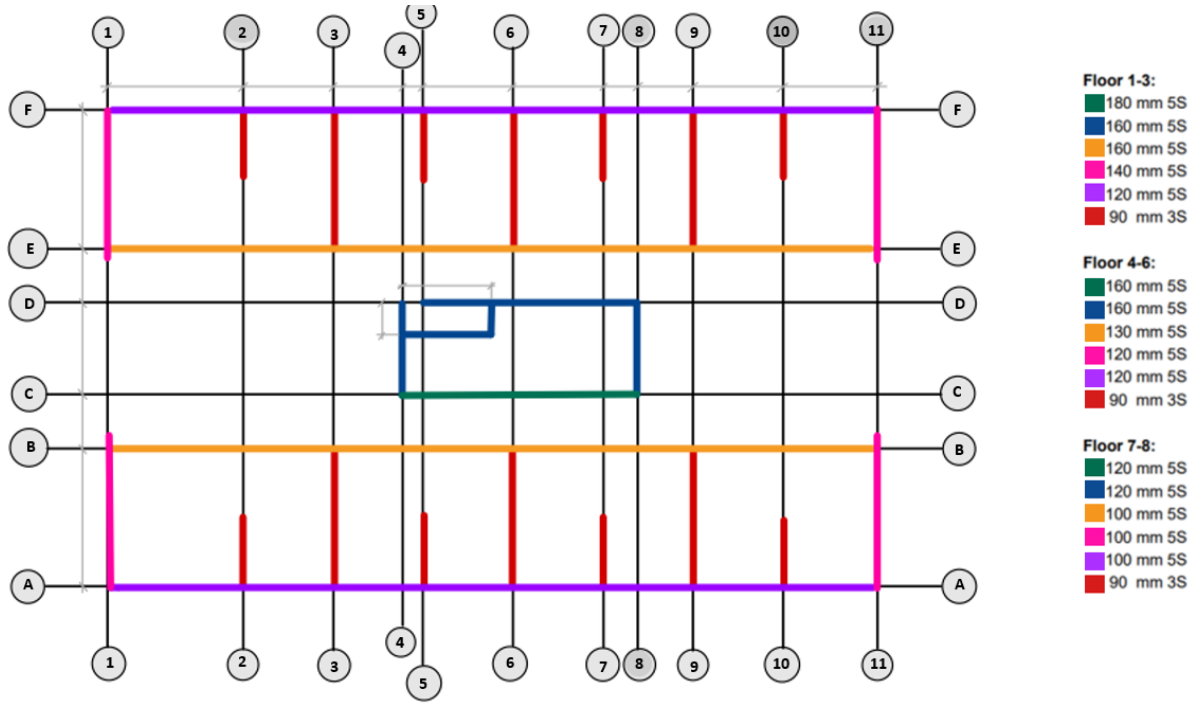

Figure 4.2 Floor plan for the reference building. Figure inspired by (Ussher et al., 2022)

The natural frequency of this building has been studied both experimentally and numerically by Aloisio et al. (2020) and Ussher et al. (2022). The experimental study by Aloisio et al. (2020) revealed the natural frequency for the first mode at 1,913 Hz, the second at 2,414 Hz, and the third at 2,693 Hz. Similarly, the numerical study by Ussher et al. (2022) showed the natural frequency for the first mode at 1,917 Hz, the second at 2,455 Hz, and the third at 2,697 Hz.

The verified FE numerical model of the reference building by Ussher et al. (2022) is the foundation for this study. Even if the reference building is in eight stories, the models herein presented are developed with added ten stories, equal to 18 stories. All models share the same height, width, and depth, with variations only in the structural system and mass participation. The primary objective of this thesis is to analyze and evaluate different structural systems and ensure their safety and comfort.

4.2 Load combination

The load combination was based on the roof's dead, live, wind, and snow load. The permanent load on a building is represented as a dead load, including the self-weight of the structure and the weight of non-structural building materials. The dead load is calculated with the thickness and density of a slab. The self-weight for a beam is calculated by the density multiplied by the

cross-section (Dominik, 2023). The variable load on the building is identified as a live load. When the live load is calculated, its needs to find the area load first, and then the area load will be multiplied by the spacing for each beam. For slabs, Eurocodes already have some general values in EN 1991-1-1.

The characteristic dead load was calculated to be 5,150 kN/m^2, and the live load was assumed to be 1,8 kN/m^2 from tables EN 1990 (for residential occupancy). Both loads were assigned to every slab as in one-way or two-way load distribution, see Figure 4.4. The self-weight for the elements was automatically calculated from SAP2000. The assigned material properties for the floor, wall, beams, and columns for the different structural systems can be found in Tables 4.1 and 4.2. Snow and wind loads were calculated according to EN 1991-1-3 and EN 1991-1-4. The loads were calculated with values assigned for the location in Norway, Ås. The calculations for wind and snow loads are found in Appendix B.

The wind is assumed to be applied horizontally on the diaphragms, as shown in Figure 4.3. The loads will flow through and transmit between different parts of a structure. The distribution of the force will vary due to the assumption of the function of a diaphragm for each model. Factors such as stiffness, deformation, and behavior under loads classify and differentiate the diaphragms. Figure 4.4 shows the idealized diaphragms as rigid diaphragms.

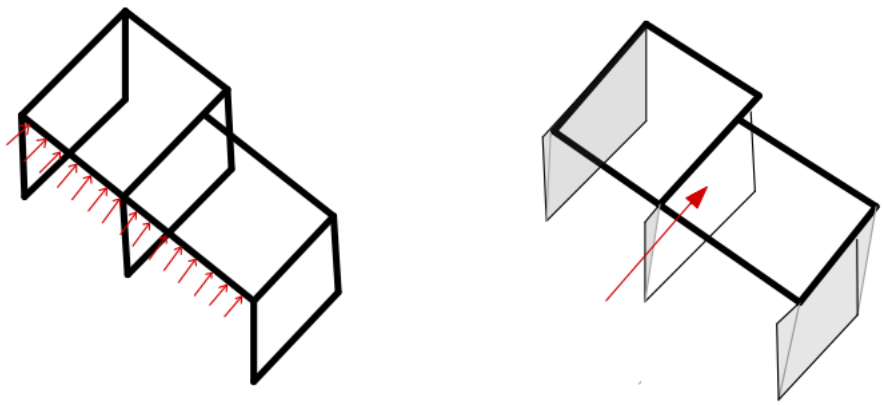

Figure 4.3 Rigid Diaphragm

The slabs had to be identified if it is a one-way or two-way slabs. This is important to assign in SAP2000 to enable load flows through the beams. The slab type was identified by dividing the longest side of the beam by the shortest side of the slab. l_y/l_x where l_y the longer length and l_x is the shorter length of the slab. For one-way slabs, the ratio $l_y/l_x > 2$, and for two-way slabs $l_y/l_x \leq 2$. The floorplan with one-way and two-way slabs for the building is displayed in

Figure 4.4. Two-way slabs are represented by squares with trapezoids, while the squares with two rectangles represent one-way slabs. It should be noted that this arrangement of the slabs in the floor types is consistent throughout all 18 floors, as the floorplan remains the same.

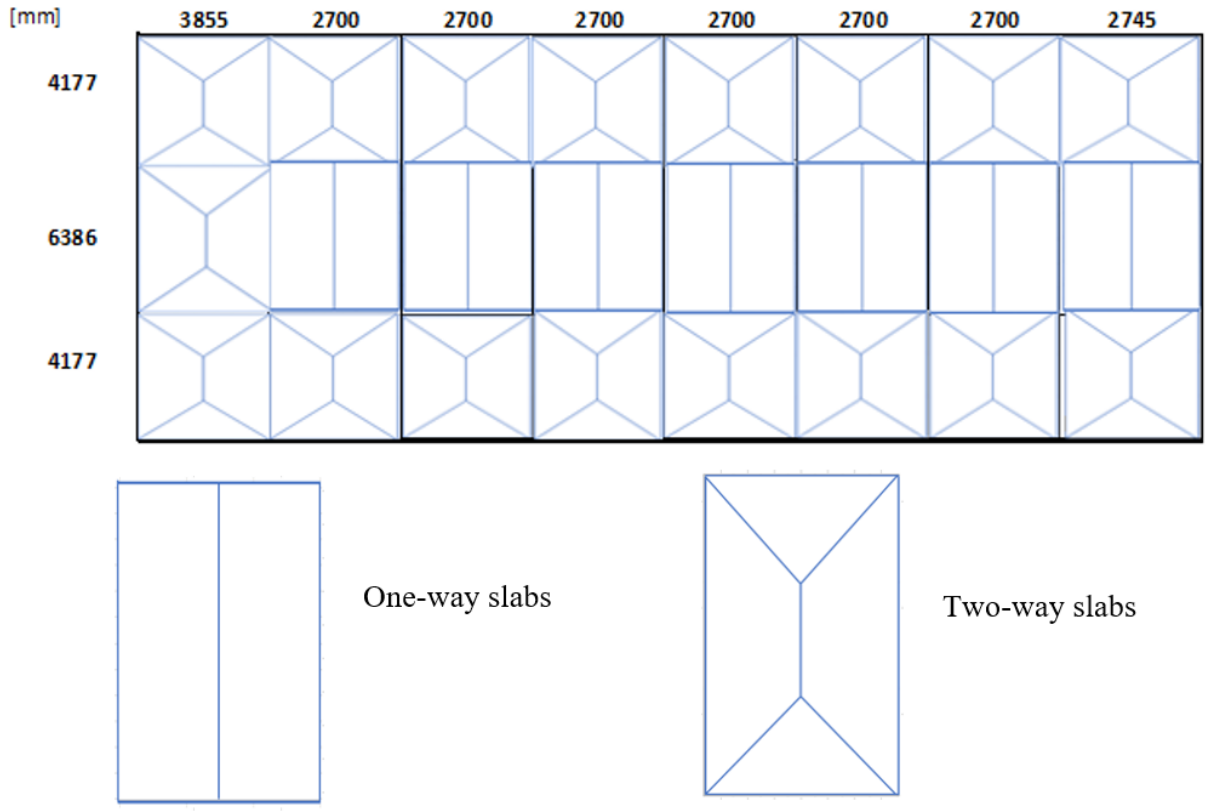

Figure 4.4 One-way and two-way slab of the floor plan

4.3 Verification of the models

Before using a model for calculations, it is crucial to verify its accuracy. It was necessary to conduct a test to confirm that the load flow of the building is equivalent to the base reaction to ensure the functionality of the SAP2000 model. The base columns and walls were fixed at the ground, and the test only focused on the dead load. The total joint reactions should add to the base reaction, as Appendix C shows. The model was suitable for determining the other parameters when the load flow matched the base reaction. Considering the ULS in this study was unnecessary, only the critical column and beam were checked. The columns and beams were evaluated for bending, compression, and buckling. Further details on the calculations can be found in Appendix D (Porteous & Kermani, 2013).

4.4 The finite element model

The three systems, frame, shear wall, and diagrid system, have been modeled in SAP2000. The dimensions of the structure are 22,8 meters in length and 14,74 meters in width. It has been determined that the story height of the building is 3 meters, resulting in an overall building height of 54 meters. It was found that using Glulam and CLT materials with a grade of c24 would be the best option for this particular structure. These materials are known for their durability and strength, making them ideal for construction projects such as this (Angelucci et al., 2022; Zhao et al., 2021a; Zhao et al., 2021b). The element properties used were taken from Tables 4.1 and 4.2 to ensure consistency and accuracy across all the models. All models were designed with identical floor plans to ensure consistency and structural simplicity throughout the structure. The floors in the reference building have a thickness of 180mm, while the roof has a thickness of 200mm. Thus, the same thickness was implemented for the floors and roof in all the models that are studied in this thesis.

Table 4.1 Glulam timber properties, (Crocetti, 2015).

		Glulam Strength class						
Property[a]	Symbol	GL 20c	GL 22c	GL 24c	GL 26c	GL 28c	GL 30c	GL 32c
Bending strength	$f_{m,g,k}$	20	22	24	26	28	30	32
Tensile strength	$f_{t,0,g,k}$	15	16	17	19	19,5	19,5	19,5
	$f_{t,90,g,k}$	0,5						
Compression strength	$f_{c,0,g,k}$	18,5	20	21,5	23,5	24	24,5	24,5
	$f_{c,90,g,k}$	2,5						
Shear strength (shear and torsion)	$f_{v,g,k}$	3,5						
Rolling shear strength	$f_{r,g,k}$	1,2						
Modulus of elasticity	$E_{0,g,\text{mean}}$	10 400	10 400	11 000	12 000	12 500	13 000	13 500
	$E_{0,g,05}$	8 600	8 600	9 100	10 000	10 400	10 800	11 200
	$E_{90,g,\text{mean}}$	300						
	$E_{90,g,05}$	250						
Shear-modulus	$G_{g,\text{mean}}$	650						
	$G_{g,05}$	540						
Rolling shear modulus	$G_{r,g,\text{mean}}$	65						
	$G_{r,g,05}$	54						
Density	$P_{g,k}$	355	355	365	385	390	390	400
	$P_{g,\text{mean}}$	390	390	400	420	420	430	440

Table 4.2 Cross-Laminated timber properties(Crocetti, 2015)

	Class	C14	C16	C18	C20	C22	C24	C27	C30	C35	C40	C45	C50
Strength properties in N/mm^2													
Bending	$f_{m,k}$	14	16	18	20	22	24	27	30	35	40	45	50
Tension parallel	$f_{t,0,k}$	7,2	8,5	10	11,5	13	14,5	16,5	19	22,5	26	30	33,5
Tension Perpendicular	$f_{t,90,k}$	0,4	0,4	0,4	0,4	0,4	0,4	0,4	0,4	0,4	0,4	0,4	0,4
Compression parallel	$f_{c,0,k}$	16	17	18	19	20	21	22	24	25	27	29	30
Compression perpendicular	$f_{c,90,k}$	2,0	2,2	2,2	2,3	2,4	2,5	2,5	2,7	2,7	2,8	2,9	3,0
Shear	$f_{v,k}$	3,0	3,2	3,4	3,6	3,8	4,0	4,0	4,0	4,0	4,0	4,0	4,0
Stiffness properties in kN/mm^2													
Mean modulus of elasticity parallel bending	$E_{m,0,mean}$	7,0	8,0	9,0	9,5	10,0	11,0	11,5	12,0	13,0	14,0	15,0	16,0
5 percentile modulus of elasticity parallel bending	$E_{m,0,k}$	4,7	5,4	6,0	6,4	6,7	7,4	7,7	8,0	8,7	9,4	10,1	10,7
Mean modulus of elasticity perpendicular	$E_{m,90,mean}$	0,23	0,27	0,30	0,32	0,33	0,37	0,38	0,40	0,43	0,47	0,50	0,53
Mean shear modulus	G_{mean}	0,44	0,50	0,56	0,59	0,63	0,69	0,72	0,75	0,81	0,88	0,94	1,00
Density in kg/m^3													
5 percentile density	p_k	290	310	320	330	340	350	360	380	390	400	410	430
Mean density	p_{mean}	350	370	380	400	410	420	430	460	470	480	490	520

4.4.1 Frame system

The frame system has a central core that has been modeled to ensure structural integrity. Throughout the entire building, the core system maintains a consistent thickness of 200mm in CLT material grade c24. Glulam columns of varying sizes are used every third story, as shown in Table 4.3. The frame system is modeled with six different sizes of glulam material. The beams spanning over the columns are the same throughout the building at 525mm x 675mm. Table 4.3 shows the column and beam size used to model the frame system. All the connections between the beams, columns, slabs, and walls are assigned to be rigid connections. This assumption was made to make the analysis easier.

Table 4.3 Frame material size

Frame		
Glulam member for the building	Story	Size [mm]
Column 1	1-3	850 x 850
Column 2	4-6	775x775
Column 3	7-9	700x700
Column 4	10-12	575x575
Column 5	13-15	550x550
Column 6	16-18	475x475
Beam	All	550 x 675
Core – CLT wall – c24	All	200 mm thick

4.4.2 Shear wall system

The shear wall and frame system were modeled with a core of 200 mm thick CLT walls in c24 material. Additionally, the outer tube of the shear wall system was modeled with the same CLT material, but a different thickness was used than the core. The outer shear walls had varying widths on the long and short sides of the building. Three walls with different widths were used on the longer side of the building. Two of these walls had widths of 3855mm and 2745mm and were placed on the sides of the long side, while the middle wall had a width of 5400mm and was placed between them, as shown in Figure 4.5. On the shorter side of the

building, two corner walls with an exact width of 4177mm were installed, as shown in Figure 4.6.

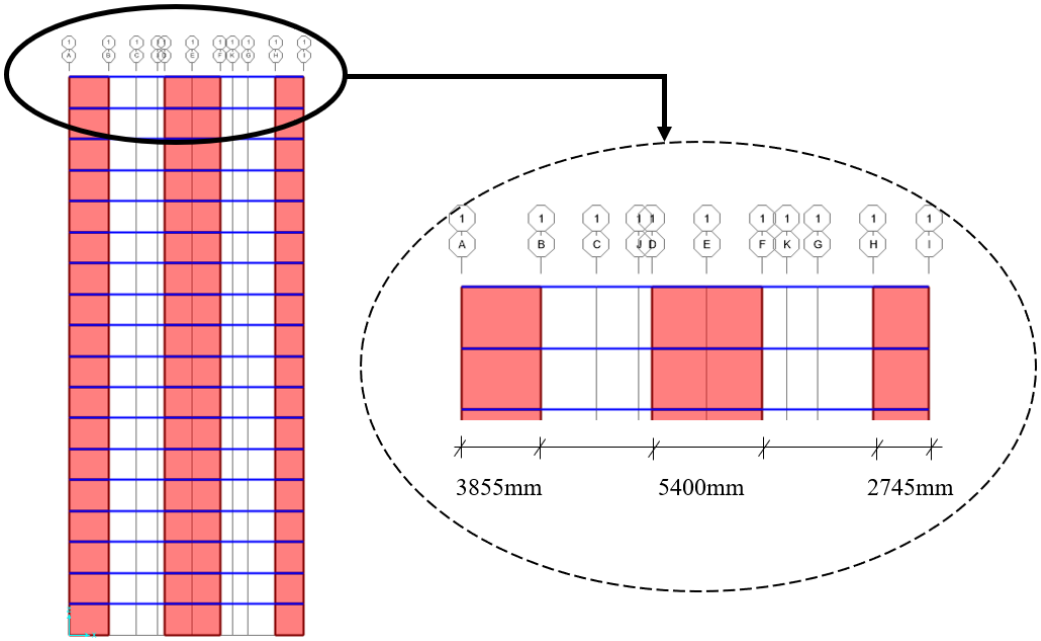

Figure 4.5 Long side of the shear wall system

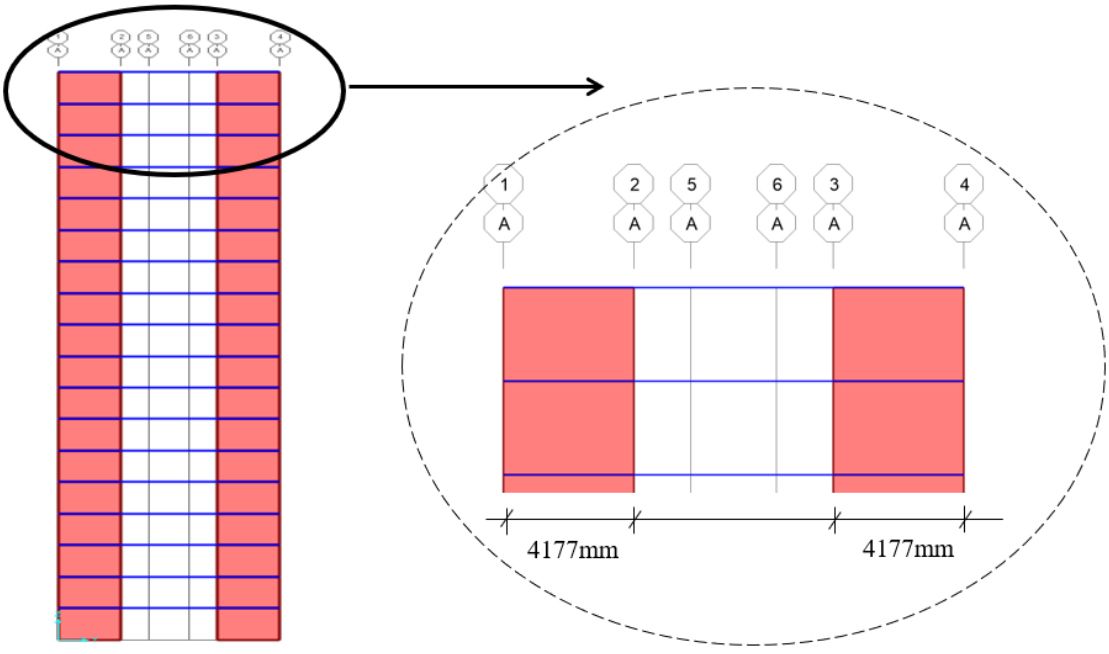

Figure 4.6 Short side of the shear wall system

The structure of the building was designed using three different thicknesses of CLT walls, which varied every sixth story. The walls were 350mm thick for the first six stories at the bottom, 300mm for the next six, and 275mm for the top six. Additionally, the building has inner glulam

columns with dimensions of 650x650mm for the first six stories, 550x550mm for the following six stories, and 450x450mm for the top six. Same-sized beams in glulam with 675x700mm were used throughout the building. Tables 4.4 and 4.5 show the element size and thickness for the CLT element and glulam for the building.

Table 4.4 CLT element size for shear wall system

Shear wall **CLT member for the building**	Story	Size of element [mm]	Thickness [mm]
CLT wall 1 – Long side (corner wall)	1-6	3855x3000 2745x3000	350
CLT wall 1 – middle	1-6	5400x3000	350
CLT wall 1 – Short side (corner wall)	1-6	4177x3000	350
CLT wall 2 – Long side (corner wall)	7-12	3855x3000 2745x3000	300
CLT wall 2 – middle	7-12	5400x3000	300
CLT wall 2 – Short side (corner wall)	7-12	4177x3000	300
CLT wall 3 – Long side (corner wall)	13-18	3855x3000 2745x3000	275
CLT wall 3 – middle	13-18	5400x3000	275
CLT wall 3 – Short side (corner wall)	13-18	4177x3000	275
CLT Core wall c24	All		200

Table 4.5 Glulam element size for shear wall system

Glulam member for the building	**Story**	**Size [mm]**	**Material**
Beam	All	675x700	GL 20c
Column 1 – inside	1-6	650x650	GL 20c
Column 2 – inside	7-12	550x550	GL 20c
Column 3 – inside	13-18	450x450	GL 20c

4.4.3 Diagrid system

The diagrid system is a unique structural framework that is made up of crosswise diagonal elements that intersect with horizontal and vertical members to create a grid-like pattern. This innovative design has been used in many modern steel buildings. The diagrid system is an efficient and innovative way to construct modern buildings, and the use of CLT walls and

glulam elements ensures that they are both strong and sustainable (Angelucci et al., 2022). The diagrid system was made in glulam with a core of CLT walls that are 300mm thick. Additionally, the material grade used for the core in the diagrid system is of higher quality than that used in the frame and shear wall system, with a CLT c30 grade being used.

The building was divided into nine sections, each consisting of two stories to model the diagrid system. The diagonal columns on the long side of the building were set at an angle of 66 degrees, while those on the short side were set at 67 degrees. This resulted in a diagonal glulam element spanning over every two stories, with a length of 6642,5mm and 6685,1mm on the long and short sides, respectively.

It is important to note that the material sizes employed across the entire building varied, and all columns (whether straight or diagonal) using dimensions of the size given in Table 4.6. Additionally, the beams used in the entire building were of the same size, 225x225mm.

Table 4.6 Element size for diagrid system

Diagrid			
Glulam member for the building	Story	Length [mm]	Size [mm]
Column 1 – Outer tube long side	1-2	6642,5	575x575
Column 1 – Outer tube short side	1-2	6685,1	575x575
Column 1 – straight	1-2	3000,0	575x575
Column – inside	1-2	3000,0	575x575
Column 2 – Outer tube long side	3-4	6642,5	525x525
Column 2 – Outer tube short side	3-4	6685,1	525x525
Column 2 – straight	3-4	3000,0	525x525
Column – inside	3-4	3000,0	525x525
Column 3 – Outer tube long side	5-6	6642,5	475x475
Column 3 – Outer tube short side	5-6	6685,1	475x475
Column 3 – straight	5-6	3000,0	475x475
Column – inside	5-6	3000,0	475x475
Column 4 – Outer tube long side	7-8	6642,5	425x425
Column 4 – Outer tube short side	7-8	6685,1	425x425
Column 4 – straight	7-8	3000,0	425x425
Column – inside	7-8	3000,0	425x425
Column 5 – Outer tube long side	9-10	6642,5	325x325
Column 5 – Outer tube short side	9-10	6685,1	325x325
Column 5 – straight	9-10	3000,0	325x325
Column – inside	9-10	3000,0	325x325

Column 6 – Outer tube long side	11-12	6642,5	275x275
Column 6 – Outer tube short side	11-12	6685,1	275x275
Column 6 – straight	11-12	3000,0	275x275
Column – inside	11-12	3000,0	275x275
Column 7 – Outer tube long side	13-14	6642,5	250x250
Column 7 – Outer tube short side	13-14	6685,1	250x250
Column 7 – straight	13-14	3000,0	250x250
Column – inside	13-14	3000,0	250x250
Column 8 – Outer tube long side	15-16	6642,5	225x225
Column 8 – Outer tube short side	15-16	6685,1	225x225
Column 8 – straight	15-16	3000,0	225x225
Column – inside	15-16	3000,0	225x225
Column 9 – Outer tube long side	17-18	6642,5	200x200
Column 9 – Outer tube short side	17-18	6685,1	200x200
Column 9 – straight	17-18	3000,0	200x200
Column – inside	17-18	3000,0	200x200
Beam	All		225x225
Core – CLT wall c30	All		300

4.5 Peak acceleration

The Eurocode does not offer guidance on analyzing the effects of wind-induced vibrations on different mass timber structural systems. Nevertheless, ISO 10137 Annex D can be utilized to assess the living conditions concerning how people respond to average building movements and horizontal acceleration with a one-year return period. Annex D evaluation curve consists of two lines indicating the acceptable horizontal movement for both office and residential buildings. The residential curve lies two-thirds of the way along the office curve, as demonstrated in Figure 4.7. In this figure, the x-axis represents the first natural frequency in a structural direction of a building, while the y-axis represents the peak acceleration. Based on the first natural frequency and peak acceleration with a one-year return period, the calculated point should not exceed the evaluation curve to achieve comfort.

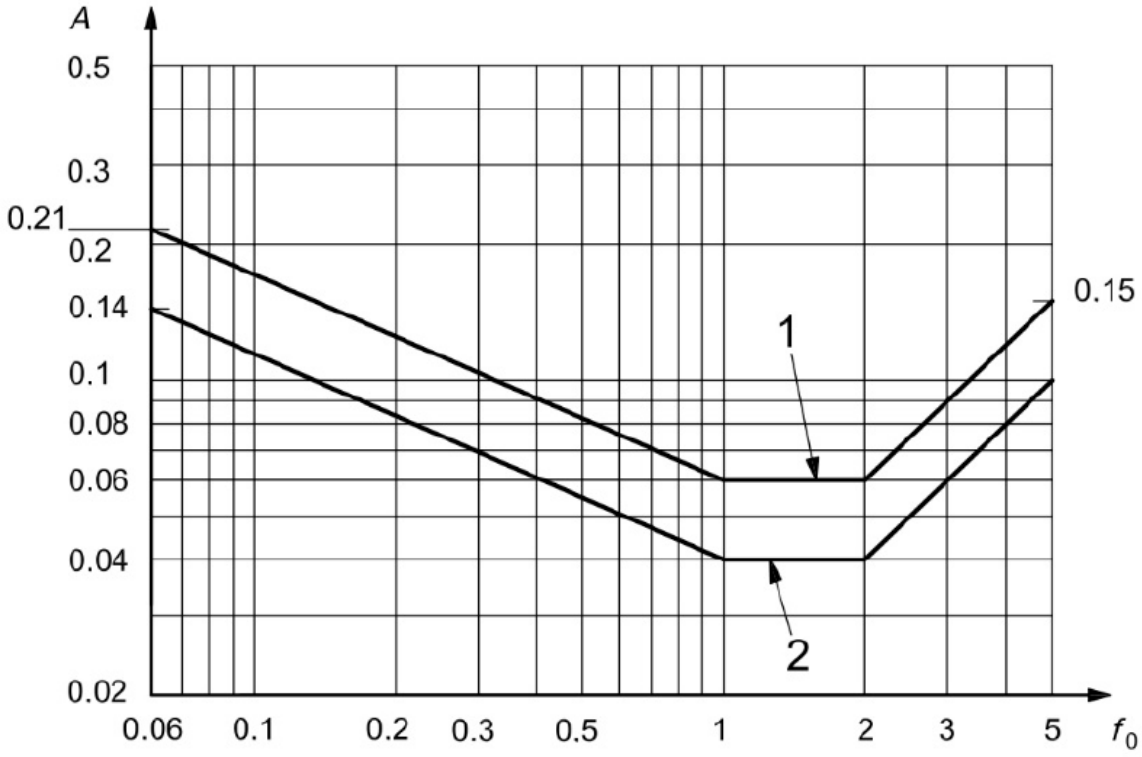

Figure 4.7 Evaluation curve from (Standardization, 2007)

4.5.1 Calculation Peak Acceleration.

It is recommended in Standardization (2007); Standardization (2009) to determine the horizontal peak acceleration, $a(z)$, at the top point of a structure, z, it must multiply the peak factor, Kp, by the standard deviation of the characteristic along-wind acceleration, $\sigma a, x(z)$. By observing the plotted peak acceleration and the first natural frequency of the structure in Figure 4.7, where it is possible to gain an understanding of the impact of the acceleration (or vibration) at the building's highest point. This calculation will be performed on all models with varying material grades on the outer tube, as shown in Expression (3.8).

The first step is to calculate the standard deviation of the characteristic along-wind acceleration, followed by calculating the peak factor. Eurocode 1991-1-4 provides two methods for determining the standard deviation, each referring to a different reference point on the building. Expression (3.9) computes the standard deviation at the building's height, while Expression (3.10) determines it for the structural point at coordinates (x,y). Eurocode 1-4 National Annex B's Expression (3.9) is mainly designed to calculate the maximum along-wind displacement at the top of the building height, which helps determine the acceleration at the top of the building,

z. Therefore, for this thesis, it will use Expression (3.9) to find the standard deviation at the top floor.

During the computation of standard deviation for various wind directions, certain coefficients and parameters remain constant because the location and building geometry remains unchanged in all models. These values, including the force coefficient (cf), air density (p), the width of the structure along the wind (b), turbulence intensity at the height (Iv(z)), mean wind velocity at the height (vm(zs)), and non-dimensional coefficient shear remains consistent across all analyzed models. Refer to Table 4.7 for a comprehensive list of these values.

Table 4.7 The parameters that remain the same when calculating the standard deviation

	cf	p [kg/m^3]	b [m]	Iv(z)	v^{2}m(z) [m/s]	$\Phi 1(z)$	kx
Value	1,2	1,25	22,8	0,144	266,56	1	1,35

As per the guidelines provided in Eurocode 1-4, the force coefficient is assumed to be identical to the net pressure coefficient, and therefore 1,2 is used (Zhao et al., 2021b). It is of note that in Norway, the air density is measured to be approximately 1,25 kg/m^3. At the top of the structure, the turbulence intensity stands at 0,144 from using Expression (3.7) from the theory section. While the mean wind velocity is determined utilizing equations from the theory section. The mean wind velocity is influenced by a one-year return period. Calculating the mean wind velocity with a one-year return period gives a peak acceleration value that allows the representation of the comfort in Figure 4.7. The Expression (3.2) from the theory section was used to calculate the wind velocity for a one-year period.

Following, Expression (3.9) needs to specify which mode shape that is taken into consideration. The fundamental mode shape, $\Phi 1(z)$, was found with $\Phi 1(z) = \left(\frac{z}{h}\right)^{\varsigma}$, where the reference point at the building (z) and height (h) are the same as the building. The ratio of $\frac{z}{h}$, where v z is the reference point, and h is the height, which is equal to 1 because the horizontal peak acceleration is concentrated at the top of the building, which has a z and h value of 54. The parameter *"*ς*"* from NS-EN 1991-1-4 varies based on the shape and structure of the building and must be selected accordingly for each model. The table below displays the chosen parameters for each structural system.

Table 4.8 Parameters

Structural system	ς	Value
Frame structure with core	ς	1,0
Shear wall with a core	ς	1,0
Diagrid structure with core	ς	1,0

When the fundamental mode shape is calculated to be $\Phi 1, x(z) = (\frac{z}{h})^{\varsigma} = 1$, the non-dimensional coefficient can be calculated as shown below in Expression (4.1):

$$K_x = \frac{(2 * \varsigma + 1) * \left\{(\varsigma + 1) * \left[\ln\left(\frac{zs}{z0}\right) + 0{,}5\right] - 1\right\}}{(\varsigma + 1)^2 * ln\left(\frac{zs}{z0}\right)} \tag{4.1}$$

Where z is the reference height of the building at 54 meters, and z0 is the roughness length of the building at 0,05 meters (Standardization, 2009). Therefore, K_x is equal to 1,35.

The equivalent mass and the square root of the resonant will vary due to the different material sizes and frequencies of the models. The method for calculating the equivalent mass can be found in the National Annex F of Eurocode 1. To determine the average mass of the building, the masses of all elements in each story were added and divided by three, as different element sizes were used in different stories. This method has been used to calculate the equivalent masses of all models. The equivalent mass was obtained by averaging the mass over 1/3 of the building's height to simplify the process (Standardization, 2009). An Excel file in Appendix E was used to calculate the equivalent mass for each model. Table 4.9 shows the corresponding mass of each model under various conditions, but only for material grade c24 for glulam and c24 for CLT.

Table 4.9 Equivalent mass for the systems

	Frame system	Shear wall system	Diagrid system
Mass [kg/m]	450745,59	503620,37	291112,76

To calculate the turbulence in resonance with a structure's vibration mode, the resonance response factor R^2 is determined using the expression from NS-EN 1991-1-4 (B.6). The standard deviation is then calculated using the square root of the resonant response factor, R. The theory section presents the Expression (3.17) for the resonance response factor, which

depends on the natural frequency of the structure and varies between models and material grades. Appendix F provides all the calculations for the different models.

Table 4.10 The resonance response factor

Structural system	Frame system	Shear wall system	Diagrid system
R	0,1425	0,1393	0,0731

It is necessary to consider all the previously mentioned expressions to determine the standard deviation. To assist with this calculation, the table below, Table 4.11, displays the corresponding values for the standard deviation.

Table 4.11 Standard deviation

Structural system	Same frequency	Same stiffness	High frequency
$\sigma a, x(z)$	0,0101	0,0089	0,0080

The peak factor (Expression (4.2)) is calculated by,

$$k_p = \sqrt{2 * \ln(v * T)} + \frac{0,6}{\sqrt{2 * \ln(v * T)}} \tag{4.2}$$

The second step in this process involves determining the peak factor, which considers the background factor (B^2) and the resonance response factor (R^2). These two factors are utilized to calculate the up-crossing frequency (v), which is a critical component in determining peak acceleration. It is important to note that the natural frequency of the system must also be taken into consideration when calculating the up-crossing frequency. This value can vary depending on the model and material grade being analyzed. The natural frequency and the up-crossing frequency are assumed to be the same.

Table 4.12 Natural frequency

Natural frequency	Frame system [Hz]	Shear wall system [Hz]	Diagrid system [Hz]
Mode 1	1,045	1,017	1,680

According to Eurocode 1-4, the averaging time for the mean wind velocity is equal to 600 seconds, denoted as (T). The peak factor is calculated and presented in Table 4.13.

Table 4.13 Peak factor

Structural system	Frame system	Shear wall system	Diagrid system
Peak factor	3,743	3,749	3,880

The calculation of the peak acceleration has been successfully completed, and the numerical result has been presented in a clear and organized manner in Table 4.14. This information is now readily available for further analysis and interpretation.

Table 4.14 Peak acceleration

Structural system	Frame system	Shear wall system	Diagrid system
Peak acc.	0,0506	0,103	0,0381

4.6 Top deflection and inter-story drift

The deflection at the top of the building was determined through analysis using the SAP2000 models. The models utilized material grade c24 for glulam and c24 in CLT to calculate the deflections. Two load combinations were analyzed for the building, both related to wind loads but in different directions, such as 0 degrees (across-wind direction) and 90 degrees (along-wind direction). The inter-story drift was calculated from the deflections using the Expression (3.19) from the theory section. This drift ratio was then determined based on the values of inter-story drift. The thorough analysis allowed for a better understanding of the building's stability.

5 Results

5.1 Natural frequency and mode

The analysis was conducted on SAP 2000 to determine the fundamental frequency of each building. The three lowest natural frequencies of swaying motion, which depend on the building's mass and stiffness, were observed to align with the wind spectra frequency range in tall timber buildings (Abrahamsen et al., 2020). The first frequency occurs along the shortest side of the building for all models. The second frequency occurs at the longest bending side of the building for shear wall and diagrid systems and as a rotational mode about the vertical axis in the frame system. The last frequency is generated from the rotational mode about the vertical axis for shear wall and diagrid systems and at the longest bending side for the frame system. Table 5.1 presents the frequency data for all models with a material grade of c24 for glulam and CLT, while Figures 5.1 – 5.9 show the mode shapes on the top of the building.

Table 5.1 The natural frequency for the first three modes

Natural frequency	Frame system [Hz]	Shear wall system [Hz]	Diagrid system [Hz]
Mode 1	1,0448	1,0169	1,6802
Mode 2	1,2304	1,3147	2,3414
Mode 3	1,3409	1,5322	3,9544

The figures below show the movement of the building in 2D and 3D of the buildings for the first three natural frequencies. The 2D figures show the pressure on the roof/top floor. Figure 5.1, 5.2, and 5.3 refers to the frame system. Figure 5.4, 5.5, and 5.5 refers to the shear wall system. Figure 5.7, 5.8, and 5.9 refers to the diagrid system.

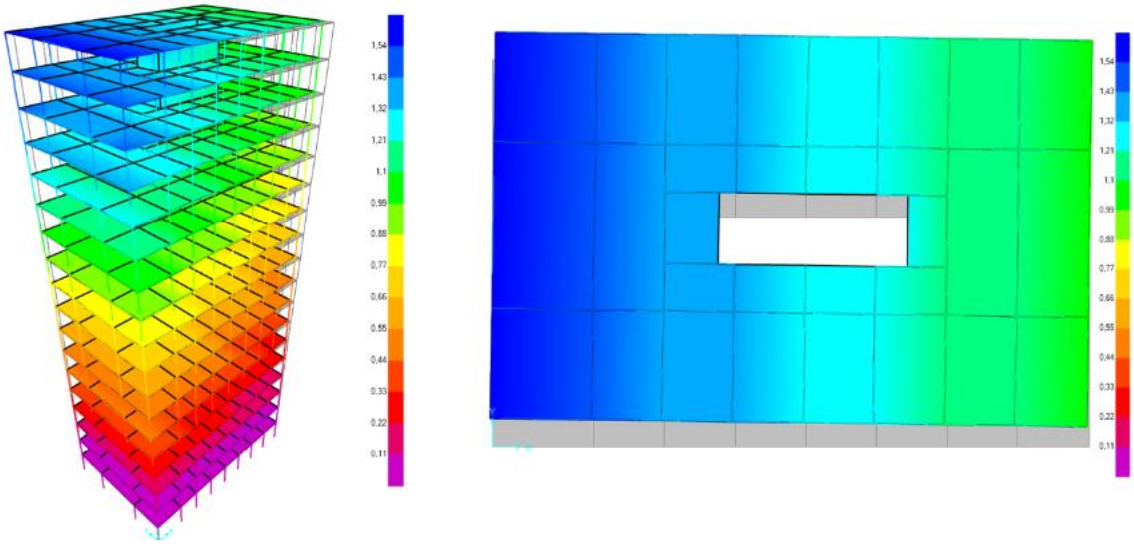

Figure 5.1 Frame system, mode 1 natural frequency 1,0448 Hz

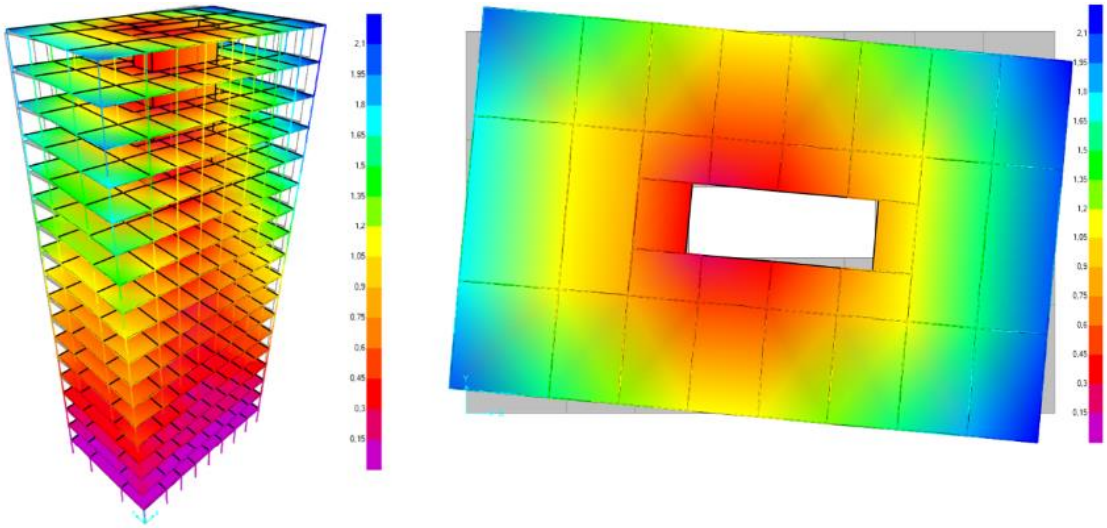

Figure 5.2 Frame system, mode 2 natural frequency 1,2304 Hz

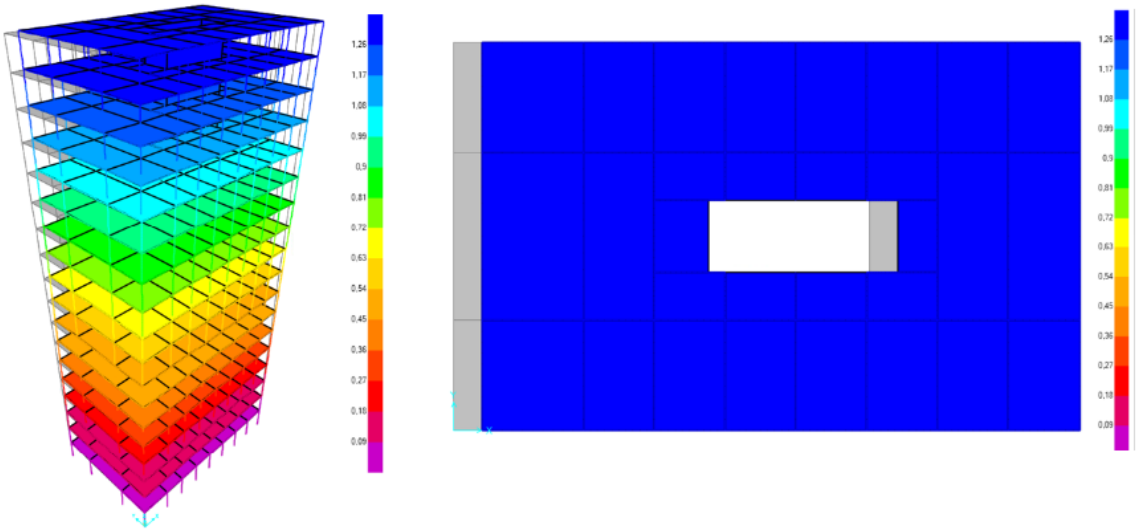

Figure 5.3 Frame system, mode 3 natural frequency 1,341 Hz

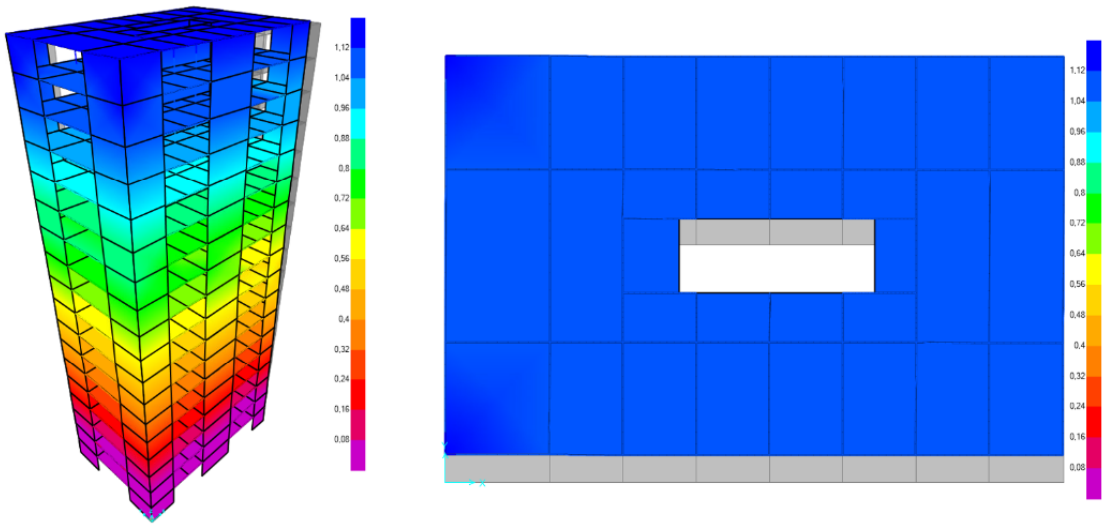

Figure 5.4 Shear wall system, mode 1 natural frequency 1,0619 Hz

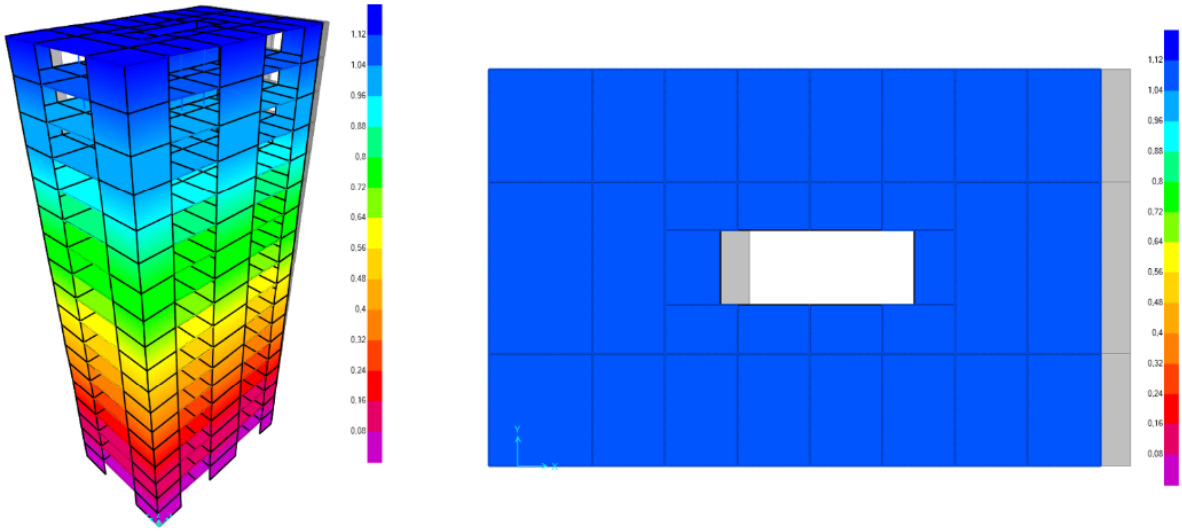

Figure 5.5 Shear wall system, mode 2 natural frequency 1,3147 Hz

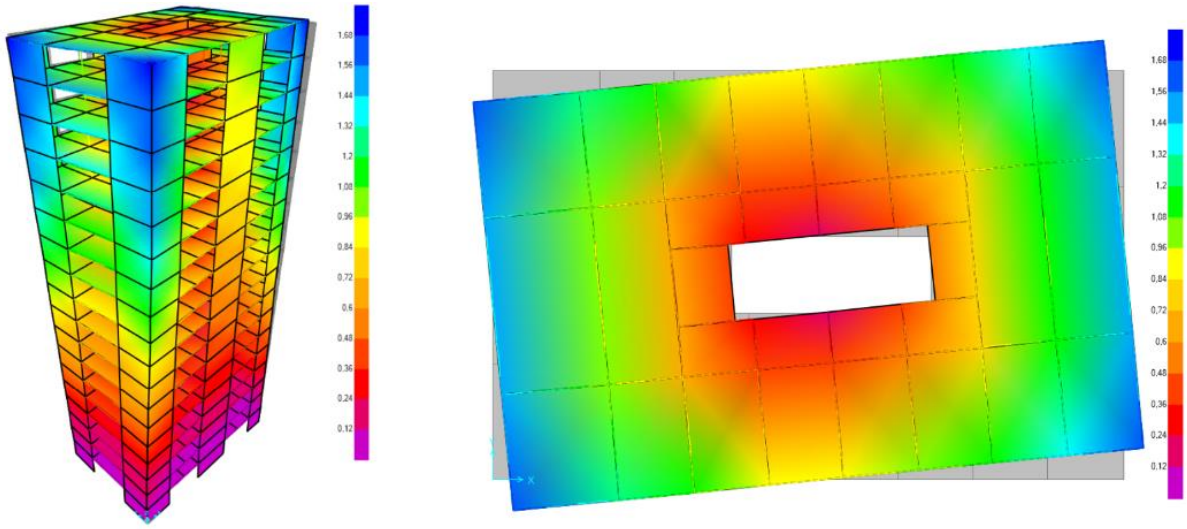

Figure 5.6 Shear wall system, mode 3 natural frequency 1,5322 Hz

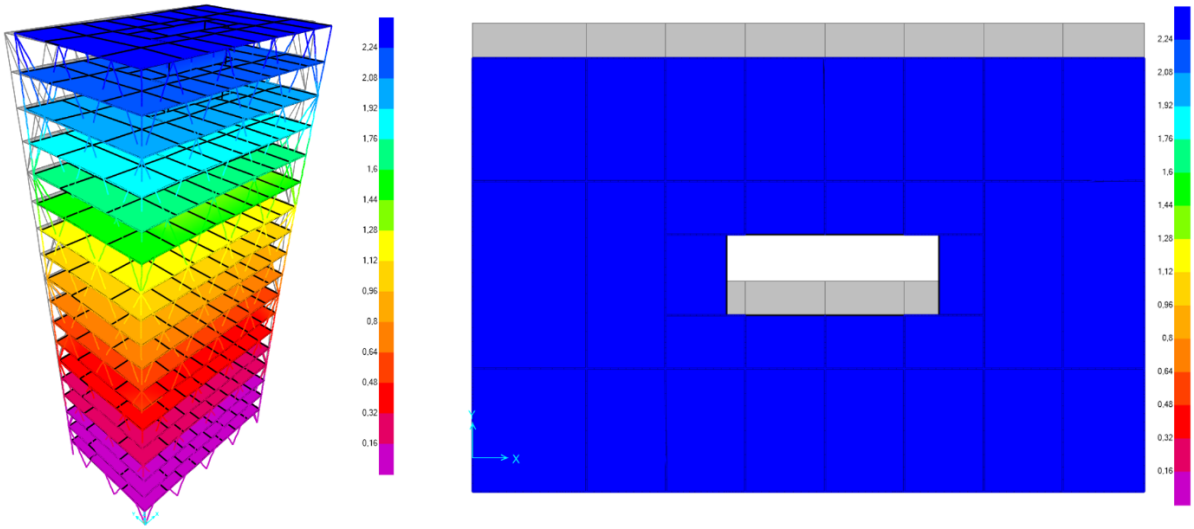

Figure 5.7 Diagrid system, mode 1 natural frequency 1,6802 Hz

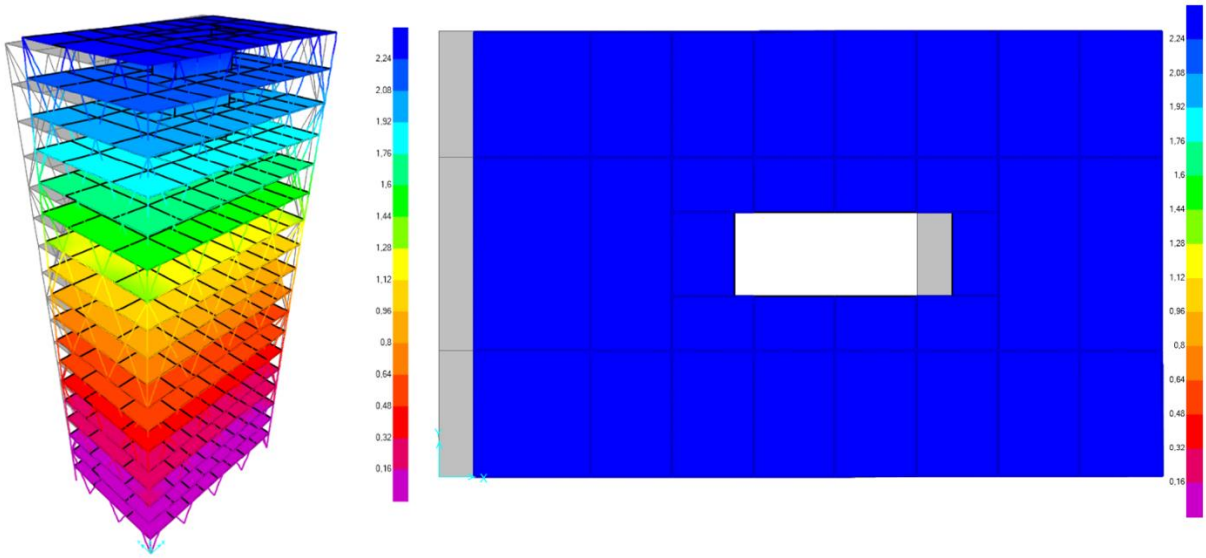

Figure 5.8 Diagrid system, mode 2 natural frequency 2,3414 Hz

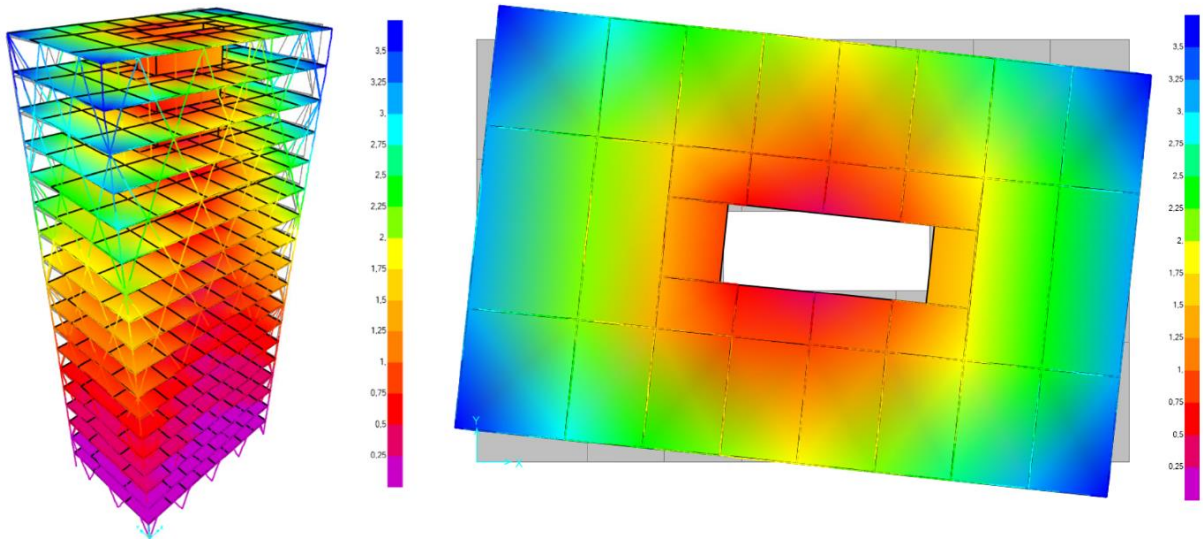

Figure 5.9 Diagrid system, mode 3 natural frequency 3,9544 Hz

5.2 Peak acceleration

ISO 10137 recommends and points out that a building should be evaluated for comfort level and have an evaluation curve, represented in Figure 4.7. Timber buildings are lightweight and are easily affected by horizontal loads. In this thesis, the focus has been on the models that satisfy the recommended limit from ISO 10137 and discusses the effectiveness of the system compared to each other. Several models have been made, but the models that had a peak acceleration level under 0,04 m/s^2 are used and presented. The other models can be found in Appendix F. Table 5.2, 5.3, and 5.4 shows the effectiveness of different material grade that vary from c20 to c32 for glulam and c20 to c40 for CLT elements for the frame, shear wall, and diagrid system.

Table 5.2 Frame system, the effectiveness of different material grade

Model	Glulam grade	Average mass	Mode stiffness	Natural frequency	Peak acceleration
A-I	C20	442642,0	72,00	0,97946	0,0390
A-II	C22	442642,0	72,00	0,97946	0,0390
A-III	C24	450745,59	71,99	0,992147	0,0379
A-IV	C26	465384,44	72,00	1,010297	0,0360
A-V	C28	465384,44	72,00	1,02225	0,0355
A-VI	C30	472703,86	71,99	1,02993	0,0347
A-VII	C32	480023,29	72,00	1,03707	0,0340

Table 5.3 Shear wall system, the effectiveness of different material grade

Model	CLT grade	Average mass	Mode stiffness	Natural frequency	Peak acceleration
B-I	C20	499101,78	73,00	0,97614	0,0351
B-II	C22	501361,08	73,00	0,99804	0,0341
B-III	C24	503620,37	72,99	1,01816	0,0332
B-IV	C27	505879,66	72,99	1,02426	0,0328
B-V	C30	512657,55	73,01	1,02845	0,0323
B-VI	C35	514916,84	73,00	1,04458	0,0316
B-VII	C40	517176,13	71,99	1,06038	0,0309

Table 5.4 Diagrid system, the effectiveness of different material grade

Model	Glulam grad	Average mass	Mode stiffness	Natural frequency	Peak acceleration
C-I	C20	289873,87	62	1,63737	0,0322
C-II	C22	289873,87	62	1,63737	0,0322
C-III	C24	291112,76	62	1,68028	0,0312
C-IV	C26	293590,54	62	1,74935	0,0295
C-V	C28	293590,54	61,99	1,78283	0,0289
C-VI	C30	294829,43	62	1,81567	0,0281
C-VII	C32	296068,32	62	1,84121	0,0276

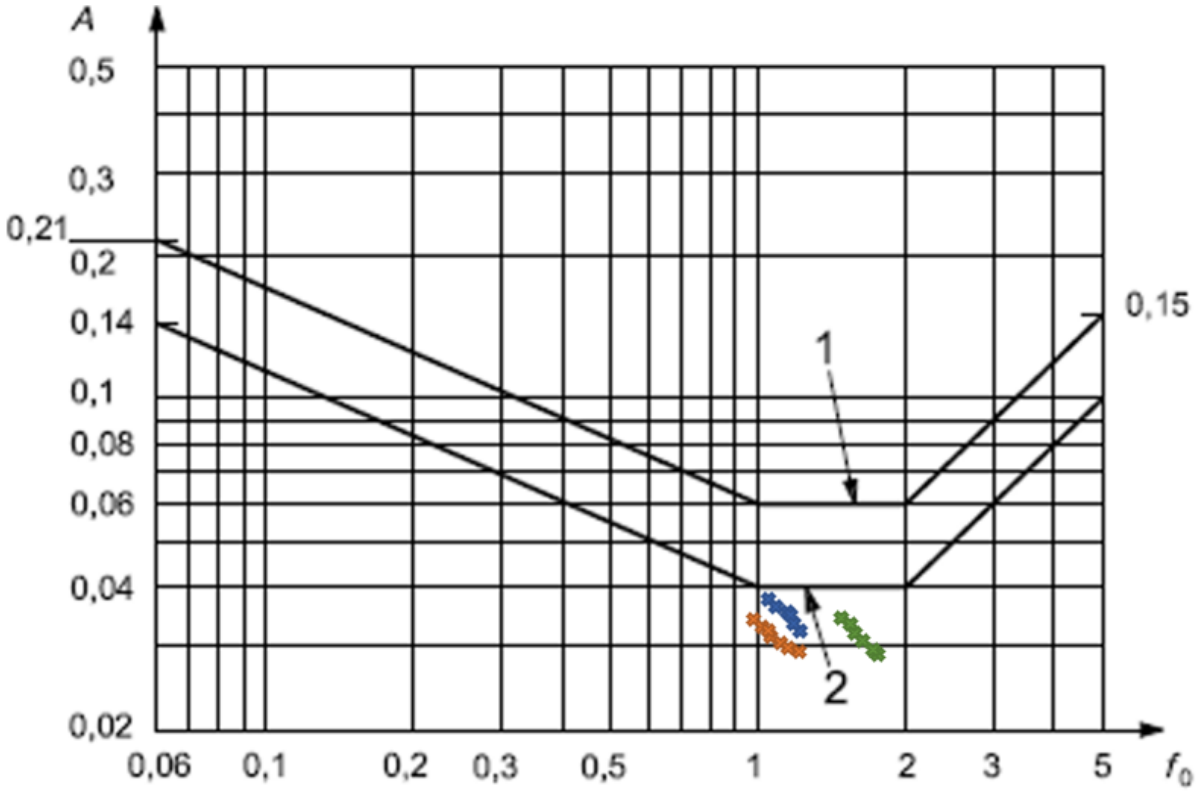

Figure 5.10 Frame (blue), Shear wall (orange), and diagrid (green) system under peak acceleration limit 0,04 m/s^2

Figure 5.10 presents the evaluation cure for the frame, shear wall, and diagrid that have material size presented in Tables 4.3 – 4.6 in the method section. To evaluate the different systems' comfort, the natural frequency and the calculated peak acceleration that is presented in Tables 5.2, 5.3, and 5.4 are used. The blue symbol represents the frame system that lays right under the line that represents the limited peak acceleration values for residential buildings. The orange symbol represents the shear wall system, and the green symbol represents the diagrid system.

The frame system had a peak acceleration range of 0,0390 m/s^2 to 0,0340 m/s^2. Depending on the material grade of the glulam elements used, the average mass of the system varied from 442 642,0 kg/m to 480 023,29 kg/m. The shear wall system, on the other hand, had a peak acceleration range of 0,0351 m/s^2 to 0,0309 m/s^2 and an average mass ranging from 499 101,78 kg/m to 517 176,13 kg/m, depending on the material grade used on CLT elements. Finally, the diagrid had a peak acceleration ranging from 0,0322 m/s^2 to 0,0276 m/s^2 and an average weight ranging from 289 873,87 kg/m to 296 068,32 kg/m.

5.3 Displacement

All the floors were assigned to be rigid diaphragms. Therefore, the displacement for all the models has been found from each story, represented in Table 5.5. Figure 5.11 was made by values found in Table 5.5. The blue graph shows the horizontal displacement for the frame system made with material size in Table 4.3 from the method section. The orange graph shows the displacement for the shear wall system made with material size from Tables 4.4 and 4.5 from the method section, and the green graph shows the horizontal displacement made from the material size from Table 4.6 from the method section for the diagrid system. Figure 5.11 represents the displacement in millimeters [mm], and the horizontal axes represent every eighteen stories. The displacement at the top of the frame system is 29,29 mm, the shear wall has a displacement of 21,53 mm, and the diagrid system has a 13,24 mm displacement.

Table 5.5 Displacement for models within acceptable peak acceleration

Load comb.	Comb2_wind 90deg – weak axis (y)		
Story	Frame	Shear wall	Diagrid
	Y [mm]	Y [mm]	Y [mm]
1	0,96	0,75	0,26
2	2,60	1,83	0,68
3	4,44	3,07	1,12
4	6,39	4,41	1,59
5	8,34	5,82	2,19
6	10,23	7,24	2,81
7	12,20	8,76	3,49
8	14,07	10,25	4,18
9	15,85	11,70	5,11
10	17,91	13,10	6,02
11	19,83	14,42	7,03
12	21,59	15,66	7,95
13	23,33	16,88	9,00
14	24,89	18,00	9,95
15	26,25	19,02	10,91
16	27,47	19,95	11,70
17	28,48	20,78	12,54
18	29,29	21,53	13,24

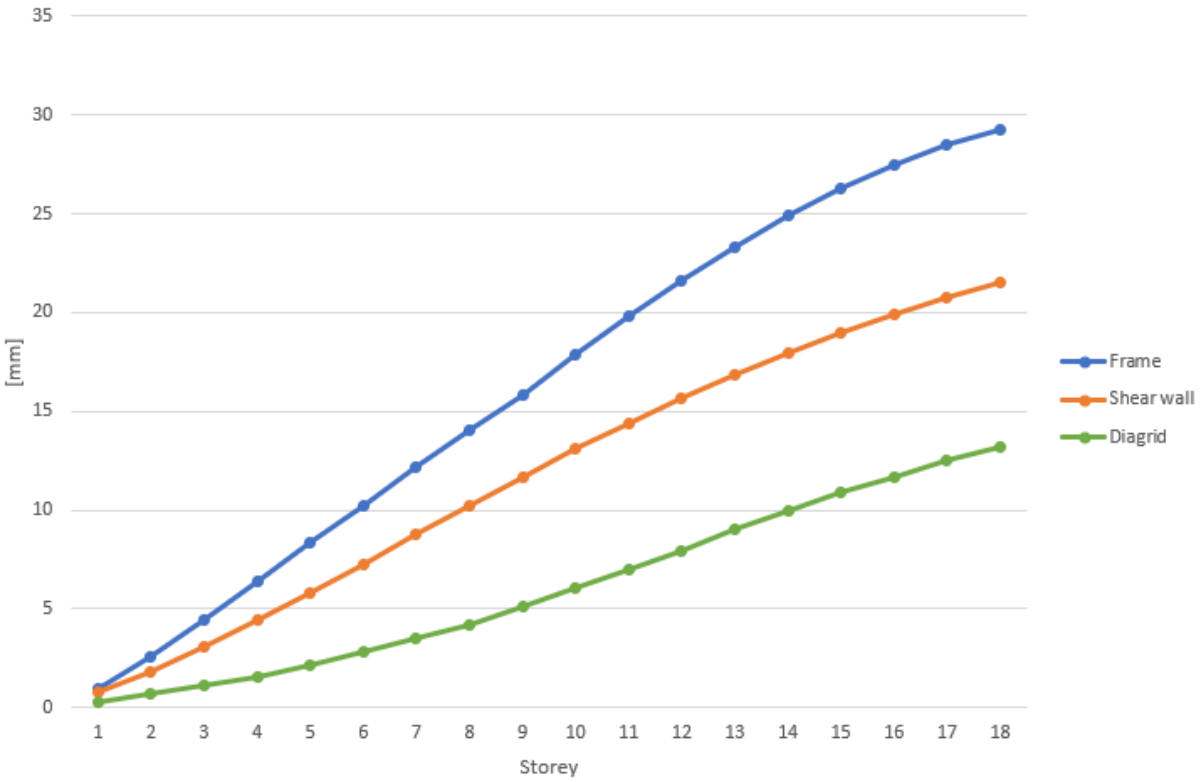

Figure 5.11 Displacement in [mm] for each story

5.4 Inter-story drift

The analysis of the drift between the floors has been conducted for the frame, shear wall, and diagrid systems. The story drift for all the stories is presented in Table 5.6 and has also been calculated and presented in Table 5.7 as the story drift ratio. The most critical value will be the maximum story drift for the systems, which can be found in Table 5.6 and in Figure 5.12. For the frame system, the maximum story drift is at the 9th floor, with a drift of 1,91 mm. The shear wall system occurs on the 7th floor, measuring 1,52 mm. Finally, for the diagrid system, the maximum drift is at the 13th floor, with a drift of 1,05 mm.

Table 5.6 Inter-story drift for models within acceptable peak acceleration

Load comb.	Comb2_wind 90deg – weak axis (y)		
Story	Frame	Shear wall	Diagrid
	Y [mm]	Y [mm]	Y [mm]
1	0,95	0,75	0,26
2	1,57	1,08	0,42
3	1,62	1,24	0,44
4	1,71	1,34	0,47
5	1,84	1,41	0,6
6	1,84	1,42	0,62
7	1,86	1,52	0,68
8	1,79	1,49	0,69
9	1,91	1,45	0,93
10	1,8	1,4	0,91
11	1,77	1,32	1,01
12	1,63	1,24	0,92
13	1,69	1,22	1,05
14	1,52	1,12	0,95
15	1,48	1,02	0,96
16	1,29	0,93	0,79
17	1,33	0,83	0,84
18	1,15	0,75	0,7

Table 5.7 Inter-story drift for models within acceptable peak acceleration

Load comb.	Comb2_wind 90deg – weak axis (y)		
Story	Frame	Shear wall	Diagrid
	Y [mm]	Y [mm]	Y [mm]
1	0,032	0,025	0,009
2	0,052	0,036	0,014
3	0,054	0,041	0,015
4	0,057	0,045	0,016
5	0,061	0,047	0,020
6	0,061	0,047	0,021
7	0,062	0,051	0,023
8	0,060	0,050	0,023
9	0,064	0,048	0,031
10	0,060	0,047	0,030
11	0,059	0,044	0,034
12	0,054	0,041	0,031
13	0,056	0,041	0,035
14	0,051	0,037	0,032
15	0,049	0,034	0,032
16	0,043	0,031	0,026
17	0,044	0,028	0,028
18	0,038	0,025	0,023

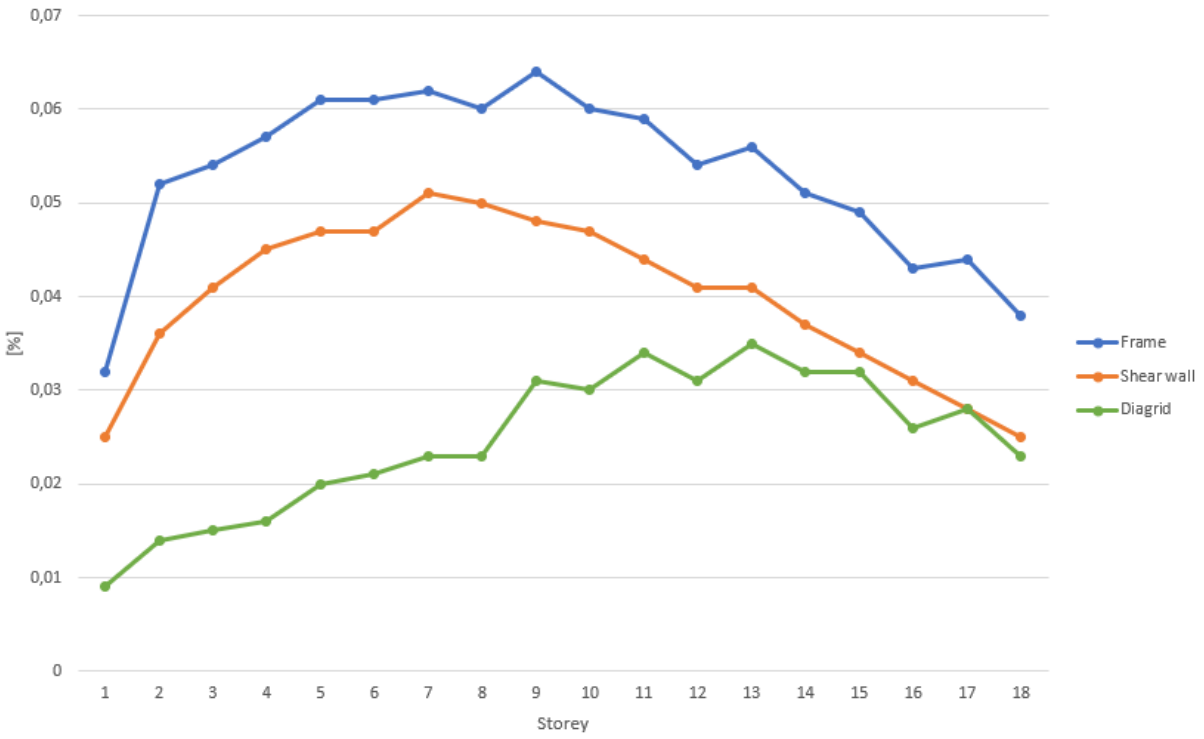

Figure 5.12 Story drift ratio in [%] for all the stories

6 Discussion

6.1 Natural frequency

The focus has been on the global serviceability behavior of different mass timber buildings. All the models have been modeled and analyzed by the finite element program SAP2000. Here, only the lowest natural frequency in the first mode is used to evaluate the comfort of the building. The numerically estimated frequency for the frame system was 0,992 Hz, the shear wall system had a frequency of 1,018 Hz, and the diagrid system had a frequency of 1,680 Hz. All the first frequencies occur along the shortest side of the building, which is the weakest bending direction. This natural frequency is based on the model size presented in Table 4.3 -4.6 in the methodology section for material grade glulam c24 and CLT c24.

Eurocode 1-4 presents an empirical formula on the fundamental frequency for tall buildings over 50 meters. The formula is represented as Expression (3.11) in the theory section. This expression is based on experimental results on tall concrete and steel buildings. With Expression (3.11), the frequency for a 54-meter-tall building should be estimated as n1 = 0,852 Hz. This indicates that the numerically modeled frame, shear wall, and diagrid system are 16,4%, 19,5%, and 97,2%, respectively, greater than the empirical formula recommended in Eurocode 1-4. Edskär (2018) presented a recommended expression for the fundamental frequency that is expressed as n1 = 55/h. In this case n1 = 55/54 = 1,019 Hz. This gives the modeled system a 2,7% smaller frequency for the frame system, 0,098% smaller frequency for the shear wall system, and 64,9% bigger frequency for the diagrid system. This shows that the frame and shear wall systems are 2,7% and 0,098%, respectively, less in stiffness than expected due to the Edskär (2018) recommended expression and 64,9% greater stiffness than expected for the diagrid system.

Based on the previous studies done on the reference building, both experimentally and numerically Ussher et al. (2022) and Aloisio et al. (2020) and the model from this thesis, it may be seen that the empirical formula provided in Eurocode for the prediction of the fundamental frequency of buildings may not be accurate enough for a timber building. This suggests that material influences like the orthotropic of CLT and the connection between various components in timber buildings all influence the prediction of the fundamental frequency.

The frequency is depended on the mass and stiffness of the building. It is getting a higher natural frequency results in high stiffness and reduced acceleration than expected from the codes

(Edskär, 2018; Zhao et al., 2021b). It is impotent to note that all the models have cores that do not have any openings. This means that the building has a "box-like" core that follows all the way from the ground to the top of the building. In real life, the core and each floor in the core will have openings in the form of door openings and stair openings that may reduce the overall stiffness of the building.

Even though the estimated numerical frequency is higher than the empirical formula expressed in Eurocode 1-4 and different from the recommended expression from Edskär (2018), the numerical frequency for the models that have been found from this study is an acceptable value. This is caused by no restrictions in Eurocode that make the numerical frequency acceptable. Moreso, the fundamental frequencies obtained in this work may be deemed acceptable due to the capabilities of the numerical models accurately simulate construction features of real-life timber buildings (Ussher et al., 2022).

6.2 Displacement and inter-story drift

The displacements for the models have also been numerically determined. It is important to note that the contribution of connections and shear deformations were not considered. All the connections for the building have been assumed to be rigid. The displacement for the system at the top of the building is 29,29 mm for the frame system, 21,53 mm for the shear wall system, and 13,24 mm for the diagrid system. In Europe, the serviceability criteria for horizontal displacement are not defined for wind-induced motions with a specific limit. Different expressions are used to check for horizontal displacement. Zhao et al. (2021b) have used an expression on $\frac{H}{500}$, where the H represents the height of the building. This expression is used as a limit for the overall global displacement and for the deflection on each story, represented as inter-story drift. When the inter-story drift is considered, the expression uses the story height as H in the expression mentioned above. From analyzing a frame structure in 10 stories, Vilguts et al. (2020) used a different expression as the limit of deflection. Vilguts et al. (2020) use a displacement limit of $\frac{H}{300}$ for global displacement and for inter-story drift, where H will represent the overall height of the building when global displacement is considered, and H will represent the story height when inter-story drift is considered. Treet, which was built in Bergen, Norway, was limited to $\frac{H}{500}$ (Abrahamsen & Malo, 2014). Therefore, the numerical models will also be limited by this expression.

According to the limit presented by Zhao et al. (2021b) and used by Abrahamsen et al. (2020), the global displacement for the models with 54 meters in height should be under $\frac{H}{500}$ =108mm. The frame system is 72,9% lower than the limit, the shear wall system is 80,1% lower than the limit, and the diagrid system is 87,7% lower than the limit.

The maximum story drift occurs on the 9th floor for the frame system, on the 7th floor for the shear wall system, and on the 13th floor for the diagrid system. The story displacement for the frame is 1,91mm, for the shear wall system, it is 1,52 mm, and for the diagrid system is 1,05 mm. This gives an inter-story drift ratio of 0,064% for the frame system, 0,051% for the shear wall system, and 0,035% for the diagrid system. Every story in the models has a height of 3 meters. Therefore, the drift limit expressed with $\frac{H}{500}$ is at 6mm, which is 68,2% lower than the limit for the frame system, 74,7% lower than the limit for the shear wall system, and 82,5% lower than the limit for the diagrid system. All displacements are within the limits. Therefore, the horizontal displacement and inter-story drift for the models are accepted.

6.3 Peak acceleration

Eurocode 1-4 and the Norwegian National Annex were used to determine the calculation of peak acceleration for all the models. Then, ISO 10137 Annex D was used to evaluate the comfort.

All three models have been satisfied under the evaluation cure requirements. With a natural frequency ranging from 1 Hz to 2 Hz, the peak acceleration was limited by 0,04 m/s^2. From Table 3.1, it may be noted that the acceleration under 0,05 m/s^2 results in situations where humans can not perceive motion. Since all the models are within 0,04 m/s^2, the motion will not be as notable. From Figure 5.10, it is noted that all the systems are within the limit, where the shear wall and diagrid system have lower peak acceleration than the frame system. The frame system in material grade c24 for the glulam has a peak acceleration of 0,0379 m/s^2, which is 5,3% lower than the limit. The shear wall with material grade in CLT c24 had a peak acceleration of 0,0332 m/s^2, which is 17% lower than the limit. Moreover, the diagrid system had peak acceleration at 0,0312 m/s^2, which is 22% lower than the limit for the system with glulam c24.

The evaluation curve presented in ISO10137 is for horizontal wind-induced vibrations for a one-year return period. The characteristics values that are used to calculate the wind actions from Eurocode 1-4 present an expression that is equivalent to a mean return period of 50 years. It is important to note that before the human response to wind-induced motions in buildings is evaluated with an evaluation curve from ISO 10137, the characteristics values from Eurocode are calculated with a one-year return period. Therefore, the expression for mean wind velocity presented by Johansson et al. (2016) was used to find the mean wind velocity with a one-year return period.

Using different material grades ranging from c20 to c32 for glulam and c20 to c40 for CLT walls, the mass for each system was increased. The mass was increased by 8,1% for the frame system, 4,4% for shear walls, and 2,3% for the diagrid system. The stiffness for the models was the same, but the frequency increased by 5,6% for the frame system, 7,91% for the shear wall system, and 11,5% for the diagrid system. The peak acceleration, on the other hand, was reduced by 15,5% for the frame system, 14,4% for the shear wall system, and 17,8% for the diagrid system.

6.4 Comparing the system

All the models had to be adjusted and modeled to achieve a comfort level related to the evaluation curve from ISO 10137. Figure 5.10 illustrates that all the models fall within the comfort level. However, the structural system chosen can significantly impact the outcome of the project. As mentioned previously, the choice that is taken regarded to building projects is highly influenced by the sustainability remark. It is important to note that the decision-making process for building projects is highly influenced by sustainability considerations. As a result, there has been an increase in the number of timber projects in recent times. However, the choices made should not only prioritize sustainability but also guarantee the safety and stability of the building. It is well-known that tall timber buildings are more susceptible to wind forces due to the light weight of the timber, resulting in a swaying motion for the building. This study and the analyses conducted on the numerical model demonstrate that tall timber buildings with a diagrid system are a sustainable and practical choice for lateral load resistance.

Table 6.1 shows the summary of the findings in percentage. The plus and minus symbols indicate whether the value exceeds (+) or falls below (-), the previously discussed limit. The

table also includes the mass of the system. This table will help to understand that the different systems respond under limits represented in Eurocodes and ISO10137.

Table 6.1 Summary of the Result

	Frame system	Shear wall system	Diagrid system
Mass [kg/m]	450 745,59	503 610,37	291 112,76
Natural frequency	+ 16,4%	+ 19,5%	+ 97,2%
Displacement	-72,9%	-80,1%	-87,7%
Story drift	-68,2%	-74,7%	-82,5%
Peak acceleration	-5,3%	-17%	-22%

Based on its performance, the diagrid system occurs as the most superior among the different models. This is due to its high natural frequency, which indicates that the building has a sturdy system that responds minimally to wind forces. Additionally, the low peak acceleration indicates a minimal response to external forces acting on the building. However, all systems had reasonable natural frequencies and peak accelerations, whereas the diagrid system had a 39,1% and 37,5% higher natural frequency than the frame and shear wall systems, respectively. Moreover, its peak acceleration was 17,7% and 6,02% lower than the frame and shear wall systems, respectively. As such, the diagrid system is considered a better option than the existing frame and shear wall systems.

The deflection of each system is a global concern and is affected by the stiffness of the structure. A stiffer system will have lower deflection or displacement. For instance, a 54-meter-tall building using the diagrid system showed a deflection of only 13,24 mm, which is 2,2 times lower than the frame system and 1,62 times lower than the shear wall system, as depicted in Figure 5.11. The different models had different structural systems, which gave a mass dependent on the system and material size that was chosen. Table 6.1 illustrates that the shear wall system has the largest mass, followed by the frame and diagrid system. Compared to the other models, the diagrid system had the lowest average mass, which is 1,55 times lower mass than the frame system and 1,73 times lower mass than the shear wall system. With the lowest mass, the diagrid performed well under the analysis.

The amount of inter-story drift in a structure is influenced by its displacement. It was observed that the diagrid system on the 8th floor and above showed larger drift in the stories compared to the frame and shear wall system. This could be recognized as the tapering of the material size,

as there was a reduction of 50mm from the system's base up to the 8th floor, followed by a 100mm reduction on the 9th floor. This highlights the importance of carefully considering the choice of material and its size when constructing a building.

The diagrid system outperformed the frame and shear wall system in terms of overall performance and comfort in the building. However, there were difficulties in comparing and modeling the timber system due to undefined expressions and limited knowledge of dynamic timber properties. Numerous experimental and numerical studies have been conducted, and it is expected that a better understanding of timber building performance will be achieved in the future.

7 Conclusion

This thesis evaluates *all-timber* systems against wind loads by modeling different structural systems, such as frame, shear wall, and diagrid systems. The goal is to determine the efficiency and effectiveness of other methods in resisting wind loads, focusing on deflection, inter-story drift, and peak acceleration.

The numerical analysis made it possible to evaluate an 18-story timber building, where the behavior of the building could easily be understood. With simple adjustments, the building could be analyzed for different materials and element sizes. This made it possible to vary and even compare different structural systems in timber buildings. One disadvantage is that with wrong adjustments, a numerical analysis can lead to wrong values. However, this is an easier way to understand and learn how structures behave and are a less expensive way to improve the knowledge of structures' behavior under different loads. Therefore, it is important also to develop numerical analysis along with tests on structures.

Based on the numerical analyses, it was found that the diagrid system performed relatively better than the frame and shear wall systems. This system had a lower mass but could respond well to lateral forces, with a higher natural frequency and lower peak acceleration. As a result, it was a stiffer system. The stiffness in the system is due to a rigid connection that has been applied to the models. However, in actual construction, the connection is flexible but somehow semi-rigid. It is essential to mention that using a diagrid system in timber building construction is a relatively new field of study. The use of diagonal columns has yet to be fully understood, and the connection system for diagonal timber columns is critical, significantly when the load exceeds a certain limit that may lead to buckling for members in compression.

In the analysis of horizontal displacement, the contributions of connections and shear deformation were not considered. The findings were based on peak acceleration with a mean wind velocity for a one-year return period and were not evaluated for other return periods. The limitations were determined using Eurocode and ISO 10137, specifically the Norwegian annex. Eurocode's current formals do not explicitly predict the fundamental frequency for timber buildings. Those formulas were developed and calibrated using conventional steel and reinforced concrete structural systems. It may be necessary that ongoing studies address the need to improve the formulas In Eurocode for adaptation to timber buildings.

After adjusting and modeling, all the models were evaluated based on the ISO 10137 comfort level. Analysis showed that the diagrid system outperformed the frame and shear wall systems, as it had a lower mass yet could respond well to lateral forces with a higher natural frequency and lower peak acceleration. The diagrid system had the lowest average mass among all the models and was 1,55 times lighter than the frame system and 1,73 times lighter than the shear wall system. Despite its low mass, the diagrid system performed impressively during the analysis.

After analyzing the natural frequencies and peak accelerations of all systems, it was observed that the diagrid system had significantly higher natural frequencies than the frame and shear wall systems, with a 39,1% and 37,5% difference, respectively. Additionally, the peak acceleration of the diagrid system was lower by 17,7% and 6,02% compared to the frame and shear wall systems, respectively. Based on these findings, the diagrid system is superior to the current frame and shear wall systems.

One major factor to consider is the deflection of each system, which is influenced by the stiffness of the structure. The diagrid system showed a deflection of only 13,24 mm, which is 2,2 times lower than the frame system and 1,62 times lower than the shear wall system.

Based on the studies, it is feasible to use timber in the construction of tall buildings to meet modern-day housing challenges. This is because the timber is light and susceptible to amplification of responses under dynamic loads. Systems such as diagrid may reduce motion responses, such as peak acceleration and lateral drift.

Further work:

- Analyzing the timber systems under seismic load/scenarios
- The connection between diagrids
- Analyze the contribution of connections and shear deformations

8 Reference

Abed, J., Rayburg, S., Rodwell, J. & Neave, M. (2022). *A Review of the Performance and Benefits of Mass Timber as an Alternative to Concrete and Steel for Improving the Sustainability of Structures*.

Abergel, T., Dulac, J., Hamilton, I., Jordan, M., Pradeep, A., Dean, B., Delmastro, C., Motherway, B., Slade, M., Nass, N., et al. (2019). *2019 Global Status Report for Buildings and Construction Towards a zero-emissions, efficient and resilient buildings and construction sector*.

Abrahamsen, R. (2017). *Mjøstårnet - Construction of an 81 m tall timber building*.

Abrahamsen, R., Bjertnæs, M. A., Bouillot, J., Brank, B., Cabaton, L., Crocetti, R., Flamand, O., Garains, F., Gavric, I., Germain, O., et al. (2020). *DYNAMIC RESPONSE OF TALL TIMBER BUILDINGS UNDER SERVICE LOAD – THE DYNATTB RESEARCH PROGRAM*.

Abrahamsen, R. B. & Malo, K. A. (2014). *STRUCTURAL DESIGN AND ASSEMBLY OF "TREET" - A 14-STOREY TIMBER RESIDENTIAL BUILDING IN NORWAY*

Ali, M. M. (2007). Structural Developments in Tall Buildings: Current Trends and Future Prospects.

Ali, M. M. & Al-Kodmany, K. (2022). *Structural Systems for Tall Buildings*

Aloisio, A., Pasca, D., Tomasi, R. & Fragiacomo, M. (2020). *Dynamic identification and model updating of an eight-storey CLT building*.

Angelucci, G., Mollaioli, F., Molle, M. & Paris, S. (2022). *Performance assessment of Timber High-rise Buildings: Structural and Technological Considerations*

archello. (2018). 25 King.

architectureanddesign. (2022). *Ascent soars to new heights as world's tallest timber building*. Tilgjengelig fra: https://www.architectureanddesign.com.au/news/ascent-soars-to-new-heights

Architizer, I. (2023). *25 King*. Tilgjengelig fra: https://architizer.com/projects/25-king/.

Arum, C. & Akinkunmi, A. (2011). *Comparison of Wind-Induced Displacement Characteristics of Buildings with Different Lateral Load Resisting System*.

Bezabeh, M. A., Bitsuamlak, G. T., Popovski, M. & Tesfamariam, S. (2018a). *Probabilistic serviceability-performance assessment of tall mass-timber buildings subjected to stochastic wind loads: Part I - structural design and wind tunnel testing*.

Bezabeh, M. A., Bitsuamlak, G. T., Popovski, M. & Tesfamariam, S. (2018b). *Probabilistic serviceability-performance assessment of tall mass-timber buildings subjected to stochastic wind loads. II: Structural reliability analysis*.

Bezabeh, M. A., Gairola, A., Bitsuamlak, G. T., Popovski, M. & Tesfamariam, S. (2018c). Structural performance of multi-story masstimber buildings under tornado-like wind field.

Bezabeh, M. A., Bitsuamlak, G. T., Popovski, M. & Tesfamariam, S. (2020). *Dynamic Response of Tall Mass-Timber Buildings to Wind Excitation*.

Carrero, T., Montaño, J., Perez, L., Doudak, G., María, H. S. & Guindos, P. (2022). *New Glulam-Framed Shear Wall Concept with Enhanced Behaviour Characteristics for Tall Timber Buildings in Seismic Areas.*

Chan, S. T. L. (2018). *ON THE WAY TO TRUE TIMBER BUILDING How to minimize the use of concrete and steel in timber high-rise buildings?*

Computers & structures, I. (2013). *CSI Analysis Reference Manual For SAP2000, ETABS, SAFE and CsiBridge*.

Crocetti, R. (2015). *Limtreboka*: Norske Limtreprodusenters Forening.

Davenport, A. G. (1967). *The Dependence of wind loads on meterological parameters*.
Dhiman, B. (2020). *Sustainability and Applications of a Timber as Structural Material: A Review*.
Dominik, L. (2023). *Live load – all you need to know*. Tilgjengelig fra: https://www.structuralbasics.com/live-load/.
Edskär, I. (2018). *Wind-Induced Vibrations in Timber Buildings-Parameter Study of Cross-Laminated Timber Residential Structures*.
Edvardsen, K. I. & Ramstad, T. Ø. (2014). *Trehus*.
Feldmann, A., Huang, H., Chang, W.-S. & Harris, R. (2016). Dynamic properties of tall Timber Structures under wind-induced Vibration.
Foster, R. M., Reynolds, T. P. S. & Ramage, M. H. (2016). *Proposal for defining a tall, timber building*.
Fragiacomo, M., Dujic, B. & Sustersic, I. (2011). *Elastic and ductile design of multi-storey crosslam massive wooden buildings under seismic actions*.
Gonchar, J. (2022). *Mass Timber on the Rise*.
Howarth, H. (2015). *Human exposure to wind-induced motion in tall buildings: and assessment of guidance in ISO 6897 and ISO 10137*.
Huebner, K. H., Dewhirst, D. L., Smith, D. E. & Byrom, T. G. (2001). *THE FINITE ELEMENT METHOD FOR ENGINEERS*.
Johansson, M., Linderholt, A., Jarnerö, K. & Landel, P. (2016). *TALL TIMBER BUILDINGS – A PRELIMINARY STUDY OF WIND-INDUCED VIBRATIONS OF A 22-STOREY BUILDING*.
Larsen, P. K. (2008). *Konstruksjonsteknikk - laster og bæresystemer*.
Leskovar, V. Z. & Permrov, M. (2021). *A Review of Architectural and Structural Design Typologies of Multi-Storey Timber Buildings in Europe*.
Lin, S. & Huang, Z. (2016). *Comparative Design of Structures*.
Malo, K. A. & Stamatopoulos, H. (2016). *Connections with threaded rods in moment resisting frames*.
Mendis, P., Ngo, T., Haritos, N., Hira, A., Samali, B. & Cheung, J. (2007). *Wind Loading on Tall Buildings*.
Orta, B., Martínez-Gaya, J. E., Cervera, J. & Aira, J. R. (2020). *Timber high rise, state of the art*.
Porteous, J. & Kermani, A. (2013). *Structural timber design to Eurocode 5*: John Wiley & Sons.
Reddy, P. S. V. B. & M.Eadukondalu. (2018). *Study of Lateral Structural Systems in Tall Buildings*
Safarik, D., Elbrecht, J. & Miranda, W. (2022). *State of Tall Timber 2022*.
Sizirici, B., Fseha, Y., Cho, C.-S., Yildiz, I. & Byon, Y.-J. (2021). *A Review of Carbon Footprint Reduction in Construction Industry, from Design to Operation*.
Skullestad, J. L., Bohne, R. A. & Lohne, J. (2016). *High-Rise Timber Buildings as a Climate Change Mitigation Measure - A Comparative LCA of Structural System Alternatives*.
Smith, I. & Frangi, A. (2018). Tall Timber Buildings: Introduction. I.
Standardization, E. C. F. (2002). *Eurocode — Basis of structural design*.
Standardization, E. C. F. (2007). *Bases for design of structures - Serviceability of buildings and walkways against vibrations*.
Standardization, E. C. F. (2009). *Eurocode 1: Actions on structures - Part 1-4: General actions - Wind actions*.
State of tall buildings. (2022). I: Habitat, T. C. o. T. B. a. U. (red.). Tilgjengelig fra: https://www.ctbuh.org/mass-timber-data.

Ussher, E., Gurholt, C.-U. D., Mikalsen, J. N., Aloisio, A. & Tomasi, R. (2022). *Effect of construction features on the dynamic performance of mid-rise CLT platform-type buildings*

Vilguts, A., Stamatopoulos, H. & Malo, K. A. (2020). *Parametric analyses and feasibility study of moment-resisting timber frames under service load*.

Wood Innovation and Design Centre.

Žemaitis, P., Linkevičius, E., Aleinikovas, M. & Tuomasjukka, D. (2021). *Sustainability impact assessment of glue laminated timber and concrete-based building materials production chains – A Lithuanian case study*.

Zhang, X., Xuan, L., Huang, W., Yuan, L. & Li, P. (2022). *Structural Design and Analysis for a Timber-Concrete Hybrid Building*.

Zhao, X., Zhang, B., Kilpatrick, T. & Sanderson, I. (2021a). *Numerical Analysis on Global Serviceability Behaviours of Tall CLT Buildings to the Eurocodes and UK National Annexes*.

Zhao, X., Zhang, B., Kilpatrick, T., Sanderson, I. & Liu, D. (2021b). *Numerical Analysis on Global Serviceability Behaviours of Tall Glulam Frame Buildings to the Eurocodes and UK National Annexes*.

Zheng, W., Lu, W., Liu, W. & Li, Y. (2019). *Lateral loading behavior of glulam frame-midply hybrid lateral systems*.

Appendix

Appendix A – Mass timber buildings

The table below provides the different timber buildings all over the world. The table provides the buildings name, where its located, the height of the building in meters, the floor/story count, what type of structural system is used, the functionality of the building, if the building is under construction or completed, and which year the building was completed. Chapter 2 is based on this table, where figures 2.2, 2.4, and 2.5 represent different cases. This table is entirely found from CTBUH.

Table A.1 Mass timber buildings

Rank	Building Name	City	Country	Region	Height (m)	Floor Count	Structural System	Function	Status (as of Feb 2022)	Completion Year
1	Ascent	Milwaukee	United States	North America	86,6	25	Concrete-Timber Hybrid	Residential	Completed	2022
2	Mjøstårnet	Brumunddal	Norway	Europe	85,4	18	All-Timber	Mixed-Use	Completed	2019
3	HoHo Wien	Vienna	Austria	Europe	84,0	24	Concrete-Timber Hybrid	Mixed-Use	Completed	2020
4	HAUT	Amsterdam	Netherlands	Europe	73,0	22	Concrete-Timber Hybrid	Residential	Completed	2022
5	Sara Kulturhus	Skellefteå	Sweden	Europe	72,8	20	Steel-Timber Hybrid	Mixed-Use	Completed	2021
6	De Karel Doorman	Rotterdam	Netherlands	Europe	70,5	22	Concrete-Steel-Timber Hybrid	Mixed-Use	Completed	2012
7	55 Southbank	Melbourne	Australia	Australia	69,7	19	Concrete-Steel-Timber Hybrid	Mixed-Use	Completed	2020
8	Roots Tower	Hamburg	Germany	Europe	65,0	19	Concrete-Timber Hybrid	Residential	Under Construction	2023
10	Baufeld 1 Suurstoffi Campus	Risch-Rotkreuz	Switzerland	Europe	60,0	15	Concrete-Timber Hybrid	Mixed-Use	Completed	2019
10	Kaj16 (Kromet)	Gothenburg	Sweden	Europe	60,0*	15	Concrete-Timber Hybrid	Mixed-Use	Proposed	2025
12	Brock Commons Tallwood House	Vancouver	Canada	North America	57,9	18	Concrete-Timber Hybrid	Residential	Completed	2017
13	Eunoia Junior College	Singapore	Singapore	South-east Asia	56,0	12	Concrete-Timber Hybrid	Institutional	Completed	2019
14	Rundeskogen Hus B	Sandnes	Norway	Europe	55,0*	16	Concrete-Timber Hybrid	Residential	Completed	2013
14	Hyperion	Bordeaux	France	Europe	55,0	16	Concrete-Timber Hybrid	Residential	Completed	2021
16	Albizzia	Lyon	France	Europe	53,0	17	Concrete-Timber Hybrid	Mixed-Use	Under Construction	2023
17	Ngytan Koriayo (Geelong Civic Precinct)	Greater Geelong	Australia	Australia	52,0*	12	Concrete-Timber Hybrid	Office	Under Construction	2022
18	503 on Tenth	Portland	United States	North America	50,0	10	All-Timber	Office	Under Construction	2023
19	Treet	Bergen	Norway	Europe	49,0	14	All-Timber	Residential	Completed	2015
20	Lighthouse Joensuu	Joensuu	Finland	Europe	48,0	14	Steel-Timber Hybrid	Residential	Completed	2019
21	25 King	Brisbane	Australia	Australia	46,8	10	Concrete-Timber Hybrid	Office	Completed	2018
22	2150 Keith Drive	Vancouver	Canada	North America	45,0	10	Concrete-Timber Hybrid	Office	Under Construction	2022
23	Palazzo Nice Meridia	Nice	France	Europe	44,0*	10	Concrete-Timber Hybrid	Office	Completed	2019
23	Hoas Tuuliniitty	Espoo	Finland	Europe	44,0*	13	All-Timber	Residential	Completed	2021
23	Cederhusen	Stockholm	Sweden	Europe	44,0*	13	Concrete-Timber Hybrid	Residential	Under Construction	2023
26	T3 Bayside	Toronto	Canada	North America	42,0	10	All-Timber	Office	Under Construction	2023
27	Tallwood 1 at District 56	Victoria	Canada	North America	41,7	12	Steel-Timber Hybrid	Residential	Under Construction	2022
28	Origine	Quebec	Canada	North America	40,9	13	Concrete-Timber Hybrid	Residential	Completed	2017
29	T3 Sterling Road Building 5A	Toronto	Canada	North America	39,8	8	All-Timber	Office	Under Construction	2023
30	INTRO Residential Tower	Cleveland	United States	North America	39,6	9	Concrete-Timber Hybrid	Residential	Completed	2022
31	77 Wade	Toronto	Canada	North America	38,2	8	Concrete-Steel-Timber Hybrid	Office	Under Construction	2022
32	Sensations	Strasbourg	France	Europe	38,0	11	Concrete-Timber Hybrid	Residential	Completed	2019
33	Rundeskogen Hus C	Sandnes	Norway	Europe	37,0*	11	Concrete-Timber Hybrid	Residential	Completed	2013
33	Monterey	Brisbane	Australia	Australia	37,0	11	Concrete-Steel-Timber Hybrid	Residential	Under Construction	2022
35	Trafalgar Place	London	United Kingdom	Europe	36,3	10	Concrete-Timber Hybrid	Residential	Completed	2015
36	Aveo Bella Vista	Sydney	Australia	Australia	36,0	11	Concrete-Timber Hybrid	Residential	Completed	2018
36	Suurstoffi 22	Risch-Rotkreuz	Switzerland	Europe	36,0	10	Concrete-Timber Hybrid	Office	Completed	2018
38	Wood and Innovation Design Centre	Prince George	Canada	North America	35,0*	8	All-Timber	Office	Completed	2014
38	Pont de Flandres Batiment 007	Paris	France	Europe	35,0*	8	Concrete-Steel-Timber Hybrid	Office	Completed	2019
38	Opalia	Saint-Ouen-sur-Seine	France	Europe	35,0*	8	Concrete-Steel-Timber Hybrid	Office	Completed	2017
38	Green Office Enjoy	Paris	France	Europe	35,0*	8	Concrete-Steel-Timber Hybrid	Office	Completed	2018
42	Rundeskogen Hus A	Sandnes	Norway	Europe	34,0*	10	Concrete-Timber Hybrid	Residential	Completed	2012
42	Hotel Jakarta	Amsterdam	Netherlands	Europe	34,0*	9	Concrete-Timber Hybrid	Hotel	Completed	2018
42	Kringsja Studentby	Oslo	Norway	Europe	34,0*	10	All-Timber	Residential	Completed	2018
42	SKAIO	Heilbronn	Germany	Europe	34,0	10	Concrete-Timber Hybrid	Residential	Completed	2019
46	Dalston Works	London	United Kingdom	Europe	33,8	10	Concrete-Timber Hybrid	Residential	Completed	2017
47	The Cube Building	London	United Kingdom	Europe	33,0	10	Concrete-Steel-Timber Hybrid	Residential	Completed	2015
48	Forte	Sydney	Australia	Australia	32,2	10	All-Timber	Residential	Completed	2012
49	Humber College Cultural Hub	Toronto	Canada	North America	33,7	8	Concrete-Timber Hybrid	Mixed-Use	Under Construction	2023
50	Cenni di Cambiamento	Milan	Italy	Europe	31,0*	9	Concrete-Timber Hybrid	Residential	Completed	2013
50	Vallen	Vaxjo	Sweden	Europe	31,0*	9	Concrete-Timber Hybrid	Residential	Completed	2015
50	Press House	London	United Kingdom	Europe	31,0*	9	Concrete-Timber Hybrid	Residential	Completed	2017
50	Botanikern	Uppsala	Sweden	Europe	31,0*	9	Concrete-Timber Hybrid	Residential	Completed	2019
50	Kajstaden	Vasteras	Sweden	Europe	31,0*	9	All-Timber	Residential	Completed	2019
55	Stadthaus	London	United Kingdom	Europe	29,0	9	Concrete-Timber Hybrid	Residential	Completed	2009
56	Carbon12	Portland	United States	North America	29,0	8	Steel-Timber Hybrid	Residential	Completed	2018
57	EDGE Suedkreuz	Berlin	Germany	Europe	28,7	8	Concrete-Timber Hybrid	Office	Completed	2022
58	Moholt 50/50	Trondheim	Norway	Europe	28,0	9	Concrete-Timber Hybrid	Residential	Completed	2016
59	Portvakten Söder	Vaxjo	Sweden	Europe	27,0*	8	Concrete-Timber Hybrid	Residential	Completed	2009
59	LCT One	Dornbirn	Austria	Europe	27,0	8	Concrete-Timber Hybrid	Office	Completed	2012
59	Pentagon I	As	Norway	Europe	27,0*	8	All-Timber	Residential	Completed	2013
59	Residences J.Ferry	Saint-Dié-des-Vosges	France	Europe	27,0*	8	All-Timber	Residential	Completed	2014
59	St. Dié-des-Vosges	Saint-Dié-des-Vosges	France	Europe	27,0*	8	All-Timber	Residential	Completed	2014
59	Contralaminada	Lleida	Spain	Europe	27,0*	8	All-Timber	Residential	Completed	2014
59	Limnologen	Vaxjo	Sweden	Europe	27,0*	8	Steel-Timber Hybrid	Residential	Completed	2014
59	The Gardens Macarthur	Sydney	Australia	Australia	27,0*	8	Concrete-Timber Hybrid	Residential	Completed	2018
59	Strandparken	Stockholm	Sweden	Europe	27,0*	8	Steel-Timber Hybrid	Residential	Completed	2014
59	Lucien Cornil Student Residence	Marseille	France	Europe	27,0*	8	Concrete-Timber Hybrid	Residential	Completed	2017
59	Hotel Nautilus	Pesaro	Italy	Europe	27,0*	8	All-Timber	Residential	Completed	2017
59	Dramsvegen	Tromso	Norway	Europe	27,0*	8	Concrete-Timber Hybrid	Residential	Completed	2017
59	Highpoint Terrace	London	United Kingdom	Europe	27,0*	8	All-Timber	Residential	Completed	2017
59	Puukuokka Housing Block	Jyvaskyla	Finland	Europe	27,0*	8	Concrete-Timber Hybrid	Residential	Completed	2018
59	Wood City Residential Buildings	Helsinki	Finland	Europe	27,0*	8	Concrete-Timber Hybrid	Residential	Completed	2018
59	Maskinparken TRE	Trondheim	Norway	Europe	27,0*	8	All-Timber	Residential	Completed	2018
59	Docenten	Vaxjo	Sweden	Europe	27,0*	8	Concrete-Timber Hybrid	Residential	Completed	2018

59	Frostaliden	Skövde	Sweden	Europe	27,0*	8	Concrete-Timber Hybrid	Residential	Completed	2018
59	Arbora Condominium	Montreal	Canada	North America	27,0*	8	All-Timber	Residential	Completed	2019
59	DAS Kelo	Rovaniemi	Finland	Europe	27,0*	8	Concrete-Timber Hybrid	Residential	Completed	2019
59	Jo & Joe	Gentilly	France	Europe	27,0*	8	Concrete-Timber Hybrid	Residential	Completed	2019
59	Trummens Strand	Vaxjo	Sweden	Europe	27,0*	8	Concrete-Timber Hybrid	Residential	Completed	2019
81	Emmons on 3rd	Seattle	United States	North America	26,3	8	Concrete-Timber Hybrid	Residential	Completed	2014
82	Bridport House	London	United Kingdom	Europe	25,6	8	All-Timber	Residential	Completed	2010
83	Holz8	Bad Aibling	Germany	Europe	31,0	8	Concrete-Timber Hybrid	Mixed-Use	Completed	2011
84	Pentagon II	As	Norway	Europe	24,0	8	All-Timber	Residential	Completed	2013
	River Beech Tower	Chicago	United States	North America	228,0	80	All-Timber	Residential	Proposed	2016
	Abebe Court Tower	Lagos	Nigeria	West Africa	87,0	26	Concrete-Timber Hybrid	Residential	Proposed	2017
	AMATA Building	São Paulo	Brazil	South America	44,0	13	All-Timber	Mixed-Use	Proposed	2022
	Ramada by Wyndham Kelowna hotel tower	Kelowna	Canada	North America	38,4	12	All-Timber	Hotel	Proposed	2022
	St Leonards Commons building B	Sydney	Australia	Australia	ND	ND	All-Timber	Office	Proposed	2023
	St Leonards Commons building C	Sydney	Australia	Australia	ND	ND	All-Timber	Office	Proposed	2023
	36-52 Wellington (T3 Melbourne)	Melbourne	Australia	Australia	63,0	15	Concrete-Timber Hybrid	Office	Under Construction	2023
	Baobab	Paris	France	Europe	120,0	35	All-Timber	Mixed-Use	Proposed	2015
	Oakwood tower 1 "The barbarican"	London	United Kingdom	Europe	300,0	80	All-Timber	Residential	Proposed	2016
	T3 Mount Pleasant	Vancouver	Canada	North America	ND	ND	All-Timber	Office	Proposed	2024
	SAWA	Rotterdam	Netherlands	Europe	50,0	16	All-Timber	Residential	Proposed	2022
	Baker's place	Madison (WI)	United States	North America	47,4	14	Steel-Timber Hybrid	Residential	Proposed	2024
	Wood'up tower	Paris	France	Europe	50,0	17	All-Timber	Residential	Proposed	2024
	W350 Tower	Tokyo	Japan	Northeast Asia	350,0	70	All-Timber	Mixed-Use	Proposed	2041
	Leadlight hotel	Perth	Australia	Australia	40,0	10	All-Timber	Hotel	Proposed	Not dated
	EuroNantes	Nantes	France	Europe	58,0	18	All-Timber	Residential	Proposed	Not dated
	Forêt Blanche	Saint-Malo	France	Europe	54,0	14	All-Timber	Mixed-Use	Proposed	Not dated
	Dock mill	Dublin	Ireland	Europe	50,0	13	All-Timber	Mixed-Use	Proposed	Not dated
	Nordic light	Oslo	Norway	Europe	ND	ND	All-Timber	Mixed-Use	Proposed	Not dated
	Rainbow tree	Cebu	Philippines	South-east Asia	115,0	32	All-Timber	Residential	Proposed	Not dated

Appendix B – Snow and wind load

Snow load

The reference building is located in Ås. Therefore, the chosen values have been based on adaptation for Ås.

Snølast:

Tabell N.A. 4.1 gir

Sk,0	3,5 [kN/m^2]	
H	95 [m]	Høyde over havet
Hg	150 [m]	Høydegrensen
H < Hg --> Sk,0 = Sk = 3,5 [kN/m^2]		Ettersom H er mindre enn Hg settes Sk,0 settes lik sk
i) S = u_i * Ce * Ct * Sk		Lasttilfelle 1 : jevnet fordelt last
ui	0,8	Formfaktor avheging av takform. Vi har valgt takvinkel
ce	1	Ekponeringsfaktor EC 1 del 1-3 tabell 5.1
ct	1	Termiskfaktor (EC 1 del 1-3 §5.2 (8)
sk	3,5 [kN/m^2]	Karakteristisk snølast
S=	**2.8 [kN/m^2**	

Wind load

For vindretning = 0

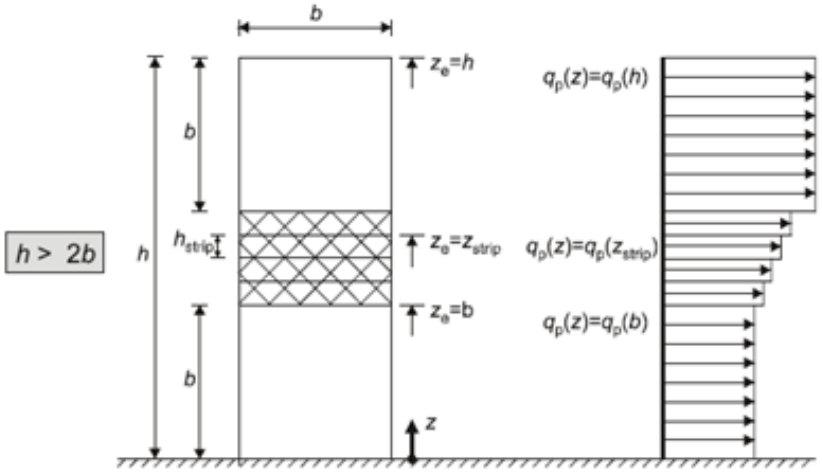

MERKNAD Hastighetstrykket bør forutsettes å være uendret over hver horisontale stripe som vurderes.

Figur 7.4 – Referansehøyde z_e, avhengig av *h* og *b*, og tilhørende hastighetstrykkprofil

h	54 m
b1	22,8 m
2b1	45,6 m
d1	14,7 m
vb	17,0940524 m/s

zmin < z < zmax

høyden på bygget z	54 m
zmin	2 m
z0	0,05 m
zmax	200 m
z0,2	0,05 m
ze = h	54 m
ze = b1	22,8 m

---

1) Peak velocity pressure

$$q_p(z) = [1 + 7 \cdot I_v(z)] \cdot \tfrac{1}{2} \cdot \rho \cdot v_m^2(z) = c_e(z) \cdot q_b \qquad (4.8)$$

qp(ze)	Iv(ze)	vm(ze)	ρ	qp(z)
qp(b1)	0,16333216	19,8850605	1,25	**529,690166**
qp(h)	0,14316974	22,6854503	1,25	**643,990878**

1.1) Mean wind velocity vm(z)

$$v_m(z) = c_r(z) \cdot c_o(z) \cdot v_b \qquad (4.3)$$

$$c_r(z) = k_r \cdot \ln\left(\frac{z}{z_0}\right) \quad \text{for} \quad z_{min} \le z \le z_{max}$$
$$c_r(z) = c_r(z_{min}) \quad \text{for} \quad z \le z_{min} \qquad (4.4)$$

cr(ze)	ze	cr(z) =
cr(b1)	22,8	1,16327363
cr(h)	54	1,3270961

vm(ze)	cr(ze)	co(z)	vm(z)
vm(b1)	1,16327363	1	19,8850605
vm(h)	1,3270961	1	22,6854503

1.2) The turbulence intensity

$$I_v(z) = \frac{\sigma_v}{v_m(z)} = \frac{k_I}{c_o(z)\cdot \ln(z/z_0)} \quad \text{for} \quad z_{min} \le z \le z_{max} \qquad (4.7)$$
$$I_v(z) = I_v(z_{min}) \quad \text{for} \quad z < z_{min}$$

$$\sigma_v = k_r \cdot v_b \cdot k_I \qquad (4.6)$$

Iv(ze)	σV	vm(z)	Iv(z)
Iv(b1)	3,24786996	19,8850605	0,16333216
Iv(h)	3,24786996	22,6854503	0,14316974

1.3) Vindlast på veggen

(figur 7.5, NS-EN 1991-1-4)

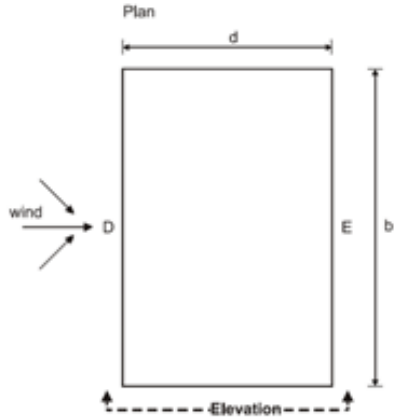

Elevation for e ≥ d

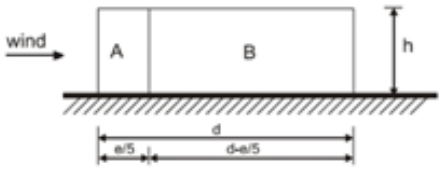

e=b or 2h,
whichever is smaller

b: crosswind dimension

e1	= b1	22,8 m
h		54 m
d1		14,7 m

Sone A1	= e1/5	4,56 m
Sone B1	=d1-(e1/5)	13,788 m
Sone D1	= b1	22,8 m
Sone E1	= b1	22,8 m

Interpolation Formula

$$y = \frac{(y_2 - y_1)}{(x_2 - x_1)} \times (x - x_1) + y_1$$

Sone	A		B		C		D		E	
h/d	$c_{pe,10}$	$c_{pe,1}$	$c_{pe,10}$	$c_{pe,1}$	$c_{pe,10}$	$c_{pe,1}$	$c_{pe,10}$	$c_{pe,1}$	$c_{pe,10}$	$c_{pe,1}$
5	-1,2	-1,4	-0,8	-1,1	-0,5		+0,8	+1,0	-0,7	
1	-1,2	-1,4	-0,8	-1,1	-0,5		+0,8	+1,0	-0,5	
≤ 0,25	-1,2	-1,4	-0,8	-1,1	-0,5		+0,7	+1,0	-0,3	

Tabell 7.1

Sone	A1	B1

h/d1	Cpe,10	Cpe,1	Cpe,10	Cpe,1
3,67346939	-1,2	-1,4	-0,8	-1,1

Sone	D1		E1	
h/d1	Cpe,10	Cpe,1	Cpe,10	Cpe,1
3,67346939	0,8	1	-0,6336735	-0,6336735

A

we(ze)	qp(ze)	Cpe,10	we(z)	
we(b1)	529,690166	-1,2	**-635,6282**	N/m^2
we(h)	643,990878	-1,2	**-772,78905**	N/m^2

B

we(ze)	qp(ze)	Cpe,10	we(z)	
we(b1)	529,690166	-0,8	**-423,75213**	N/m^2
we(h)	643,990878	-0,8	**-515,1927**	N/m^2

D

we(ze)	qp(ze)	Cpe,10	we(z)	
we(b1)	529,690166	0,8	**423,752133**	N/m^2
we(h)	643,990878	0,8	**515,192703**	N/m^2

E

we(ze)	qp(ze)	Cpe,10	we(z)	
we(b1)	529,690166	-0,6336735	**-335,65061**	N/m^2
we(h)	643,990878	-0,6336735	**-408,07993**	N/m^2

1.4) Vindlast på tak

(figur 7.5, NS-EN 1991-1-4)

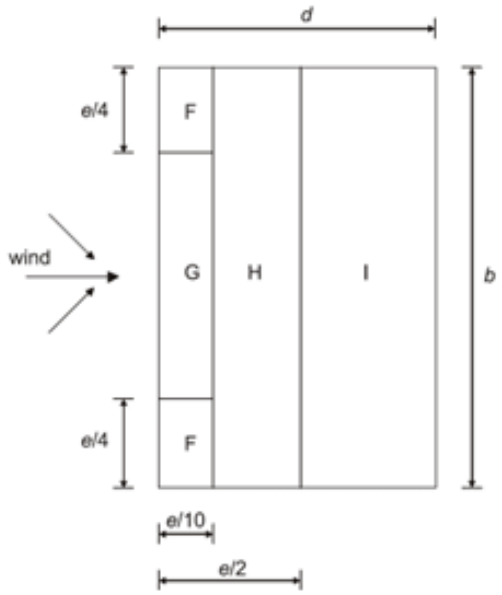

e = *b* or 2*h*
whichever is smaller

b : crosswind dimension

e1	= b1	22,8 m
h		54 m
d1	= 14,7	14,7 m

Sone F1	= e1/4	5,7 m
Sone G1	= e1/2	11,4 m
Sone H1	= b1	22,8 m
Sone I1	= b1	22,8 m

Tabell 7.2 – Utvendige formfaktorer for flate tak

Taktype	Sone							
	F		G		H		I	
	$c_{pe,10}$	$c_{pe,1}$	$c_{pe,10}$	$c_{pe,1}$	$c_{pe,10}$	$c_{pe,1}$	$c_{pe,10}$	$c_{pe,1}$
Skarp takavslutning	-1,8	-2,5	-1,2	-2,0	-0,7	-1,2	+0,2	
							-0,2	

F

we(ze)	qp(ze)	Cpe,10	we(z)	
we(b1)	529,690166	-1,8	-953,4423	
we(h)	643,990878	-1,8	**-1159,1836**	N/m^2

G

we(ze)	qp(ze)	Cpe,10	we(z)	
we(b1)	529,690166	-1,2	-635,6282	
we(h)	643,990878	-1,2	**-772,78905**	N/m^2

H

we(ze)	qp(ze)	Cpe,10	we(z)	
we(b1)	529,690166	-0,7	-370,78312	
we(h)	643,990878	-0,7	**-450,79361**	N/m^2

I

we(ze)	qp(ze)	Cpe,10	we(z)	
we(b1)	529,690166	0,2	105,938033	
we(h)	643,990878	0,2	**128,798176**	N/m^2
we(b1)	529,690166	-0,2	-105,93803	
we(h)	643,990878	-0,2	**-128,79818**	N/m^2

For vindretning = 90

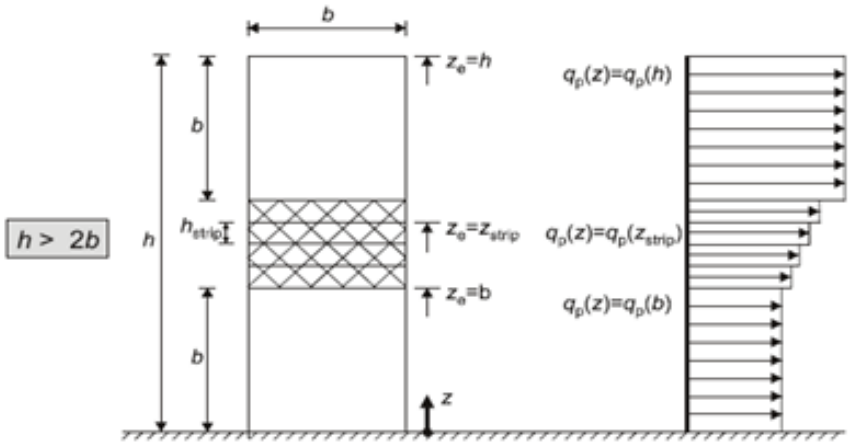

MERKNAD Hastighetstrykket bør forutsettes å være uendret over hver horisontale stripe som vurderes.

Figur 7.4 – Referansehøyde z_e, avhengig av *h* og *b*, og tilhørende hastighetstrykkprofil

h	54 m
b2	14,7 m
2 b2	29,4 m
d2	22,8 m
vb	22 m/s

zmin < z < zmax

høyden på bygget z	54 m
zmin	2 m
z0	0,05 m
zmax	200 m
z0,2	0,05 m
ze = h	54 m
ze = b2	14,7 m

---

1) Peak velocity pressure

$$q_p(z) = \left[1 + 7 \cdot I_v(z)\right] \cdot \tfrac{1}{2} \cdot \rho \cdot v_m^2(z) = c_e(z) \cdot q_b \qquad (4.8)$$

qp(ze)	Iv(ze)	vm(ze)	ρ	**qp(z)**
qp(b2)	0,17594545	23,7573634	1,25	**787,220482**
qp(h)	0,14316974	29,1961142	1,25	**1066,68212**

1.1) Mean wind velocity vm(z)

$$v_m(z) = c_r(z) \cdot c_o(z) \cdot v_b \qquad (4.3)$$

$$c_r(z) = k_r \cdot \ln\left(\frac{z}{z_0}\right) \quad \text{for} \quad z_{min} \le z \le z_{max}$$
$$c_r(z) = c_r(z_{min}) \quad \text{for} \quad z \le z_{min} \qquad (4.4)$$

cr(ze)	ze	cr(z) =
cr(b2)	14,7	1,07988016
cr(h)	54	1,3270961

vm(ze)	cr(ze)	co(z)	vm(z)
vm(b2)	1,07988016	1	23,7573634
vm(h)	1,3270961	1	29,1961142

1.2) The turbulence intensity

$$I_v(z) = \frac{\sigma_v}{v_m(z)} = \frac{k_I}{c_o(z)\cdot \ln(z/z_0)} \quad \text{for} \quad z_{min} \le z \le z_{max} \qquad (4.7)$$

$$I_v(z) = I_v(z_{min}) \quad \text{for} \quad z < z_{min}$$

$$\sigma_v = k_r \cdot v_b \cdot k_I \qquad (4.6)$$

Iv(ze)	σV	vm(z)	Iv(z)
Iv(b2)	4,18	23,7573634	0,17594545
Iv(h)	4,18	29,1961142	0,14316974

1.3) Vindlast på veggen

(figur 7.5, NS-EN 1991-1-4)

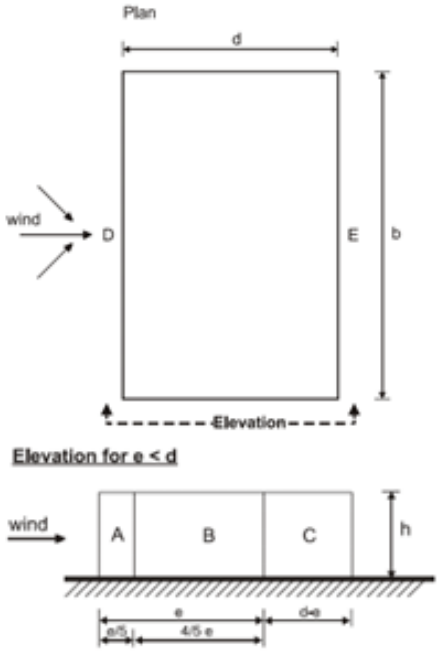

e=b or 2h,
whichever is smaller

b: crosswind dimension

e2	= b2	14,7 m
h		54 m
d2		22,8 m

Sone A2	= e2/5	2,94 m
Sone B2	=(4/5)e2	11,76 m
Sone C2	= d-e	8,1 m
Sone D2	= b2	14,7 m
Sone E2	= b2	14,7 m

Interpolation Formula

$$y = \frac{(y_2 - y_1)}{(x_2 - x_1)} \times (x - x_1) + y_1$$

Sone	A		B		C		D		E	
h/d	$c_{pe,10}$	$c_{pe,1}$	$c_{pe,10}$	$c_{pe,1}$	$c_{pe,10}$	$c_{pe,1}$	$c_{pe,10}$	$c_{pe,1}$	$c_{pe,10}$	$c_{pe,1}$
5	-1,2	-1,4	-0,8	-1,1	-0,5		+0,8	+1,0	-0,7	
1	-1,2	-1,4	-0,8	-1,1	-0,5		+0,8	+1,0	-0,5	
≤ 0,25	-1,2	-1,4	-0,8	-1,1	-0,5		+0,7	+1,0	-0,3	

Tabell 7.1

Sone	A2	B2	C2

h/d1	Cpe,10	Cpe,1	Cpe,10	Cpe,1	Cpe,10	Cpe,1
2,36842105	-1,2	-1,4	-0,8	-1,1	-0,5	-0,5

Sone	D2		E2	
h/d1	Cpe,10	Cpe,1	Cpe,10	Cpe,1
2,36842105	0,8	1	-0,5684211	-0,5684211

A

we(ze)	qp(ze)	Cpe,10	we(z)	
we(b2)	787,220482	-1,2	**-944,66458**	N/m^2
we(h)	1066,68212	-1,2	**-1280,0185**	N/m^2

B

we(ze)	qp(ze)	Cpe,10	we(z)	
we(b2)	787,220482	-0,8	**-629,77639**	N/m^2
we(h)	1066,68212	-0,8	**-853,34569**	N/m^2

C

we(ze)	qp(ze)	Cpe,10	we(z)	
we(b2)	787,220482	-0,5	**-393,61024**	N/m^2
we(h)	1066,68212	-0,5	**-533,34106**	N/m^2

D

we(ze)	qp(ze)	Cpe,10	we(z)	
we(b2)	787,220482	0,8	**629,776385**	N/m^2
we(h)	1066,68212	0,8	**853,345694**	N/m^2

E

we(ze)	qp(ze)	Cpe,10	we(z)	
we(b2)	787,220482	-0,5684211	**-447,47269**	N/m^2
we(h)	1066,68212	-0,5684211	**-606,32457**	N/m^2

1.4) Vindlast på tak

(figur 7.5, NS-EN 1991-1-4)

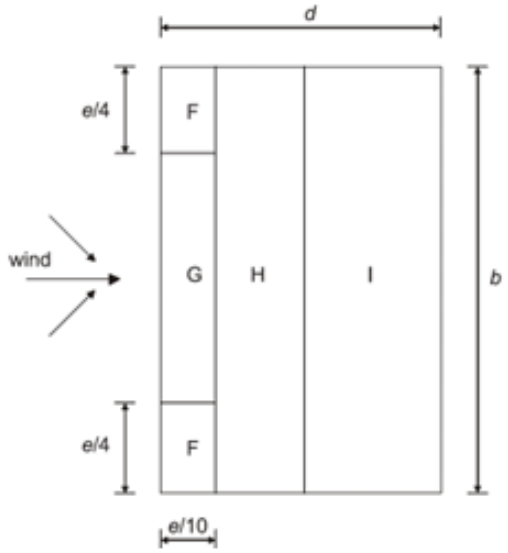

e = *b* or 2*h*
whichever is smaller

b : crosswind dimension

e2	= b2	14,7 m
h		54 m
d2		22,8 m

Sone F2	= e2/4	3,675 m
Sone G2	= e2/2	7,35 m
Sone H2	= b2	14,7 m
Sone I2	= b2	14,7 m

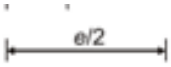

Tabell 7.2 – Utvendige formfaktorer for flate tak

Taktype	Sone							
	F		G		H		I	
	$c_{pe,10}$	$c_{pe,1}$	$c_{pe,10}$	$c_{pe,1}$	$c_{pe,10}$	$c_{pe,1}$	$c_{pe,10}$	$c_{pe,1}$
Skarp takavslutning	-1,8	-2,5	-1,2	-2,0	-0,7	-1,2	+0,2	
							-0,2	

F

we(ze)	qp(ze)	Cpe,10	we(z)
we(b2)	787,220482	-1,8	**-1416,9969**
we(h)	1066,68212	-1,8	**-1920,0278**

G

we(ze)	qp(ze)	Cpe,10	we(z)
we(b2)	787,220482	-1,2	**-944,66458**
we(h)	1066,68212	-1,2	**-1280,0185**

H

we(ze)	qp(ze)	Cpe,10	we(z)
we(b2)	787,220482	-0,7	**-551,05434**
we(h)	1066,68212	-0,7	**-746,67748**

I

we(ze)	qp(ze)	Cpe,10	we(z)
we(b2)	787,220482	0,2	**157,444096**
we(h)	1066,68212	0,2	**213,336423**
we(b2)	787,220482	-0,2	**-157,4441**
we(h)	1066,68212	-0,2	**-213,33642**

Appendix C – Verification of SAP2000 Models

To verify if the models were working the right way in SAP2000, the joint force was checked to see if it matched the base reactions at the bottom. This method was done to all the models. Only the dead load was considered. Therefore, the base reaction, under GlobalFZ, from the tables was used as the base reaction. The tables presented below are from sap2000. All the joint reactions that occur under dead load were summed and checked if the base reaction and the sum of joint reactions for dead loads were the same.

Frame

Base reaction

TABLE: Base Reactions

OutputCase	CaseType	GlobalFX	GlobalFY	GlobalFZ
Text	Text	KN	KN	KN
DEAD	LinStatic	-684	-684	12258,764
COMB1_wind 0deg	Combination	-1118,004	-684	12782,287
COMB2_wind 90deg	Combination	-684	-1355,323	12782,287

TABLE: Base Reactions

OutputCase	CaseType	GlobalMX	GlobalMY	GlobalMZ
Text	Text	KN-mm	KN-mm	KN-mm
DEAD	LinStatic	108814409	-1,6E+08	-3052464
COMB1_wind 0deg	Combination	112672768	-1,79E+08	146148,51
COMB2_wind 90deg	Combination	132294099	-1,66E+08	-10705546

TABLE: Base Reactions

OutputCase	CaseType	GlobalX	GlobalY	GlobalZ
Text	Text	mm	mm	mm
DEAD	LinStatic	0	0	0
COMB1_wind 0deg	Combination	0	0	0
COMB2_wind 90deg	Combination	0	0	0

TABLE: Base Reactions

OutputCase	CaseType	XCentroidFX	YCentroidFX	ZCentroidFX
Text	Text	mm	mm	mm
DEAD	LinStatic	13210,99	7389,03	0
COMB1_wind 0deg	Combination	12756,4	7381,65	0
COMB2_wind 90deg	Combination	13251,54	7578,06	0

TABLE: Base Reactions

OutputCase	CaseType	XCentroidFY	YCentroidFY	ZCentroidFY
Text	Text	mm	mm	mm
DEAD	LinStatic	11853,55	8003,91	0
COMB1_wind 0deg	Combination	11853,55	8020,56	0
COMB2_wind 90deg	Combination	11729,66	7698,35	0

TABLE: Base Reactions

OutputCase	CaseType	XCentroidFZ	YCentroidFZ	ZCentroidFZ
Text	Text	mm	mm	mm
DEAD	LinStatic	12940,98	8729,13	0
COMB1_wind 0deg	Combination	13795,4	8673,47	0
COMB2_wind 90deg	Combination	12872,03	10061,67	0

Joint reaction

TABLE: Joint Reactions								
Joint	OutputCase	CaseType	F1	F2	F3	M1	M2	M3
Text	Text	Text	KN	KN	KN	KN-mm	KN-mm	KN-mm
1	DEAD	LinStatic	-19,618	-8,003	60,375	10288,46	-17167,43	977,55
1	COMB1_wind 0deg	Combination	-48,042	-34,988	-41,612	10358,44	-28497,38	1241,51
1	COMB2_wind 90deg	Combination	-49,838	-31,646	-144,913	21483	-15974,37	2709,78
2	DEAD	LinStatic	-71,395	75,057	397,011	9664,24	-16629,27	367,69
2	COMB1_wind 0deg	Combination	-103,912	106,14	529,633	9620,8	-27930,24	631,63
2	COMB2_wind 90deg	Combination	-39,817	52,405	193,679	19361,63	-17243,37	1486,81
37	DEAD	LinStatic	42,598	-40,795	476,887	10346,73	-18617,84	198,75
37	COMB1_wind 0deg	Combination	14,174	-13,81	374,9	10276,75	-29947,79	-65,21
37	COMB2_wind 90deg	Combination	76,743	-68,552	712,131	21545,53	-19796,01	1934,81
74	DEAD	LinStatic	-133,838	-123,505	812,899	10056,72	-14526,52	-414,7
74	COMB1_wind 0deg	Combination	-166,354	-154,588	945,521	10100,16	-25827,49	-678,64
74	COMB2_wind 90deg	Combination	-169,344	-149,907	1044,866	19754,17	-13883,48	708,22
680	DEAD	LinStatic	-11,609	-14,68	37,492	49116,54	-33813,11	3,68
680	COMB1_wind 0deg	Combination	-19,015	-14,694	-9,65	49119,01	-56815,71	3,68
680	COMB2_wind 90deg	Combination	-10,979	-30,335	-67,633	103495,1	-31542,71	47,25
681	DEAD	LinStatic	-14,138	-14,613	110,25	48983,81	-34280,55	3,68
681	COMB1_wind 0deg	Combination	-22,907	-14,626	92,595	48986,22	-57535,36	3,68
681	COMB2_wind 90deg	Combination	-13,338	-30,055	-1,556	102201,8	-31978,89	47,25
682	DEAD	LinStatic	-14,197	-14,638	122,612	48904,1	-34291,48	3,68
682	COMB1_wind 0deg	Combination	-23,08	-14,662	123,06	48908,53	-57567,23	3,68
682	COMB2_wind 90deg	Combination	-13,386	-29,823	7,084	101289,09	-31987,77	47,25
683	DEAD	LinStatic	-14,212	-14,659	123,419	48823,73	-34294,28	3,68
683	COMB1_wind 0deg	Combination	-23,123	-14,689	129,717	48829,2	-57575,23	3,68
683	COMB2_wind 90deg	Combination	-13,387	-29,627	6,543	100383,32	-31988,01	47,25
684	DEAD	LinStatic	-14,19	-14,633	123,476	48734,59	-34290,23	3,68
684	COMB1_wind 0deg	Combination	-23,101	-14,637	134,211	48735,22	-57571,19	3,68
684	COMB2_wind 90deg	Combination	-13,354	-29,369	4,843	99465,93	-31981,88	47,25
685	DEAD	LinStatic	-14,176	-14,536	131,988	48632,31	-34287,64	3,68
685	COMB1_wind 0deg	Combination	-23,085	-14,509	147,743	48627,43	-57568,13	3,68
685	COMB2_wind 90deg	Combination	-13,334	-29,016	17,423	98531,01	-31978,22	47,25
686	DEAD	LinStatic	-14,166	-14,482	139,72	48538,03	-34285,73	3,68
686	COMB1_wind 0deg	Combination	-23,062	-14,451	161,122	48532,41	-57563,95	3,68
686	COMB2_wind 90deg	Combination	-13,316	-28,708	28,392	97604,54	-31974,84	47,25
687	DEAD	LinStatic	-14,132	-14,424	150,652	48442,98	-34279,47	3,68
687	COMB1_wind 0deg	Combination	-22,957	-14,4	184,005	48438,63	-57544,48	3,68
687	COMB2_wind 90deg	Combination	-13,287	-28,369	43,183	96672,14	-31969,47	47,25
688	DEAD	LinStatic	-12,304	-14,415	193,988	48355,66	-33941,57	3,68
688	COMB1_wind 0deg	Combination	-19,795	-14,385	278,214	48350,12	-56960,03	3,68
688	COMB2_wind 90deg	Combination	-11,585	-27,99	86,486	95718,02	-31654,83	47,25
689	DEAD	LinStatic	-11,745	-16,709	281,91	49491,49	-33968,62	3,68
689	COMB1_wind 0deg	Combination	-19,344	-16,708	234,687	49491,48	-57007,01	3,68
689	COMB2_wind 90deg	Combination	-11,47	-34,857	332,358	104331,1	-32978,88	47,25
690	DEAD	LinStatic	-15,019	-16,605	360,12	49352,02	-34573,97	3,68
690	COMB1_wind 0deg	Combination	-24,223	-16,62	334,101	49354,79	-57909,05	3,68
690	COMB2_wind 90deg	Combination	-14,761	-34,534	397,412	103029,82	-33587,29	47,25
691	DEAD	LinStatic	-15,082	-17,829	290,04	49493,93	-34585,49	3,68
691	COMB1_wind 0deg	Combination	-24,315	-18,424	260,474	49603,96	-57926,07	3,68

691	COMB2_wind 90deg	Combination	-14,946	-35,701	290,429	102375,89	-33621,48	47,25
692	DEAD	LinStatic	-14,237	-18,782	237,503	49585,9	-34429,33	3,68
692	COMB1_wind 0deg	Combination	-23,18	-19,089	217,305	49642,6	-57716,09	3,68
692	COMB2_wind 90deg	Combination	-13,733	-37,061	201,721	101757,61	-33397,22	47,25
693	DEAD	LinStatic	-14,225	-14,919	336,67	48787,38	-34427,13	3,68
693	COMB1_wind 0deg	Combination	-23,164	-14,931	344,923	48789,64	-57713,22	3,68
693	COMB2_wind 90deg	Combination	-13,789	-29,93	367,383	99569,61	-33407,59	47,25
694	DEAD	LinStatic	-14,388	-17,471	325,87	49174,96	-34457,31	3,68
694	COMB1_wind 0deg	Combination	-23,3	-17,346	361,449	49151,85	-57738,41	3,68
694	COMB2_wind 90deg	Combination	-14,208	-34,589	306,876	99561,33	-33485,14	47,25
695	DEAD	LinStatic	-14,446	-16,266	381,626	48867,96	-34467,93	3,68
695	COMB1_wind 0deg	Combination	-23,65	-15,546	440,398	48734,71	-57803	3,68
695	COMB2_wind 90deg	Combination	-13,91	-33,185	368,268	98432,24	-33430,1	47,25
696	DEAD	LinStatic	-14,794	-16,385	410,843	48805,61	-34532,28	3,68
696	COMB1_wind 0deg	Combination	-24,09	-16,36	458,839	48801,04	-57884,33	3,68
696	COMB2_wind 90deg	Combination	-14,302	-32,554	437,678	97445,86	-33502,46	47,25
697	DEAD	LinStatic	-12,774	-16,445	437,617	48730,96	-34158,86	3,68
697	COMB1_wind 0deg	Combination	-20,505	-16,428	533,731	48727,88	-57221,58	3,68
697	COMB2_wind 90deg	Combination	-12,447	-32,158	471,346	96488,56	-33159,63	47,25
698	DEAD	LinStatic	-11,771	-18,195	229,804	49766,3	-34172,72	3,68
698	COMB1_wind 0deg	Combination	-19,37	-18,195	182,581	49766,32	-57211,11	3,68
698	COMB2_wind 90deg	Combination	-12,048	-36,358	216,472	104608,6	-35142,6	47,25
699	DEAD	LinStatic	-14,918	-18,548	326,758	49711,3	-34754,49	3,68
699	COMB1_wind 0deg	Combination	-24,121	-18,533	300,739	49708,53	-58089,57	3,68
699	COMB2_wind 90deg	Combination	-15,191	-36,489	324,094	103391,13	-35723,75	47,25
700	DEAD	LinStatic	-14,749	-17,699	317,662	49469,98	-34723,35	3,68
700	COMB1_wind 0deg	Combination	-23,983	-17,104	288,096	49359,94	-58063,94	3,68
700	COMB2_wind 90deg	Combination	-14,907	-35,577	346,237	102352,98	-35671,28	47,25
701	DEAD	LinStatic	-14,583	-17,965	326,316	49434,88	-34692,67	3,68
701	COMB1_wind 0deg	Combination	-23,526	-17,658	306,117	49378,19	-57979,43	3,68
701	COMB2_wind 90deg	Combination	-15,101	-36,256	386,307	101608,9	-35707	47,25
702	DEAD	LinStatic	-14,419	-16,074	299,154	49001,02	-34662,38	3,68
702	COMB1_wind 0deg	Combination	-23,358	-16,062	307,407	48998,75	-57948,47	3,68
702	COMB2_wind 90deg	Combination	-14,856	-31,085	290,281	99783,26	-35661,77	47,25
703	DEAD	LinStatic	-14,094	-18,086	383,331	49288,67	-34602,33	3,68
703	COMB1_wind 0deg	Combination	-23,006	-18,211	418,911	49311,78	-57883,42	3,68
703	COMB2_wind 90deg	Combination	-14,263	-35,213	424,631	99676,74	-35552,21	47,25
704	DEAD	LinStatic	-14,826	-19,367	428,854	49441,08	-34737,51	3,68
704	COMB1_wind 0deg	Combination	-24,029	-20,087	487,626	49574,33	-58072,58	3,68
704	COMB2_wind 90deg	Combination	-15,342	-36,291	466,779	99006,31	-35751,68	47,25
705	DEAD	LinStatic	-15,096	-18,291	383,084	49158,02	-34787,46	3,68
705	COMB1_wind 0deg	Combination	-24,392	-18,316	431,08	49162,6	-58139,51	3,68
705	COMB2_wind 90deg	Combination	-15,572	-34,468	384,058	97799,8	-35794,22	47,25
706	DEAD	LinStatic	-12,882	-17,842	392,607	48989,21	-34378,09	3,68
706	COMB1_wind 0deg	Combination	-20,612	-17,858	488,721	48992,29	-57440,81	3,68
706	COMB2_wind 90deg	Combination	-13,203	-33,566	387,435	96748,82	-35356,26	47,25
707	DEAD	LinStatic	-11,664	-15,724	257,483	49309,55	-34283,43	3,68
707	COMB1_wind 0deg	Combination	-19,07	-15,711	210,34	49307,09	-57286,03	3,68
707	COMB2_wind 90deg	Combination	-12,292	-31,394	389,656	103690,92	-36533,1	47,25
708	DEAD	LinStatic	-14,27	-15,964	341,611	49233,44	-34765,23	3,68

708	COMB1_wind 0deg	Combination	-23,04	-15,951	323,956	49231,04	-58020,04	3,68
708	COMB2_wind 90deg	Combination	-15,07	-31,417	480,769	102453,53	-37046,63	47,25
709	DEAD	LinStatic	-14,335	-15,859	359,134	49129,75	-34777,21	3,68
709	COMB1_wind 0deg	Combination	-23,218	-15,835	359,582	49125,33	-58052,97	3,68
709	COMB2_wind 90deg	Combination	-15,151	-31,048	500,434	101515,66	-37061,65	47,25
710	DEAD	LinStatic	-14,368	-15,832	362,623	49040,54	-34783,27	3,68
710	COMB1_wind 0deg	Combination	-23,279	-15,802	368,921	49035,07	-58064,23	3,68
710	COMB2_wind 90deg	Combination	-15,196	-30,8	503,293	100600,17	-37069,99	47,25
711	DEAD	LinStatic	-14,361	-15,833	367,546	48956,36	-34782,03	3,68
711	COMB1_wind 0deg	Combination	-23,272	-15,829	378,281	48955,73	-58062,99	3,68
711	COMB2_wind 90deg	Combination	-15,196	-30,567	508,855	99687,46	-37069,96	47,25
712	DEAD	LinStatic	-14,356	-15,854	370,891	48876,07	-34781,03	3,68
712	COMB1_wind 0deg	Combination	-23,264	-15,881	386,645	48880,96	-58061,53	3,68
712	COMB2_wind 90deg	Combination	-15,193	-30,334	507,958	98774,65	-37069,4	47,25
713	DEAD	LinStatic	-14,365	-15,842	374,974	48789,47	-34782,71	3,68
713	COMB1_wind 0deg	Combination	-23,261	-15,872	396,375	48795,09	-58060,93	3,68
713	COMB2_wind 90deg	Combination	-15,21	-30,071	508,987	97856,51	-37072,63	47,25
714	DEAD	LinStatic	-14,34	-15,784	379,17	48694,53	-34778,09	3,68
714	COMB1_wind 0deg	Combination	-23,165	-15,808	412,523	48698,89	-58043,1	3,68
714	COMB2_wind 90deg	Combination	-15,184	-29,738	508,851	96925,28	-37067,8	47,25
715	DEAD	LinStatic	-12,517	-15,503	414,795	48556,87	-34441,18	3,68
715	COMB1_wind 0deg	Combination	-20,009	-15,533	499,02	48562,4	-57459,64	3,68
715	COMB2_wind 90deg	Combination	-13,238	-29,09	543,191	95921,33	-36707,93	47,25

SUM	DEAD	12258,77

When all the joint reaction under F3 was summed, the total dead load was 12 258,8 kN. The base reaction for the frame model was 12 258,76 kN. Therefore, this model is good to use for further analysis.

Shear wall
base reaction

TABLE: Base Reactions				
OutputCase	CaseType	GlobalFX	GlobalFY	GlobalFZ
Text	Text	KN	KN	KN
DEAD	**LinStatic**	**-662**	**-662**	**17238,852**
COMB1_wind 0deg	Combination	-1096,004	-662	17762,375
COMB2_wind 90deg	Combination	-662	-1333,323	17762,375

TABLE: Base Reactions				
OutputCase	CaseType	GlobalMX	GlobalMY	GlobalMZ
Text	Text	KN-mm	KN-mm	KN-mm
DEAD	LinStatic	145517679	-216390933	-2956012
COMB1_wind 0deg	Combination	149376038,2	-234969081	242600,51
COMB2_wind 90deg	Combination	168997369,3	-222284063	-10609093,8

TABLE: Base Reactions				
OutputCase	CaseType	GlobalX	GlobalY	GlobalZ
Text	Text	mm	mm	mm
DEAD	LinStatic	0	0	0
COMB1_wind 0deg	Combination	0	0	0
COMB2_wind 90deg	Combination	0	0	0

TABLE: Base Reactions				
OutputCase	CaseType	XCentroidFX	YCentroidFX	ZCentroidFX
Text	Text	mm	mm	mm
DEAD	LinStatic	19170,17	7302,35	0
COMB1_wind 0deg	Combination	16220,15	7329,14	0
COMB2_wind 90deg	Combination	19410,51	7386,88	0

TABLE: Base Reactions				
OutputCase	CaseType	XCentroidFY	YCentroidFY	ZCentroidFY
Text	Text	mm	mm	mm
DEAD	LinStatic	11747,52	11947,3	0
COMB1_wind 0deg	Combination	11747,52	12076,49	0
COMB2_wind 90deg	Combination	11614,25	9714,51	0

TABLE: Base Reactions				
OutputCase	CaseType	XCentroidFZ	YCentroidFZ	ZCentroidFZ
Text	Text	mm	mm	mm
DEAD	LinStatic	12528,33	8410,54	0
COMB1_wind 0deg	Combination	13189,25	8379,87	0
COMB2_wind 90deg	Combination	12490,85	9453,53	0

Joint reaction

TABLE: Joint Reactions								
Joint	OutputCase	CaseType	F1	F2	F3	M1	M2	M3
Text	Text	Text	KN	KN	KN	KN-mm	KN-mm	KN-mm
1	DEAD	LinStatic	55,0	69,1	379,6	19942,8	-12798,0	-720,3
1	COMB1_wind 0deg	Combination	39,4	45,9	268,6	19529,4	-21511,2	745,1
1	COMB2_wind 90deg	Combination	-8,4	33,0	103,5	41778,2	-11116,1	-2491,0
2	DEAD	LinStatic	-108,7	-4,0	331,9	11290,5	-11880,6	-2272,0
2	COMB1_wind 0deg	Combination	-136,0	-4,0	396,0	12138,7	-20182,9	-3309,6
2	COMB2_wind 90deg	Combination	-37,7	-8,5	152,3	22889,5	-11393,2	-3786,1
3	DEAD	LinStatic	37,5	-3,0	96,1	6838,8	-9710,3	-954,5
3	COMB1_wind 0deg	Combination	28,7	-3,0	74,6	6143,8	-15003,4	-1563,8
3	COMB2_wind 90deg	Combination	-44,9	-6,3	-60,3	16318,2	-10380,5	192,1
4	DEAD	LinStatic	-91,7	136,9	641,9	20053,0	-11361,7	3422,8
4	COMB1_wind 0deg	Combination	-112,2	168,0	789,4	20380,5	-17496,2	5776,5
4	COMB2_wind 90deg	Combination	-14,4	91,9	368,4	38879,3	-13288,3	4435,2
5	DEAD	LinStatic	84,3	-6,2	413,2	10941,8	-18004,4	-3908,5
5	COMB1_wind 0deg	Combination	60,9	-6,2	361,2	10237,4	-29764,6	-5142,6
5	COMB2_wind 90deg	Combination	49,1	-13,2	271,3	24416,0	-17887,9	-5196,6
6	DEAD	LinStatic	-173,3	-6,3	639,5	13727,9	-17555,2	-874,4
6	COMB1_wind 0deg	Combination	-208,3	-6,3	738,4	14448,1	-29285,3	-2108,9
6	COMB2_wind 90deg	Combination	-137,3	-13,3	494,4	26871,3	-17284,1	961,6
7	DEAD	LinStatic	181,5	-148,5	954,0	20115,7	-14483,2	-4563,3
7	COMB1_wind 0deg	Combination	166,0	-125,4	843,1	20529,1	-23196,4	-6028,7
7	COMB2_wind 90deg	Combination	255,0	-194,8	1291,4	41990,4	-16133,7	-6322,1
8	DEAD	LinStatic	-245,9	-4,6	681,7	11249,1	-11948,3	-1545,4
8	COMB1_wind 0deg	Combination	-273,2	-4,6	745,8	10400,9	-20250,6	-507,8
8	COMB2_wind 90deg	Combination	-327,1	-9,2	890,5	22810,3	-12430,5	-3012,0
9	DEAD	LinStatic	208,3	-3,5	421,3	11135,6	-7837,2	2520,5
9	COMB1_wind 0deg	Combination	199,5	-3,6	399,8	11830,7	-13130,4	3129,8
9	COMB2_wind 90deg	Combination	300,1	-6,8	596,9	20532,3	-7168,2	3593,1
10	DEAD	LinStatic	-249,8	-233,2	1211,5	17996,3	-6254,6	-3062,6
10	COMB1_wind 0deg	Combination	-270,3	-264,3	1359,0	17668,8	-12389,1	-5416,3
10	COMB2_wind 90deg	Combination	-336,6	-287,6	1533,4	36904,3	-4328,7	-2113,9
11	DEAD	LinStatic	162,8	-7,3	725,8	14071,6	-17142,2	-127,6
11	COMB1_wind 0deg	Combination	139,4	-7,3	673,8	14775,9	-28902,4	1106,5
11	COMB2_wind 90deg	Combination	208,4	-14,3	910,1	27538,3	-17245,3	-1412,4
12	DEAD	LinStatic	-248,1	-7,3	944,5	12525,5	-17018,6	2851,7
12	COMB1_wind 0deg	Combination	-283,1	-7,2	1043,5	11805,3	-28748,7	4086,2
12	COMB2_wind 90deg	Combination	-294,6	-14,3	1131,7	25657,3	-17285,3	4691,5
13	DEAD	LinStatic	-3,0	-156,8	492,6	18840,9	-8825,8	2461,8
13	COMB1_wind 0deg	Combination	-5,2	-130,6	423,0	18663,3	-14487,5	3583,9
13	COMB2_wind 90deg	Combination	-3,1	-225,2	668,3	39706,7	-10989,9	5420,4
14	DEAD	LinStatic	-2,8	41,3	204,1	19900,0	-5285,4	1997,7
14	COMB1_wind 0deg	Combination	-5,0	15,1	134,4	20077,6	-10947,1	875,5
14	COMB2_wind 90deg	Combination	-2,7	-16,9	60,4	40764,5	-3146,2	4919,8
15	DEAD	LinStatic	-3,4	-236,9	705,9	19881,1	-6763,6	-811,4
15	COMB1_wind 0deg	Combination	-5,5	-270,3	801,0	20037,8	-12740,4	768,6
15	COMB2_wind 90deg	Combination	-3,2	-292,6	844,8	39876,0	-4199,9	-4063,5
16	DEAD	LinStatic	-3,6	132,1	453,2	19841,6	-12293,1	-6645,5
16	COMB1_wind 0deg	Combination	-5,8	165,5	548,3	19684,8	-18269,9	-8225,5

16	COMB2_wind 90deg	Combination	-3,8	85,7	343,4	39836,0	-14847,1	-9888,1
690	DEAD	LinStatic	-8,8	-9,6	404,9	17240,4	-12946,2	-4,7
690	COMB1_wind 0deg	Combination	-13,4	-10,0	396,1	17428,9	-21227,1	-4,7
690	COMB2_wind 90deg	Combination	-9,7	-19,2	436,7	35781,6	-13389,7	-2,6
691	DEAD	LinStatic	-8,4	-10,3	308,1	17664,2	-12694,1	-4,7
691	COMB1_wind 0deg	Combination	-13,0	-10,7	284,6	17905,4	-20980,1	-4,7
691	COMB2_wind 90deg	Combination	-8,6	-19,4	279,7	35942,4	-12778,1	-2,6
692	DEAD	LinStatic	-7,5	-10,8	275,2	18004,0	-12210,2	-4,7
692	COMB1_wind 0deg	Combination	-11,8	-10,7	254,9	17954,2	-20345,2	-4,7
692	COMB2_wind 90deg	Combination	-7,3	-20,7	240,4	36676,2	-12092,9	-2,6
693	DEAD	LinStatic	-7,3	-8,4	346,2	16740,7	-12121,5	-4,7
693	COMB1_wind 0deg	Combination	-11,5	-8,4	354,3	16750,7	-20208,1	-4,7
693	COMB2_wind 90deg	Combination	-7,3	-15,8	334,4	34018,9	-12040,1	-2,6
694	DEAD	LinStatic	-7,6	-11,0	362,7	18265,7	-12259,0	-4,7
694	COMB1_wind 0deg	Combination	-11,9	-11,3	399,2	18401,8	-20379,3	-4,7
694	COMB2_wind 90deg	Combination	-7,7	-20,6	334,4	36681,6	-12275,3	-2,6
695	DEAD	LinStatic	-7,5	-9,5	385,7	17480,2	-12229,6	-4,7
695	COMB1_wind 0deg	Combination	-12,1	-9,0	432,2	17216,7	-20501,2	-4,7
695	COMB2_wind 90deg	Combination	-7,2	-18,6	351,8	35589,1	-12031,9	-2,6
696	DEAD	LinStatic	-6,9	-8,9	433,5	17237,0	-11913,4	-4,7
696	COMB1_wind 0deg	Combination	-11,5	-8,6	462,9	17078,8	-20185,7	-4,7
696	COMB2_wind 90deg	Combination	-5,8	-18,2	470,9	35411,5	-11244,4	-2,6
699	DEAD	LinStatic	-7,0	-10,4	367,4	17684,1	-11813,2	-4,7
699	COMB1_wind 0deg	Combination	-11,6	-10,1	358,7	17495,6	-20094,2	-4,7
699	COMB2_wind 90deg	Combination	-6,1	-20,0	357,9	36225,5	-11367,8	-2,6
700	DEAD	LinStatic	-7,8	-9,1	381,3	17007,3	-12216,4	-4,7
700	COMB1_wind 0deg	Combination	-12,4	-8,6	357,8	16766,1	-20502,4	-4,7
700	COMB2_wind 90deg	Combination	-7,5	-18,2	431,1	35283,6	-12132,8	-2,6
701	DEAD	LinStatic	-7,6	-10,1	359,9	17651,8	-12111,3	-4,7
701	COMB1_wind 0deg	Combination	-11,9	-10,2	339,5	17701,6	-20246,3	-4,7
701	COMB2_wind 90deg	Combination	-7,7	-20,0	414,8	36320,8	-12228,7	-2,6
702	DEAD	LinStatic	-7,3	-8,0	386,2	16533,0	-11954,8	-4,7
702	COMB1_wind 0deg	Combination	-11,5	-8,0	394,3	16523,0	-20041,4	-4,7
702	COMB2_wind 90deg	Combination	-7,4	-15,4	417,2	33806,4	-12033,5	-2,6
703	DEAD	LinStatic	-7,2	-9,6	433,3	17490,8	-11901,2	-4,7
703	COMB1_wind 0deg	Combination	-11,5	-9,4	469,8	17354,7	-20021,5	-4,7
703	COMB2_wind 90deg	Combination	-7,1	-19,2	480,9	35903,2	-11879,6	-2,6
704	DEAD	LinStatic	-7,9	-10,3	468,0	17924,2	-12277,0	-4,7
704	COMB1_wind 0deg	Combination	-12,4	-10,8	514,5	18187,7	-20548,6	-4,7
704	COMB2_wind 90deg	Combination	-8,1	-19,4	521,5	36031,0	-12469,0	-2,6
705	DEAD	LinStatic	-9,0	-11,3	379,2	18553,5	-12895,0	-4,7
705	COMB1_wind 0deg	Combination	-13,6	-11,6	408,6	18711,7	-21167,2	-4,7
705	COMB2_wind 90deg	Combination	-10,1	-20,6	361,8	36726,8	-13557,3	-2,6
931	DEAD	LinStatic	24,9	34,0	369,8	9033,4	-15510,7	255,6
931	COMB1_wind 0deg	Combination	2,2	14,3	299,3	9083,5	-24977,0	458,4
931	COMB2_wind 90deg	Combination	2,7	14,2	220,4	18590,7	-15066,3	756,3
932	DEAD	LinStatic	-101,9	99,0	635,1	8844,1	-13397,3	-20,7
932	COMB1_wind 0deg	Combination	-130,3	124,3	747,8	8817,3	-22746,5	182,0
932	COMB2_wind 90deg	Combination	-79,5	79,3	485,8	17857,9	-14153,2	207,3
933	DEAD	LinStatic	72,5	-77,0	689,8	8882,0	-15914,1	-481,6

933	COMB1_wind 0deg	Combination	49,8	-57,3	619,4	8832,0	-25380,5	-684,3
933	COMB2_wind 90deg	Combination	100,0	-102,1	878,6	18439,5	-16351,4	19,3
934	DEAD	LinStatic	-148,8	-142,4	955,8	9078,3	-11435,7	-762,2
934	COMB1_wind 0deg	Combination	-177,2	-167,8	1068,6	9105,1	-20784,9	-965,0
934	COMB2_wind 90deg	Combination	-176,5	-167,2	1143,6	18092,2	-10662,3	-534,0
SUM	DEAD	LinStatic			17238,9			

Diagrid

Base reaction

TABLE: Base Reactions						
OutputCase	CaseType	StepType	StepNum	GlobalFX	GlobalFY	GlobalFZ
Text	Text	Text	Unitless	KN	KN	KN
MODAL	LinModal	Mode	1	-0,003579	69,671	-0,024
MODAL	LinModal	Mode	2	-136,253	-0,003265	-0,709
MODAL	LinModal	Mode	3	-0,403	-0,549	-0,00604
MODAL	LinModal	Mode	4	0,046	377,447	-1,642
MODAL	LinModal	Mode	5	-724,637	0,072	38,636
MODAL	LinModal	Mode	6	24,888	-3,021	-242,313
MODAL	LinModal	Mode	7	2,363	68,505	-15,807
MODAL	LinModal	Mode	8	-78,433	461,543	-1138,951
MODAL	LinModal	Mode	9	-69,551	-521,853	-987,869
MODAL	LinModal	Mode	10	6,594	45,082	96,794
MODAL	LinModal	Mode	11	3,517	-84,793	24,845
MODAL	LinModal	Mode	12	-53,623	-4,029	659,138
COMB1_wind 0deg	Combination			-434,004	-2,726E-11	3688,887
COMB2_wind 90deg	Combination			-7,247E-11	-671,323	3688,887

TABLE: Base Reactions						
OutputCase	CaseType	StepType	StepNum	GlobalMX	GlobalMY	GlobalMZ
Text	Text	Text	Unitless	KN-mm	KN-mm	KN-mm
MODAL	LinModal	Mode	1	-2888494,9	120,36	790854,01
MODAL	LinModal	Mode	2	-4949,79	-5649267,1	1000595,7
MODAL	LinModal	Mode	3	-25926,42	-35359,04	3264865,9
MODAL	LinModal	Mode	4	-4639101,3	18944,7	4294489,1
MODAL	LinModal	Mode	5	283268,47	-8053894,9	5335531,3
MODAL	LinModal	Mode	6	-1708437,8	3869362,15	-207180,19
MODAL	LinModal	Mode	7	-1406488,9	282695,38	692954,65
MODAL	LinModal	Mode	8	-12498282	9369824,07	5815968,7
MODAL	LinModal	Mode	9	-2684545,2	8040194,79	-6073627,9
MODAL	LinModal	Mode	10	331570,7	-934423,18	-8700604,6
MODAL	LinModal	Mode	11	-3014896,6	-327322,51	-1216991,9
MODAL	LinModal	Mode	12	4615552,93	-5945949,7	187744,15
COMB1_wind 0deg	Combination			27187094,5	-54613668	3198612,5
COMB2_wind 90deg	Combination			46808425,6	-41928649	-7653081,9

TABLE: Base Reactions						
OutputCase	CaseType	StepType	StepNum	GlobalX	GlobalY	GlobalZ
Text	Text	Text	Unitless	mm	mm	mm
MODAL	LinModal	Mode	1	0	0	0
MODAL	LinModal	Mode	2	0	0	0
MODAL	LinModal	Mode	3	0	0	0
MODAL	LinModal	Mode	4	0	0	0
MODAL	LinModal	Mode	5	0	0	0
MODAL	LinModal	Mode	6	0	0	0
MODAL	LinModal	Mode	7	0	0	0
MODAL	LinModal	Mode	8	0	0	0
MODAL	LinModal	Mode	9	0	0	0
MODAL	LinModal	Mode	10	0	0	0
MODAL	LinModal	Mode	11	0	0	0
MODAL	LinModal	Mode	12	0	0	0
COMB1_wind 0deg	Combination			0	0	0
COMB2_wind 90deg	Combination			0	0	0

TABLE: Base Reactions						
OutputCase	CaseType	StepType	StepNum	XCentroidFX	YCentroidFX	ZCentroidFX
Text	Text	Text	Unitless	mm	mm	mm
MODAL	LinModal	Mode	1	52456626,5	-938645,99	0
MODAL	LinModal	Mode	2	11504,53	5935,25	0
MODAL	LinModal	Mode	3	8395,63	3338112,15	0
MODAL	LinModal	Mode	4	-7938359,4	331376,15	0
MODAL	LinModal	Mode	5	11534,55	6895,15	0
MODAL	LinModal	Mode	6	13452,89	6574,99	0
MODAL	LinModal	Mode	7	-4331,68	19469,23	0
MODAL	LinModal	Mode	8	12383,58	6188,34	0
MODAL	LinModal	Mode	9	4166,39	3085,12	0
MODAL	LinModal	Mode	10	4107,18	565585,45	0
MODAL	LinModal	Mode	11	2009,45	37205,71	0
MODAL	LinModal	Mode	12	14552,98	6580,56	0
COMB1_wind 0deg	Combination			13380,44	6399,33	0
COMB2_wind 90deg	Combination			0	0	0

TABLE: Base Reactions						
OutputCase	CaseType	StepType	StepNum	XCentroidFY	YCentroidFY	ZCentroidFY
Text	Text	Text	Unitless	mm	mm	mm
MODAL	LinModal	Mode	1	11399,67	5419,37	0
MODAL	LinModal	Mode	2	-58681339	-115715,08	0
MODAL	LinModal	Mode	3	-3483882,9	6489,95	0
MODAL	LinModal	Mode	4	11418,47	6522,29	0
MODAL	LinModal	Mode	5	4700772,98	-61932,66	0
MODAL	LinModal	Mode	6	14394,57	3085,74	0
MODAL	LinModal	Mode	7	10790,87	6781,3	0
MODAL	LinModal	Mode	8	11549,86	7012,08	0
MODAL	LinModal	Mode	9	12047,22	6570,9	0
MODAL	LinModal	Mode	10	-109633,34	6528,5	0
MODAL	LinModal	Mode	11	12799,7	7359,89	0
MODAL	LinModal	Mode	12	40911,25	37208,54	0
COMB1_wind 0deg	Combination			0	0	0
COMB2_wind 90deg	Combination			11471,65	6541,15	0

TABLE: Base Reactions						
OutputCase	CaseType	StepType	StepNum	XCentroidFZ	YCentroidFZ	ZCentroidFZ
Text	Text	Text	Unitless	mm	mm	mm
MODAL	LinModal	Mode	1	5178,5	118786289	0
MODAL	LinModal	Mode	2	-7912190,1	6965,16	0
MODAL	LinModal	Mode	3	-6332302,4	4131689,95	0
MODAL	LinModal	Mode	4	11530,84	2743542,07	0
MODAL	LinModal	Mode	5	203402,21	7328,88	0
MODAL	LinModal	Mode	6	15940,47	7058,16	0
MODAL	LinModal	Mode	7	17845,79	87444,38	0
MODAL	LinModal	Mode	8	8245,74	10823,64	0
MODAL	LinModal	Mode	9	8158,72	2903,88	0
MODAL	LinModal	Mode	10	9613,66	3554,28	0
MODAL	LinModal	Mode	11	13183,39	-122524,04	0
MODAL	LinModal	Mode	12	8999,63	6985,82	0
COMB1_wind 0deg	Combination			14769,65	7365,04	0
COMB2_wind 90deg	Combination			11366,16	12612,18	0

Appendix D – ULS check

Beam

1. Glulam beam geometric properties		GL20c	g =	9.81	m/s^2
Breadth of each beam	b		300	mm	
Depth of each beam	h		500	mm	
Effective span of each beam	lc1	=0,9*l	5.13	m	
	lc2	=0,9*l	4.5	m	
Bearing length of each end of a beam					
			20c8		
Section modulus of each beam about the y-y axis	Wy	= (b*h^2)/6	12500000	mm^3	
2. Glulam properties				1000	
			N/mm^2	kN/m^2	
			kg/m^3	kN/m^3	
Characteristic bending strength	fm,g,k	1000	20	20000	kN/m^2
Characteristic shear strength	fv,g,k		3.5	3500	kN/m^2
Characteristic bearing strength	fc,90,g,k		2.5	2500	kN/m^2
Mean modulus of elasticity parallel to grain	E0,g,mean		10400	10400000	kN/m^2 kN/m^2
Mean shear modulus	G0,g,mean		650	650000	kN/m^2
Mean density of each beam	ρg,k		355	3.48255	kN/m^3
	ρg,mean		390	3.8259	kN/m^3

3. Partial safety factors					
Permanent actions	γG		1.2		
Variable actions	γQ		1.5		
Factor for quasi-permanent value of variable action	ψ2		0		
Material factor for glulam at ULS	γM		1.15		

Cross Section	Section Modulus
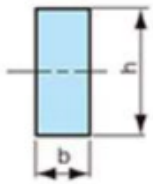	$\frac{1}{6}bh^2$

4. Actions					
Self-weight of a beam	Gk,selfwt	= b*h*g*pm	0.573885	kN	

Design action from the self-weight of a beam	Fd,selfwt	= γG * Gk,selwt	0.688662	kN	
Snow load	S		2.8	kN/m^2	
	formfactor	S*μ	2.24	kN/m^2	
	S1	5,7m	11.4912	kN/m	
	S2	5m	10.08	kN/m	
Characteristic permanent action on a beam	Gk,p		3	kN/m	
Characteristic variable short-term action on a beam	Qk,p		2	kN/m	
Design action from permanent actionm short-term action and self-weight for the critical load case at the ULS	Fd,p1,roof		18.779862	kN/m	on roof
	Fd,p2,roof		17.368662	kN/m	on roof
	Fd,p		6.6	kN/m	in building

5. Modification factors					
Factor for short-duration loading and service class 1	kmod,short		0.9		
Size factor for depth less than 600 mm	kh		1		
Lateral stability of a beam	kcrit		1		
Modification factor for the influence of cracks	kcr		0.67		
Bearing factor	kc,90		1.75		
Deformation factor for service class 1	kdef		0.6		
Load sharing factor	ksys		1		

6. Bending strength							
The design load case will be due to a combination of the self-weight of the beam plus the permanent and variable loading							
Design bending moment			Md1,roof	(Fd,p1,roof*(1	61.7784688	kNm	roof
			Md2,roof	(Fd,p2,roof*(1	47.5365257	kNm	roof
Design bending stress			σm,y,d1,roof		4942.2775	kN/m^2	roof
			σm,y,d2,roof		3802.92206	kN/m^2	roof
Design bending strength			fm,yd,roof		15652.1739	kN/m^2	roof
Design bending strength taking lateral torsional buckling effect into account			fmr,y,d,roof		15652.1739		roof
			Md1		21.7114425	kNm	innside
			Md2		16.70625	kNm	innside
			σm,y,d1		1736.9154	kN/m^2	innside
			σm,y,d2		1336.5	kN/m^2	innside
			fm,yd		15652.1739	kN/m^2	innside
			fmr,y,d		15652.1739		
σm,y,d1,roof							
fm,yd,roof	Check	0.3157566	OK				
σm,y,d2,roof							
fm,yd,roof	Check	0.2429645	OK				
σm,y,d1							
fm,yd	Check	0.1109696	OK				
σm,y,d2							
fm,yd	Check	0.0853875	OK				

7. Shear strength							
The design load case will be due to a combination of self-weight of the beam plus the							
permanent and variable loading:							
Design value of the end shear force			Vd1,roof	(Fd,p1*l)/2	48.170346	kN	roof
			Vd2,roof	(Fd,p2*l)/2	39.0794895	kN	roof
			Vd1		16.929	kN	innside
			Vd2		14.85	kN	innside
Effective shear width of the beam			bef	kcr*b	201	mm	
Design shear stress			tv,d1,roof	(3/2)*(Vd/(bef*h))	718.960389	kN/m^2	
			tv,d2,roof	(3/2)*(Vd/(bef*h))	583.275963	kN/m^2	
			tv,d1		252.671642	kN/m^2	
			tv,d2		221.641791	kN/m^2	
Design shear strength			fv,d	(kmod,short*ksys*fv,g,k)/ym	2739.13043	kN/m^2	
tv,d1,roof							
fv,d	Check	0.2624776	OK				
tv,d2,roof							
fv,d	Check	0.212942	OK				
tv,d1							
fv,d	Check	0.0922452	OK				
tv,d2							
fv,d	Check	0.0809168	OK				

8. Bearing strength							
The design load case will be due to a combination of self-weight of the beam plus the							
permanent and variable loading:							
Design value of the end reaction			Vd1,roof		48.170346	kN	roof
			Vd2,roof		39.0794895	kN	roof
			Vd1		16.929	kN	innside
			Vd2		14.85	kN	innside
Effective contact area			Aef		9000		
Design bearing stress			σc,90,d1,roof		41.8872574		
			σc,90,d2,roof		33.9821648		
			σc,90,d1		14.7208696		
			σc,90,d2		12.9130435		

Design bearing strength			fc,90,d		1956.52174		
Factored design bearing strength			kc,90		1.75		
			fc,90,d*kc,90		3423.91304		
σc,90,d1,roof							
fc,90,d*kc,90	Check	0.0122337	OK				
σc,90,d2,roof							
fc,90,d*kc,90	Check	0.0099249	OK				
σc,90,d1							
fc,90,d*kc,90	Check	0.0042994	OK				
σc,90,d2							
fc,90,d*kc,90	Check	0.0037714	OK				

9. Beam deflection							
uinst ,DL	(((5*(Gk,selfwt+Gk,p))*(l^4))/(32*E0,g,mean*b*(h^3)))*(1+(0,96*(E0,g,mean/G0,g,mean))*((h/l)^						
uinst,DL1	1.136363874						
uinst, DL2	0.698486184						
uinst,Q	(((5*(Qk,p))*(l^4))/(32*E0,g,mean*b*(h^3)))*(1+(0,96*(E0,g,mean/G0,g,mean))*((h/l)^2))						
uinst,Q1	0.635926379						
uinst,Q2	0.390883413						
uinst	= uinst,DL + uinst,Q						
uinst1	1.772290254						
uinst2	1.089369598						
			Check	uinst1<winst1	OK		
winst	= l/300			uinst2<winst2	OK		
winst1	17.1						
winst2	15						
ufin,G	= uinst,dl*(1+kdef)						
ufin,G1	1.818182199						
ufin,G2	1.117577894						
ufin,Q	= uinst,Q*(1+(w2*kdef))						
ufin,Q1	0.635926379						
ufin,Q2	0.390883413						
unet,fin	= ufin,G + ufin,Q						
unet,fin1	2.454108579						
unet,fin2	1.508461308						
			Check	unet,fin1<wnet,fin1		OK	
wnet,fin	= l/250			unet,fin2<wnet,fin2		OK	
wnet,fin1	20.52						
wnet,fin2	18						

Columns

1. Glulam column geometric properties					
Length	L		3	m	
Effectiv length of the column buckling y-y	Le,y	= 0,5*L	1.5	m	
Effectiv length of the column buckling z-z	Le,z	= 0,5*L	1.5	m	
Effective length of the member acting as a beam with a constant moment along	lef	= L	3	m	
Width of the column	b		200	mm	
Depth of the column	h		200	mm	
Cross-section area of the column	A	= b*h	40000	mm^2	
Second moment of area of the column about the y-y axes	Iy	=(b*h^3)/12	133333333.3	mm^4	
Section modulus about the y-y axes	Wy	=(h*(b^2))/6	1333333.333	mm^3	
Radius of gyration about the y-y axis	iy	=rot(Iy/A)	57.73502692	mm	
Slenderness ratio about the y-y axis	λy	=Le,y/iy	25.98076211		
Second moment of area of the column about the z-z axis	Iz	=(h*b^3)/12	133333333.3	mm^4	
Section modulus about the z-z axes	Wz	=(b*(h^2))/6	1333333.333	mm^3	
Radius of gyration of the column about the z-z axis	iz	=rot(Iz/A)	57.73502692	mm	
Slenderness ratio about the z-z axis	λz	=Le,z/iz	25.98076211		

2. Glulam properties					
				1000	
			N/mm^2	kN/m^2	
			kg/m^3	kN/m^3	
Characteristic bending strength	fm,g,k		20	20000	kN/m^2
Characteristic shear strength	fv,g,k		3.5	3500	kN/m^2
Characteristic bearing strength	fc,90,g,k		2.5	2500	kN/m^2
Compression strength	fc,0,g,k		18.5	18500	kN/m^2
Mean modulus of elasticity parallel to grain	E0,g,mean		10400	10400000	kN/m^2 kN/m^2
Mean shear modulus	G0,g,mean		650	650000	kN/m^2
Mean density of each beam	ρg,k		355	3.48255	kN/m^3
	ρg,mean		390	3.8259	kN/m^3

3. Partial safety factors					
Permanent actions	γG		1.2		
Variable actions	γQ		1.5		
Factor for quasi-permanent value of variable action	ψ2		0		
Material factor for glulam at ULS	γM		1.15		

4. Actions						
Characteristic permanent compressive action		Gk		40	kN	
Characteristic medium-term compressive variable action		Qk		75	kN	
Wind load		Wb1		1.065	kN/m^2	
		Wb2		1.065	kN/m^2	
Design compressive action for the critical load combination		Nd		160.5	kN	
5. Modification factors						
Factor for short-duration loading and service class 1		kmod,short		0.9		
Size factor for depth less than 600 mm		kh		1		
Lateral stability of a beam		kcrit		1		
Modification factor for the influence of cracks		kcr		0.67		
Bearing factor		kc,90		1.75		
Deformation factor for service class 1		kdef		0.6		
Load sharing factor		ksys		1		
6. Strength of column						
Design bending moment about the end		Md1	= (W1*L)/2	0.9585	kNm	
		Md2	= (W2*L)/2	0.9585	kNm	
Design bending stress about the end		σmdy1	=Md1/Wy	0.718875	N/mm^2	
		σmdy2	=Md2/Wy	0.718875	N/mm^2	
		σmdz1	=Md1/Wz	0.718875	N/mm^2	
		σmdz2	=Md2/Wz	0.718875	N/mm^2	
design bending strength about the y-y		fmd		15.65217391	N/mm^2	
Redistribution factor for a rectangular section		km		0.7		
Critical bending stress		σm,crit	=(pi*(b^2)*(	331.2324094	N/mm^2	
Relative slenderness for bending		λrel,m	=rot((fmgk)/σm,crit)	0.217380669		
Bending strength greater than bending stress				OK		

7. Axial compression condition					
Design compression stress	σc,0,d	=Nd/A	4012.5	kN/m^2	
Design compression strength	fc,0,d		14478.26087	kN/m^2	
Buckling resistance condition					
Relative slenderness about the y-y axis	λrel,y		0.348795769		
Relative slenderness about the z-z axis	λrel,z		0.348795769		
Factor for glulam	βc		0.1		
Factor ky	ky		0.563269033		
Instability factor about the y-y axis	ky,c		0.994479447		
Factor kz	kz		0.563269033		
Instability factor about the z-z axis	kz,c		0.994479447		
Combined stress conditions					
compression stress condition about the y-y axis	(σc,0,d/(kc,y*fc,0,d)) + (σm,y,d/fm,y,d)		0.324606222		
compression stress condition about the z-z axis	(σc,0,d/(kc,z*fc,0,d)) + (km*(σm,y,d/fm,y,d))		0.310827784		
Combined stress condition	((σm,y,d/(kcrit*fm,y,d))^2)+(σc,0,d/(kz,c*fc,0,d))		0.28078749		

Appendix E – Equivalent Mass

Frame

	Story	Element	Size [mm]	Height or length [mm]	Area [m^2]	Nr. of elements		Area tot. [m^2]	Material	Weight [kg/m^3]	(Equvialent) mass [kg/m]
		Column									
825	1-3	Column	825x825	3	0.680625	36	108	73.5075	GL 22c	390	86003.775
775	4-6	Column	775x775	3	0.600625	36	108	64.8675	GL 22c	390	75894.975
525	1-6	Beam	525x675	4.177	0.354375	18	108	38.2725	GL 22c	390	62347.0507
675				6.386	0.354375	9	54	19.1363	GL 22c	390	47659.5961
				3.855	0.354375	4	24	8.505	GL 22c	390	12786.8423
				2.7	0.354375	24	144	51.03	GL 22c	390	53734.59
				2.745	0.354375	4	24	8.505	GL 22c	390	9105.02775
	1-6	Slab	4177x3855	0.18	16.102335	2	12	193.228	CLT c14	350	12173.3653
			6386x3855	0.18	24.61803	1	6	147.708	CLT c14	350	9305.61534
			4177x2700	0.18	11.2779	12	72	812.009	CLT c14	350	51156.5544
			6386x2700	0.18	17.2422	6	36	620.719	CLT c14	350	39105.3096
			2745x4177	0.18	11.465865	2	12	137.59	CLT c14	350	8668.19394
			2745x6386	0.18	17.52957	1	6	105.177	CLT c14	350	6626.17746
	1-6	CLT Core	2746x3000	0.2	8.238	2	12	98.856	CLT c24	420	8303.904
			7224x3000	0.2	21.672	2	12	260.064	CLT c24	420	21845.376
										Total	504716.4

675	7-9	Column	675x675	3	0.455625	36	108	49.2075	GL 22c	390	57572.775
500	10-12	Column	500x500	3	0.25	36	108	27	GL 22c	390	31590
525	7-12	Beam	425x675	4.177	0.354375	18	108	38.2725	GL 22c	390	62347.0507
675				6.386	0.354375	9	54	19.1363	GL 22c	390	47659.5961
				3.855	0.354375	4	24	8.505	GL 22c	390	12786.8423
				2.7	0.354375	24	144	51.03	GL 22c	390	53734.59
				2.745	0.354375	4	24	8.505	GL 22c	390	9105.02775
	7-12	Slab	4177x3855	0.18	16.102335	2	12	193.228	CLT c14	350	12173.3653
			6386x3855	0.18	24.61803	1	6	147.708	CLT c14	350	9305.61534
			4177x2700	0.18	11.2779	12	72	812.009	CLT c14	350	51156.5544
			6386x2700	0.18	17.2422	6	36	620.719	CLT c14	350	39105.3096
			2745x4177	0.18	11.465865	2	12	137.59	CLT c14	350	8668.19394
			2745x6386	0.18	17.52957	1	6	105.177	CLT c14	350	6626.17746
	7-12	CLT Core	2746x3000	0.2	8.238	2	12	98.856	CLT c24	420	8303.904
			7224x3000	0.2	21.672	2	12	260.064	CLT c24	420	21845.376
										Total	431980.4

450	1-3	Column	450x450	3	0.2025	36	108	21.87	GL 22c	390	25587.9
425	4-6	Column	425x425	3	0.180625	36	108	19.5075	GL 22c	390	22823.775
525	1-6	Beam	425x675	4.177	0.354375	18	108	38.2725	GL 22c	390	62347.0507
675				6.386	0.354375	9	54	19.1363	GL 22c	390	47659.5961
				3.855	0.354375	4	24	8.505	GL 22c	390	12786.8423
				2.7	0.354375	24	144	51.03	GL 22c	390	53734.59
				2.745	0.354375	4	24	8.505	GL 22c	390	9105.02775
1-6	Slab	4177x3855	0.18	16.102335	2	10	161.023	CLT c14	350	10144.4711
		6386x3855	0.18	24.61803	1	5	123.09	CLT c14	350	7754.67945
		4177x2700	0.18	11.2779	12	60	676.674	CLT c14	350	42630.462
		6386x2700	0.18	17.2422	6	30	517.266	CLT c14	350	32587.758
		2745x4177	0.18	11.465865	2	10	114.659	CLT c14	350	7223.49495
		2745x6386	0.18	17.52957	1	5	87.6479	CLT c14	350	5521.81455
1-6	Slab	4177x3855	0.2	16.102335	2	2	32.2047	CLT c14	350	2254.3269
		6386x3855	0.2	24.61803	1	1	24.618	CLT c14	350	1723.2621
		4177x2700	0.2	11.2779	12	12	135.335	CLT c14	350	9473.436
		6386x2700	0.2	17.2422	6	6	103.453	CLT c14	350	7241.724
		2745x4177	0.2	11.465865	2	2	22.9317	CLT c14	350	1605.2211
		2745x6386	0.2	17.52957	1	1	17.5296	CLT c14	350	1227.0699
1-6	CLT Core	2746x3000	0.2	8.238	2	12	98.856	CLT c24	420	8303.904
		7224x3000	0.2	21.672	2	12	260.064	CLT c24	420	21845.376

Total	393581.8

Avrage mass	443426.17
Equivalent mass	24634.79

Shear wall

	Story	Element	Size [mm]	Height [mm]	Area [m^2]	Nr. of elements		Area tot. [m^2]	Material	Weight [kg/m^3]	Equvialent mass [kg/m]
650	1-6	Column	650x650	3	0.4225	14	84	35.49	GL 22c	390	41523.3
675	1-6	Beam	260x400	4.177	0.4725	18	108	51.03	GL 22c	390	83129.4009
700				6.386	0.4725	9	54	25.515	GL 22c	390	63546.1281
				3.855	0.4725	4	24	11.34	GL 22c	390	17049.123
				2.7	0.4725	24	144	68.04	GL 22c	390	71646.12
				2.745	0.4725	4	24	11.34	GL 22c	390	12140.037
	1-6	Slab	4177x3855	0.18	16.102335	2	12	193.228	CLT c14	350	12173.3653
			6386x3855	0.18	24.61803	1	6	147.7082	CLT c14	350	9305.61534
			4177x2700	0.18	11.2779	12	72	812.0088	CLT c14	350	51156.5544
			6386x2700	0.18	17.2422	6	36	620.7192	CLT c14	350	39105.3096
			2745x4177	0.18	11.465865	2	12	137.5904	CLT c14	350	8668.19394
			2745x6386	0.18	17.52957	1	6	105.1774	CLT c14	350	6626.17746
350	1-6	CLT wall	3855x3000	0.35	11.565	2	12	138.78	CLT c22	480	23315.04
			5400x3000	0.35	16.2	2	12	194.4	CLT c22	480	32659.2
			4177x3000	0.35	12.531	4	24	300.744	CLT c22	480	50524.992
			2745x3000	0.35	8.235	2	12	98.82	CLT c22	480	16601.76
	1-6	CLT Core	2746x3000	0.2	0.8238	2	12	9.8856	CLT c24	420	830.3904
			7224x3000	0.2	2.1672	2	12	26.0064	CLT c24	420	2184.5376

Total 542185.2

550	7-12	Column	550x550	3	0.3025	14	84	25.41	GL 22c	390	29729.7
675	7-12	Beam	260x400	4.177	0.4725	18	108	51.03	GL 22c	390	83129.4009
700				6.386	0.4725	9	54	25.515	GL 22c	390	63546.1281
				3.855	0.4725	4	24	11.34	GL 22c	390	17049.123
				2.7	0.4725	24	144	68.04	GL 22c	390	71646.12
				2.745	0.4725	4	24	11.34	GL 22c	390	12140.037
	7-12	Slab	4177x3855	0.18	16.102335	2	12	193.228	CLT c14	350	12173.3653
			6386x3855	0.18	24.61803	1	6	147.7082	CLT c14	350	9305.61534
			4177x2700	0.18	11.2779	12	72	812.0088	CLT c14	350	51156.5544
			6386x2700	0.18	17.2422	6	36	620.7192	CLT c14	350	39105.3096
			2745x4177	0.18	11.465865	2	12	137.5904	CLT c14	350	8668.19394
			2745x6386	0.18	17.52957	1	6	105.1774	CLT c14	350	6626.17746
300	7-12	CLT wall	3855x3000	0.3	11.565	2	12	138.78	CLT c22	480	19984.32
			5400x3000	0.3	16.2	2	12	194.4	CLT c22	480	27993.6
			4177x3000	0.3	12.531	4	24	300.744	CLT c22	480	43307.136
			2745x3000	0.3	8.235	2	12	98.82	CLT c22	480	14230.08
	7-12	CLT Core	2746x3000	0.2	0.8238	2	12	9.8856	CLT c24	420	830.3904
			7224x3000	0.2	2.1672	2	12	26.0064	CLT c24	420	2184.5376

Total 512805.8

450	13-18	Column	550x550	3	0.2025	14	84	17.01	GL 22c	390	19901.7
675	13-18	Beam	260x400	4.177	0.4725	18	108	51.03	GL 22c	390	83129.4009
700				6.386	0.4725	9	54	25.515	GL 22c	390	63546.1281
				3.855	0.4725	4	24	11.34	GL 22c	390	17049.123
				2.7	0.4725	24	144	68.04	GL 22c	390	71646.12
				2.745	0.4725	4	24	11.34	GL 22c	390	12140.037
	13-18	Slab	4177x3855	0.18	16.102335	2	10	161.0234	CLT c14	350	10144.4711
			6386x3855	0.18	24.61803	1	5	123.0902	CLT c14	350	7754.67945
			4177x2700	0.18	11.2779	12	60	676.674	CLT c14	350	42630.462
			6386x2700	0.18	17.2422	6	30	517.266	CLT c14	350	32587.758
			2745x4177	0.18	11.465865	2	10	114.6587	CLT c14	350	7223.49495
			2745x6386	0.18	17.52957	1	5	87.64785	CLT c14	350	5521.81455
	13-18	Slab	4177x3855	0.2	16.102335	2	2	32.20467	CLT c14	350	2254.3269
			6386x3855	0.2	24.61803	1	1	24.61803	CLT c14	350	1723.2621
			4177x2700	0.2	11.2779	12	12	135.3348	CLT c14	350	9473.436
			6386x2700	0.2	17.2422	6	6	103.4532	CLT c14	350	7241.724
			2745x4177	0.2	11.465865	2	2	22.93173	CLT c14	350	1605.2211
			2745x6386	0.2	17.52957	1	1	17.52957	CLT c14	350	1227.0699
275	13-18	CLT wall	3855x3000	0.275	11.565	2	12	138.78	CLT c22	480	18318.96
			5400x3000	0.275	16.2	2	12	194.4	CLT c22	480	25660.8
			4177x3000	0.275	12.531	4	24	300.744	CLT c22	480	39698.208
			2745x3000	0.275	8.235	2	12	98.82	CLT c22	480	13044.24
	13-18	CLT Core	2746x3000	0.2	0.8238	2	12	9.8856	CLT c24	420	830.3904
			7224x3000	0.2	2.1672	2	12	26.0064	CLT c24	420	2184.5376

Total	496537.4

Avrage mass	517176.13
Equivalent mass	28732.01

Diagrid

	Story	Element	Size [mm]	Height or length [mm]	Area [m^2]	Nr. of elements		Area tot. [m^2]	Material	Weight [kg/m^3]	Equvialent mass [kg/m]
575	1-2	Long side	575x575	6.6424769	0.330625	16	16	5.29	GL 22c	390	13704.0941
575		short side	200x200	3.3425553	0.330625	10	10	3.30625	GL 22c	390	4310.01615
575		straight	200x200	3	0.330625	4	8	2.645	GL 22c	390	3094.65
575		inside	150x150	3	0.330625	14	28	9.2575	GL 22c	390	10831.275
525	3-4	Long side	575x575	6.6424769	0.275625	16	16	4.41	GL 22c	390	11424.396
525		short side	200x200	3.3425553	0.275625	10	10	2.75625	GL 22c	390	3593.03804
525		straight	200x200	3	0.275625	4	8	2.205	GL 22c	390	2579.85
525		inside	150x150	3	0.275625	14	28	7.7175	GL 22c	390	9029.475
475	5-6	Long side	575x575	6.6424769	0.225625	16	16	3.61	GL 22c	390	9351.94323
475		short side	200x200	3.3425553	0.225625	10	10	2.25625	GL 22c	390	2941.23975
475		straight	200x200	3	0.225625	4	8	1.805	GL 22c	390	2111.85
475		inside	150x150	3	0.225625	14	28	6.3175	GL 22c	390	7391.475
	1-6	Beam	150x200	4.177	0.01	18	90	0.9	GL 22c	390	1466.127
				6.386	0.01	9	54	0.54	GL 22c	390	1344.8916
				3.855	0.01	4	24	0.24	GL 22c	390	360.828
				2.7	0.01	24	144	1.44	GL 22c	390	1516.32
				2.745	0.01	4	24	0.24	GL 22c	390	256.932
	1-6	Slab	4177x3855	0.18	16.102335	2	12	193.22802	CLT c14	350	12173.3653
			6386x3855	0.18	24.61803	1	6	147.70818	GL 22c	350	9305.61534
			4177x2700	0.18	11.2779	12	72	812.0088	GL 22c	350	51156.5544
			6386x2700	0.18	17.2422	6	36	620.7192	GL 22c	350	39105.3096
			2745x4177	0.18	11.465865	2	12	137.59038	GL 22c	350	8668.19394
			2745x6386	0.18	17.52957	1	6	105.17742	GL 22c	350	6626.17746
	1-6	CLT Core	2746x3000	300	8.238	2	12	98.856	CLT c18	460	45473.76
			7224x3000	300	21.672	2	12	260.064	CLT c18	460	119629.44
										Total	377446.817
425	7-8	Long side	575x575	6.6424769	0.180625	16	16	2.89	GL 22c	390	7486.73571
425		short side	200x200	3.3425553	0.180625	10	10	1.80625	GL 22c	390	2354.6213
425		straight	200x200	3	0.180625	4	8	1.445	GL 22c	390	1690.65
425		inside	150x150	3	0.180625	14	28	5.0575	GL 22c	390	5917.275
325	9-10	Long side	575x575	6.6424769	0.105625	16	16	1.69	GL 22c	390	4378.05652
325		short side	200x200	3.3425553	0.105625	10	10	1.05625	GL 22c	390	1376.92387
325		straight	200x200	3	0.105625	4	8	0.845	GL 22c	390	988.65
325		inside	150x150	3	0.105625	14	28	2.9575	GL 22c	390	3460.275
275	11-12	Long side	575x575	6.6424769	0.075625	16	16	1.21	GL 22c	390	3134.58485
275		short side	200x200	3.3425553	0.075625	10	10	0.75625	GL 22c	390	985.844904
275		straight	200x200	3	0.075625	4	8	0.605	GL 22c	390	707.85
275		inside	150x150	3	0.075625	14	28	2.1175	GL 22c	390	2477.475
	13-18	Beam	150x200	4.177	0.01	18	90	0.9	GL 22c	390	1466.127

			6.386	0.01	9	54	0.54	GL 22c	390	1344.8916
			3.855	0.01	4	24	0.24	GL 22c	390	360.828
			2.7	0.01	24	144	1.44	GL 22c	390	1516.32
			2.745	0.01	4	24	0.24	GL 22c	390	256.932
7-12	Slab	4177x3855	0.18	16.102335	2	12	193.22802	CLT c14	350	12173.3653
		6386x3855	0.18	24.61803	1	6	147.70818	GL 22c	350	9305.61534
		4177x2700	0.18	11.2779	12	72	812.0088	GL 22c	350	51156.5544
		6386x2700	0.18	17.2422	6	36	620.7192	GL 22c	350	39105.3096
		2745x4177	0.18	11.465865	2	12	137.59038	GL 22c	350	8668.19394
		2745x6386	0.18	17.52957	1	6	105.17742	GL 22c	350	6626.17746
7-12	CLT Core	2746x3000	150	0.5492	2	12	6.5904	CLT c18	460	3031.584
		7224x3000	150	1.4448	2	12	17.3376	CLT c18	460	7975.296

Total	177946.137

250	13-14	Long side	575x575	6.6424769	0.0625	16	16	1	GL 22c	390	2590.56599
250		short side	200x200	3.3425553	0.0625	10	10	0.625	GL 22c	390	814.747854
250		straight	200x200	3	0.0625	4	8	0.5	GL 22c	390	585
250		inside	150x150	3	0.0625	14	28	1.75	GL 22c	390	2047.5
225	15-16	Long side	575x575	6.6424769	0.050625	16	16	0.81	GL 22c	390	2098.35845
225		short side	200x200	3.3425553	0.050625	10	10	0.50625	GL 22c	390	659.945762
225		straight	200x200	3	0.050625	4	8	0.405	GL 22c	390	473.85
225		inside	150x150	3	0.050625	14	28	1.4175	GL 22c	390	1658.475
200	17-18	Long side	575x575	6.6424769	0.04	16	16	0.64	GL 22c	390	1657.96223
200		short side	200x200	3.3425553	0.04	10	10	0.4	GL 22c	390	521.438627
200		straight	200x200	3	0.04	4	8	0.32	GL 22c	390	374.4
200		inside	150x150	3	0.04	14	28	1.12	GL 22c	390	1310.4
	13-18	Beam	150x200	4.177	0.01	18	90	0.9	GL 22c	390	1466.127
				6.386	0.01	9	54	0.54	GL 22c	390	1344.8916
				3.855	0.01	4	24	0.24	GL 22c	390	360.828
				2.7	0.01	24	144	1.44	GL 22c	390	1516.32
				2.745	0.01	4	24	0.24	GL 22c	390	256.932
	13-18	Slab	4177x3855	0.18	16.102335	2	10	161.02335	CLT c14	350	10144.4711
			6386x3855	0.18	24.61803	1	5	123.09015	GL 22c	350	7754.67945
			4177x2700	0.18	11.2779	12	60	676.674	GL 22c	350	42630.462
			6386x2700	0.18	17.2422	6	30	517.266	GL 22c	350	32587.758
			2745x4177	0.18	11.465865	2	10	114.65865	GL 22c	350	7223.49495
			2745x6386	0.18	17.52957	1	5	87.64785	GL 22c	350	5521.81455
	13-18	Slab	4177x3855	0.2	16.102335	2	2	32.20467	CLT c14	350	2254.3269
			6386x3855	0.2	24.61803	1	1	24.61803	GL 22c	350	1723.2621
			4177x2700	0.2	11.2779	12	12	135.3348	GL 22c	350	9473.436
			6386x2700	0.2	17.2422	6	6	103.4532	GL 22c	350	7241.724
			2745x4177	0.2	11.465865	2	2	22.93173	GL 22c	350	1605.2211
			2745x6386	0.2	17.52957	1	1	17.52957	GL 22c	350	1227.0699
	13-18	CLT Core	2746x3000	300	8.238	2	12	98.856	CLT c18	460	45473.76
			7224x3000	300	21.672	2	12	260.064	CLT c18	460	119629.44

Total	314228.663
Avrage mass	289873.87
Equivalent mass	16104.10

Appendix F – Peak acceleration

1.1.1 Same frequency

8.1.1.1 Frame

Frame		
Glulam member for the building	Story	Size [mm]
Column 1	1-3	825 x 825
Column 2	4-6	775 x 775
Column 3	7-9	675 x 675
Column 4	10-12	500 x 500
Column 5	13-15	450 x 450
Column 6	16-18	425 x 425
Beam	All	425 x 675
Core – CLT Wall c30	All	300 x 300

	C20	C22	C24	C26	C28	C30	C32
	Value	Value	Value	Value	Value	Value	Value
m	396878,4	396878,4	411905,25	424730,83	424730,83	431143,621	437556,411
m_e	22048,8	22048,8	22883,63	23596,16	23596,16	23952,42	24308,69
$n_{1,x}$	0,847	0,847	0,857	0,872	0,882	0,888	0,894
δa	0,0149	0,0149	0,0142	0,0136	0,0134	0,0131	0,0128
δ	0,0749	0,0749	0,0742	0,0736	0,0734	0,0731	0,0728
f_L	7,8759	7,8759	7,9689	8,1084	8,2014	8,2572	8,3130
$S_L(zs)$	0,0351	0,0351	0,0348	0,0344	0,0342	0,0340	0,0339
η_h	12,8866	12,8866	13,0387	13,2669	13,4191	13,5104	13,6017
η_b	5,4410	5,4410	5,5052	5,6016	5,6658	5,7044	5,7429
R_h	0,0746	0,0746	0,0738	0,0725	0,0717	0,0713	0,0708
R_b	0,1669	0,1669	0,1651	0,1626	0,1609	0,1599	0,1590
R^2	0,0288	0,0288	0,0282	0,0272	0,0265	0,0262	0,0258
R	0,1696	0,1696	0,1679	0,1650	0,1628	0,1618	0,1607
v	0,8470	0,8470	0,8570	0,8720	0,8820	0,8880	0,8940
kp(zs)	3,7001	3,7001	3,7032	3,7079	3,7110	3,7128	3,7146
σa(z)	0,0137	0,0137	0,0130	0,0124	0,0123	0,0120	0,0117
$a_{1,x}(z)$	0,0506	0,0506	0,0483	0,0461	0,0455	0,0446	0,0436

Model	Grade – glulam	Average mass	Mode stiffness	Frequency	Peak acceleration
	C20	396878,4	70,00	0,847	0,0506
	C22	396878,4	70,00	0,847	0,0506
	C24	411905,25	69,99	0,857	0,0483
	C26	431143,621	70,00	0,872	0,0461

	C28	437556,411	71,00	0,882	0,0455
	C30	424730,83	71,00	0,888	0,0446
	C32	424730,83	71,00	0,894	0,0436

8.1.1.2 Shear wall

Shear wall			
CLT member for the building	Story	Size of element [mm]	Thickness [mm]
CLT wall 1 – Long side (corner wall)	1-6	3855x3000 2745x3000	300
CLT wall 1 – middle	1-6	5400x3000	300
CLT wall 1 – Short side (corner wall)	1-6	4177x3000	300
CLT wall 2 – Long side (corner wall)	7-12	3855x3000 2745x3000	225
CLT wall 2 – middle	7-12	5400x3000	225
CLT wall 2 – Short side (corner wall)	7-12	4177x3000	225
CLT wall 3 – Long side (corner wall)	13-18	3855x3000 2745x3000	175
CLT wall 3 – middle	13-18	5400x3000	175
CLT wall 3 – Short side (corner wall)	13-18	4177x3000	175
Core – CLT Wall c30	All	2746x3000 7224x3000	300

Glulam member for the building	**Story**	**Size [mm]**	**Material**
Beam	All	260x400	GL 20c
Column 1 – inside	1-6	600x600	GL 20c
Column 2 – inside	7-12	500x500	GL 20c
Column 2 – inside	13-18	400x400	GL 20c

	C20	C22	C24	C27	C30	C35	C40
	Value	Value	Value	Value	Value	Value	Value
m	292395,3	293548,4	294701,51	295854,63	299313,98	300467,09	301620,21
m_e	16244,18	16308,24	16372,31	16436,37	16628,55	16692,62	16756,68
$n_{1,x}$	0,662	0,679	0,694	0,699	0,705	0,717	0,730

δa	0,0260	0,0252	0,0246	0,0243	0,0238	0,0233	0,0228
δ	0,0860	0,0852	0,0846	0,0843	0,0838	0,0833	0,0828
f_L	6,1557	6,3138	6,4533	6,4997	6,5555	6,6671	6,7880
$S_L(zs)$	0,0411	0,0404	0,0399	0,0397	0,0395	0,0391	0,0386
η_h	10,0719	10,3306	10,5588	10,6349	10,7261	10,9087	11,1065
η_b	4,2526	4,3618	4,4582	4,4903	4,5288	4,6059	4,6894
R_h	0,0944	0,0921	0,0902	0,0896	0,0889	0,0875	0,0860
R_b	0,2075	0,2030	0,1992	0,1979	0,1964	0,1935	0,1905
R^2	0,0462	0,0438	0,0418	0,0412	0,0406	0,0392	0,0377
R	0,2149	0,2093	0,2045	0,2030	0,2015	0,1979	0,1941
v	0,6620	0,6790	0,6940	0,6990	0,7050	0,7170	0,7300
kp(zs)	3,6330	3,6400	3,6460	3,6479	3,6503	3,6549	3,6598
σa(z)	0,0235	0,0228	0,0222	0,0219	0,0215	0,0211	0,0206
$a_{1,x}(z)$	0,0854	0,0830	0,0809	0,0801	0,0786	0,0770	0,0753

Model	Grade – glulam	Average mass	Mode stiffness	Frequency	Peak acceleration
	C20	258633,8	67,01	0,835	0,0756
	C22	260343,6	66,99	0,845	0,0744
	C24	262053,29	65,99	0,863	0,0733
	C27	263763,02	65,99	0,868	0,0729
	C30	268892,23	65,99	0,869	0,0728
	C35	270601,97	65,99	0,882	0,0718
	C40	272311,7	66,01	0,894	0,0708

8.1.1.3 Diagrids

Diagrid			
Glulam member for the building	Story	Length [mm]	Size [mm]
Column 1 – Outer tube long side	1-6	6642,5	100x100
Column 1 – Outer tube short side	1-6	6685,1	200x200
Column 1 – straight	1-6	3000	100x100
Column – inside	1-6	3000	200x200
Column 2 – Outer tube long side	7-12	6642,5	100x100
Column 2 – Outer tube short side	7-12	6685,1	150x150
Column 2 – straight	7-12	3000	100x100
Column – inside	7-12	3000	150x150
Column 3 – Outer tube long side	13-18	6642,5	100x100
Column 3 – Outer tube short side	13-18	6685,1	100x100
Column 3 – straight	13-18	3000	100x100

Column – inside	13-18	3000	100x100
Beam	All		100x100
CLT Core – c20	All		150x150

	C20	C22	C24	C26	C28	C30	C32
	Value	Value	Value	Value	Value	Value	Value
m	125223,5	125223,5	125474,47	125976,5	125976,5	126227,52	126478,53
m_e	6956,86	6956,86	6970,80	6998,69	6998,69	7012,64	7026,59
$n_{1,x}$	0,854	0,854	0,872	0,901	0,915	0,929	0,943
δa	0,0470	0,0470	0,0459	0,0443	0,0436	0,0429	0,0421
δ	0,1070	0,1070	0,1059	0,1043	0,1036	0,1029	0,1021
f_L	7,9410	7,9410	8,1084	8,3781	8,5083	8,6384	8,7686
$S_L(zs)$	0,0349	0,0349	0,0344	0,0337	0,0334	0,0330	0,0327
η_h	12,9931	12,9931	13,2669	13,7082	13,9212	14,1342	14,3472
η_b	5,4860	5,4860	5,6016	5,7879	5,8778	5,9678	6,0577
R_h	0,0740	0,0740	0,0725	0,0703	0,0693	0,0682	0,0673
R_b	0,1657	0,1657	0,1626	0,1578	0,1557	0,1535	0,1515
R^2	0,0197	0,0197	0,0189	0,0177	0,0171	0,0166	0,0161
R	0,1405	0,1405	0,1375	0,1330	0,1309	0,1289	0,1269
v	0,8540	0,8540	0,8720	0,9010	0,9150	0,9290	0,9430
kp(zs)	3,7023	3,7023	3,7079	3,7167	3,7209	3,7249	3,7289
σa(z)	0,0359	0,0359	0,0351	0,0338	0,0332	0,0327	0,0321
$a_{1,x}(z)$	0,1328	0,1328	0,1300	0,1255	0,1237	0,1217	0,1197

Model	Grade – glulam	Average mass	Mode stiffness	Frequency	Peak acceleration
	C20	125223,5	64,99	0,854	0,1328
	C22	125223,5	64,99	0,854	0,1328
	C24	125474,47	65,01	0,872	0,1300
	C26	125976,5	64,99	0,901	0,1255
	C28	125976,5	65,01	0,915	0,1237
	C30	126227,52	64,99	0,929	0,1217
	C32	126478,53	65,01	0,943	0,1197

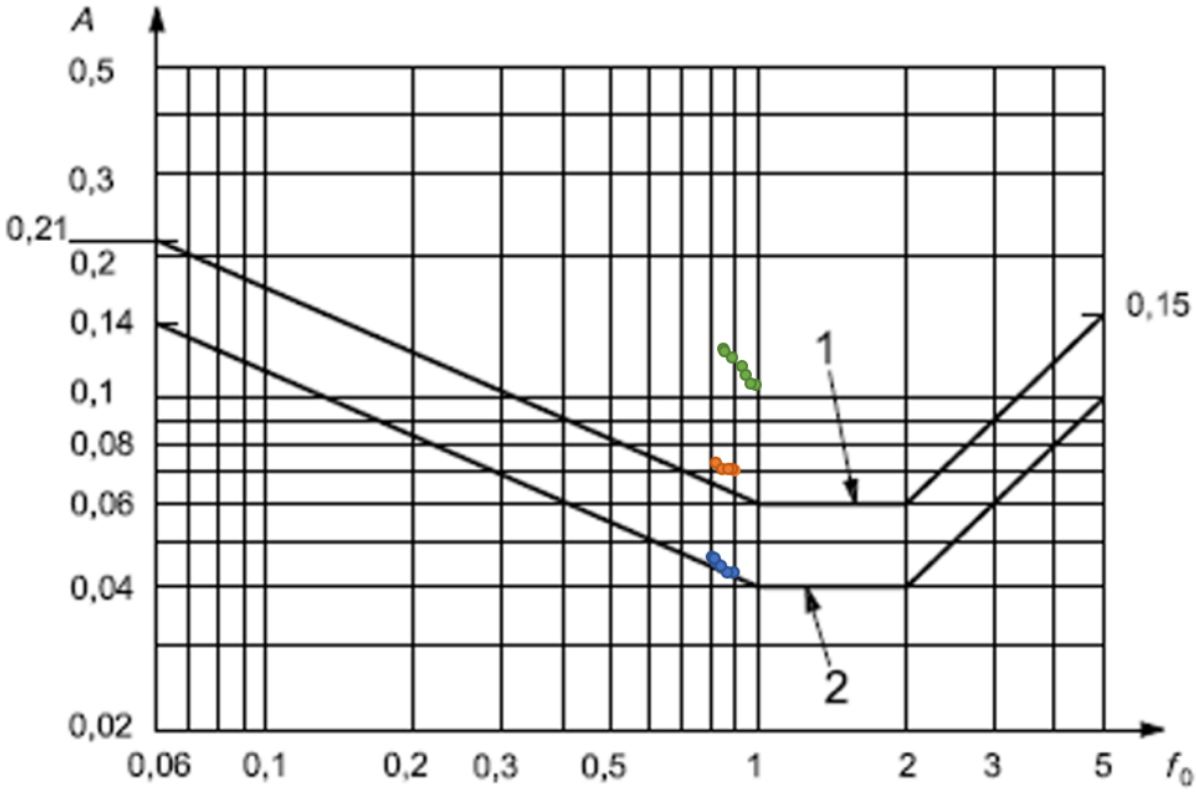

1.1.2 Low frequency

8.1.1.4 Frame

Frame		
Glulam member for the building	Story	Size [mm]
Column 1	1-6	600 x 600
Column 2	7-12	500 x 500
Column 3	13-18	400 x 400
Beam	All	300 x 400
Core – CLT C18	All	200 mm thick

	C20	C22	C24	C26	C28	C30	C32

	Value	Value	Value	Value	Value	Value	Value
m	260865,3	260865,3	264140,28	270690,3	270690,3	273965,26	277240,25
m_e	14492,52	14492,52	14674,46	15038,348	15038,348	15220,292	15402,236
$n_{1,x}$	0,620	0,620	0,629	0,642	0,649	0,656	0,661
δa	0,0311	0,0311	0,0302	0,0289	0,0286	0,0280	0,0274
δ	0,0911	0,0911	0,0902	0,0889	0,0886	0,0880	0,0874
f_L	5,7652	5,7652	5,8488	5,9697	6,0348	6,0999	6,1464
$S_L(zs)$	0,0429	0,0429	0,0425	0,0419	0,0416	0,0413	0,0411
η_h	9,4329	9,4329	9,5698	9,7676	9,8741	9,9806	10,0567
η_b	3,9828	3,9828	4,0406	4,1241	4,1691	4,2140	4,2462
R_h	0,1004	0,1004	0,0990	0,0971	0,0961	0,0952	0,0945
R_b	0,2196	0,2196	0,2169	0,2131	0,2111	0,2092	0,2078
R^2	0,0512	0,0512	0,0499	0,0482	0,0471	0,0462	0,0456
R	0,2263	0,2263	0,2233	0,2194	0,2169	0,2149	0,2135
v	0,6200	0,6200	0,6290	0,6420	0,6490	0,6560	0,6610
kp(zs)	3,6150	3,6150	3,6190	3,6246	3,6276	3,6305	3,6326
σa(z)	0,0277	0,0277	0,0270	0,0259	0,0256	0,0251	0,0246
$a_{1,x}(z)$	0,1003	0,1003	0,0979	0,0940	0,0930	0,0911	0,0895

Model	Grade – glulam	Average mass	Mode stiffness	Frequency	Peak acceleration
	C20	260865,3	72,99	0,620	0,1003
	C22	260865,3	72,99	0,620	0,1003
	C24	264140,28	73,01	0,629	0,0979
	C26	270690,3	72,99	0,642	0,0940
	C28	270690,3	72,99	0,649	0,0930
	C30	273965,26	73,02	0,656	0,0911
	C32	277240,25	72,99	0,661	0,0895

8.1.1.5 Shear wall

Shear wall

CLT member for the building	Story	Size of element [mm]	Thickness [mm]
CLT wall 1 – Long side (corner wall)	1-3	3855x3000 2745x3000	225
CLT wall 1 – middle	1-3	5400x3000	225
CLT wall 1 – Long side (corner wall)	4-6	3855x3000 2745x3000	200
CLT wall 1 – middle	4-6	5400x3000	200
CLT wall 1 – Short side (corner wall)	1-6	4177x3000	200
CLT wall 2 – Long side (corner wall)	7-9	3855x3000	175

		2745x3000	
CLT wall 2 – middle	7-9	5400x3000	175
CLT wall 2 – Long side (corner wall)	10-12	3855x3000 2745x3000	150
CLT wall 2 – middle	10-12	5400x3000	150
CLT wall 2 – Short side (corner wall)	7-12	4177x3000	150
CLT wall 3 – Long side (corner wall)	13-15	3855x3000 2745x3000	125
CLT wall 3 – middle	13-15	5400x3000	125
CLT wall 3 – Long side (corner wall)	16-18	3855x3000 2745x3000	100
CLT wall 3 – middle	16-18	5400x3000	100
CLT wall 3 – Short side (corner wall)	13-18	4177x3000	100
Core – CLT c20	All		200

Glulam member for the building	**Story**	**Size [mm]**	**Material**
Beam c22	All	450 x 550	GL 20c
Column 1 – inside c22	All	300 x 300	GL 20c

	C20	C22	C24	C27	C30	C35	C40
	Value	Value	Value	Value	Value	Value	Value
m	292395,3	293548,4	294701,51	295854,63	299313,98	300467,09	301620,21
m_e	16244,18	16308,24	16372,31	16436,37	16628,55	16692,62	16756,68
$n_{1,x}$	0,662	0,679	0,694	0,699	0,705	0,717	0,730

δa	0,0260	0,0252	0,0246	0,0243	0,0238	0,0233	0,0228
δ	0,0860	0,0852	0,0846	0,0843	0,0838	0,0833	0,0828
f_L	6,1557	6,3138	6,4533	6,4997	6,5555	6,6671	6,7880
$S_L(zs)$	0,0411	0,0404	0,0399	0,0397	0,0395	0,0391	0,0386
η_h	10,0719	10,3306	10,5588	10,6349	10,7261	10,9087	11,1065
η_b	4,2526	4,3618	4,4582	4,4903	4,5288	4,6059	4,6894
R_h	0,0944	0,0921	0,0902	0,0896	0,0889	0,0875	0,0860
R_b	0,2075	0,2030	0,1992	0,1979	0,1964	0,1935	0,1905
R^2	0,0462	0,0438	0,0418	0,0412	0,0406	0,0392	0,0377
R	0,2149	0,2093	0,2045	0,2030	0,2015	0,1979	0,1941
v	0,6620	0,6790	0,6940	0,6990	0,7050	0,7170	0,7300
kp(zs)	3,6330	3,6400	3,6460	3,6479	3,6503	3,6549	3,6598
σa(z)	0,0235	0,0228	0,0222	0,0219	0,0215	0,0211	0,0206
$a_{1,x}(z)$	0,0854	0,0830	0,0809	0,0801	0,0786	0,0770	0,0753

Model	Grade – glulam	Average mass	Mode stiffness	Frequency	Peak acceleration
	C20	292395,3	72,02	0,662	0,0854
	C22	293548,4	71,99	0,679	0,0830
	C24	294701,51	72,02	0,694	0,0809
	C27	295854,63	71,98	0,699	0,0801
	C30	299313,98	70,98	0,705	0,0786
	C35	300467,09	70,99	0,717	0,0770
	C40	301620,21	70,98	0,730	0,0753

8.1.1.6 Diagrids

Diagrid

Glulam member for the building	Story	Length [mm]	Size [mm]
Column 1 – Outer tube long side	All	6642,5	150x150
Column 1 – Outer tube short side	All	6685,1	200x200
Column 1 – straight	All	3000	150x150
Column – inside	All	3000	200x200
Beam	All		200x300
CLT core – c18			200

	C20	C22	C24	C26	C28	C30	C32
	Value	Value	Value	Value	Value	Value	Value
m	153551,1	153551,1	154540,67	156519,94	156519,94	157509,57	158499,21

m_e	8530,61326	8530,61326	8585,59292	8695,55223	8695,55223	8750,53189	8805,51155
$n_{1,x}$	0,774	0,774	0,779	0,819	0,833	0,846	0,859
δa	0,0423	0,0423	0,0420	0,0392	0,0385	0,0377	0,0369
δ	0,1023	0,1023	0,1020	0,0992	0,0985	0,0977	0,0969
f_L	7,1971	7,1971	7,1971	7,6156	7,7458	7,8666	7,9875
$S_L(zs)$	0,0372	0,0372	0,0372	0,0358	0,0355	0,0351	0,0348
η_h	11,7759	11,7759	11,7759	12,4606	12,6736	12,8714	13,0692
η_b	4,9721	4,9721	4,9721	5,2611	5,3511	5,4346	5,5181
R_h	0,0813	0,0813	0,0813	0,0770	0,0758	0,0747	0,0736
R_b	0,1809	0,1809	0,1809	0,1720	0,1694	0,1671	0,1648
R^2	0,0264	0,0264	0,0265	0,0236	0,0228	0,0221	0,0215
R	0,1624	0,1624	0,1626	0,1537	0,1510	0,1487	0,1465
v	0,7740	0,7740	0,7740	0,8190	0,8330	0,8460	0,8590
kp(zs)	3,6757	3,6757	3,6757	3,6910	3,6956	3,6998	3,7039
$\sigma a(z)$	0,0338	0,0338	0,0337	0,0314	0,0309	0,0302	0,0296
$a_{1,x}(z)$	0,1244	0,1244	0,1237	0,1159	0,1140	0,1117	0,1095

Model	Grade – glulam	Average mass	Mode stiffness	Frequency	Peak acceleration
	C20	153551,1	69,00	0,774	0,1244
	C22	153551,1	69,00	0,774	0,1244
	C24	154540,67	69,00	0,779	0,1237
	C26	156519,94	69,00	0,819	0,1159
	C28	156519,94	69,00	0,833	0,1140
	C30	157509,57	71,23	0,846	0,1117
	C32	158499,21	68,99	0,859	0,1095

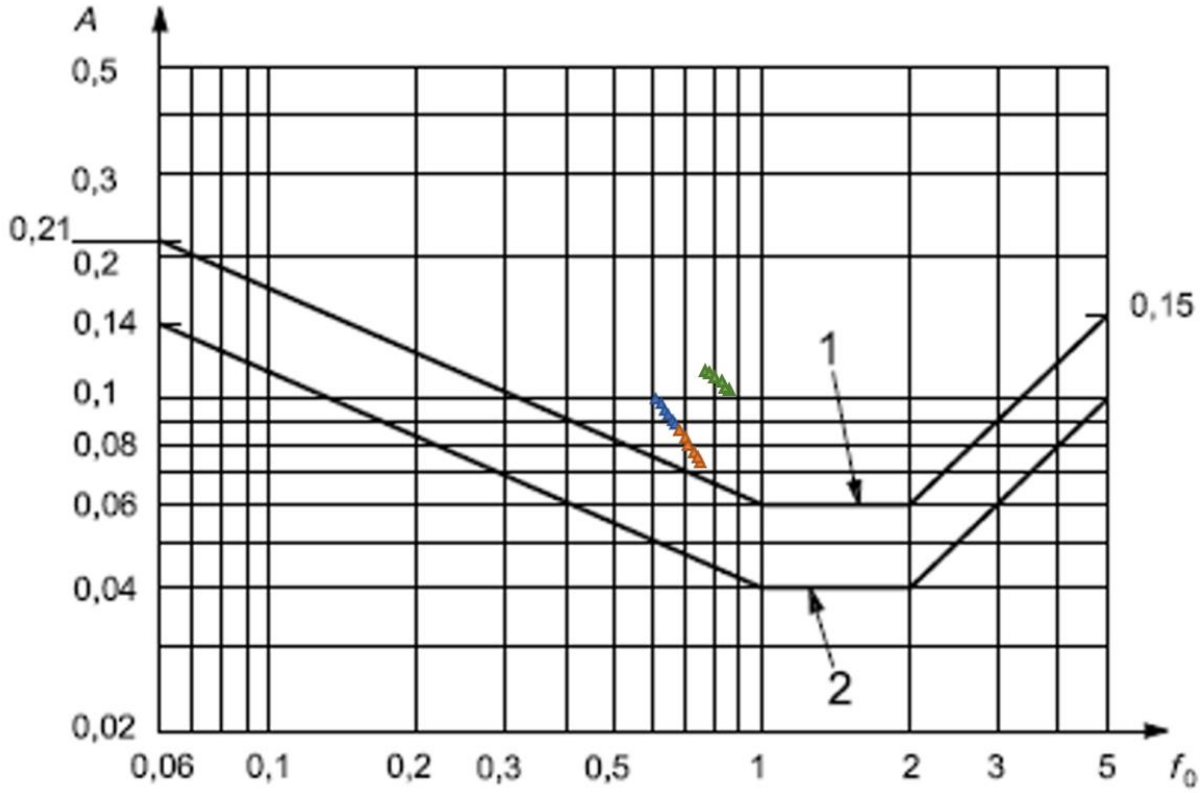

1.1.3 High frequency

8.1.1.7 Frame

Frame		
Glulam member for the building	Story	Size [mm]
Column 1	1-3	825 x 825
Column 2	4-6	775x775
Column 3	7-9	675x675
Column 4	10-12	500 x 500
Column 5	13-15	450x450
Column 6	16-18	425x425
Beam	All	525 x 675
Core – CLT wall – c24	All	200 mm thick

	C20	C22	C24	C26	C28	C30	C32
	Value	Value	Value	Value	Value	Value	Value
m	435612,9	435612,9	443295,02	458659,17	458659,17	466341,25	474023,32
m_e	24200,72	24200,72	24627,501	25481,065	25481,065	25907,8471	26334,6291
$n_{1,x}$	1,015	1,015	1,029	1,047	1,06	1,068	1,075
δa	0,0114	0,0114	0,0110	0,0105	0,0103	0,0101	0,0099
δ	0,0714	0,0714	0,0710	0,0705	0,0703	0,0701	0,0699
f_L	9,4381	9,4381	9,5683	9,7357	9,8566	9,9309	9,9960
$S_L(zs)$	0,0312	0,0312	0,0309	0,0306	0,0303	0,0302	0,0301
η_h	15,4426	15,4426	15,6556	15,9295	16,1272	16,2490	16,3555

η_b	6,5202	6,5202	6,6101	6,7258	6,8093	6,8607	6,9056
R_h	0,0627	0,0627	0,0618	0,0608	0,0601	0,0596	0,0593
R_b	0,1416	0,1416	0,1398	0,1376	0,1361	0,1351	0,1343
R^2	0,0191	0,0191	0,0186	0,0179	0,0174	0,0171	0,0169
R	0,1384	0,1384	0,1363	0,1339	0,1319	0,1309	0,1300
v	1,0150	1,0150	1,0290	1,0470	1,0600	1,0680	1,0750
kp(zs)	3,7486	3,7486	3,7522	3,7568	3,7601	3,7621	3,7638
σa(z)	0,0102	0,0102	0,0098	0,0093	0,0092	0,0090	0,0088
$a_{1,x}(z)$	0,0381	0,0381	0,0369	0,0351	0,0346	0,0338	0,0330

Model	Grade – glulam	Average mass	Mode stiffness	Frequency	Peak acceleration
	C20	435612,9	72,00	1,015	0,0381
	C22	435612,9	72,00	1,015	0,0381
	C24	443295,02	71,99	1,029	0,0369
	C26	458659,17	72,00	1,047	0,0351
	C28	458659,17	72,00	1,06	0,0346
	C30	466341,25	71,99	1,068	0,0338
	C32	474023,32	72,00	1,075	0,0330

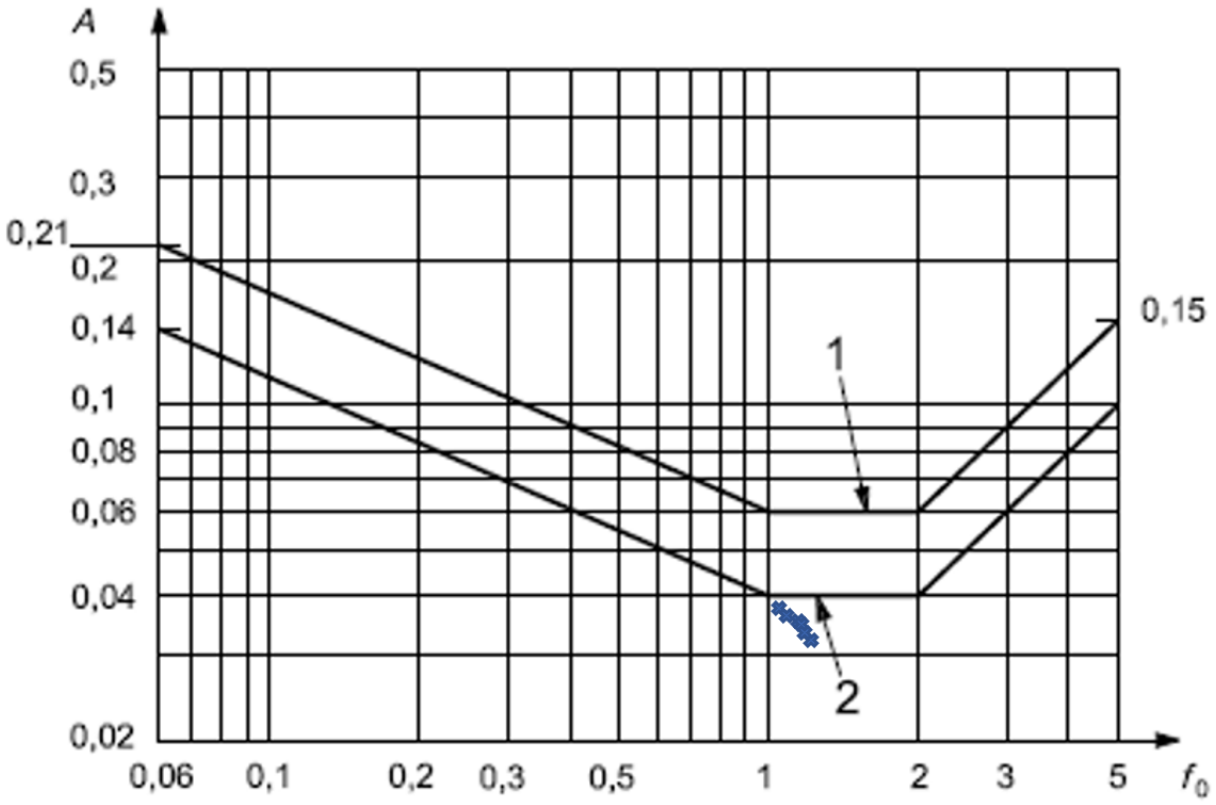

8.1.1.8 Shear wall

Shear wall

CLT member for the building	Story	Size of element [mm]	Thickness [mm]
CLT wall 1 – Long side (corner wall)	1-6	3855x3000 2745x3000	350
CLT wall 1 – middle	1-6	5400x3000	350
CLT wall 1 – Short side (corner wall)	1-6	4177x3000	350
CLT wall 2 – Long side (corner wall)	7-12	3855x3000 2745x3000	300
CLT wall 2 – middle	7-12	5400x3000	300
CLT wall 2 – Short side (corner wall)	7-12	4177x3000	300
CLT wall 3 – Long side (corner wall)	13-18	3855x3000 2745x3000	275
CLT wall 3 – middle	13-18	5400x3000	275
CLT wall 3 – Short side (corner wall)	13-18	4177x3000	275

Glulam member for the building	Story	Size [mm]	Material
Beam	All	675x700	GL 20c
Column 1 – inside	1-6	650x650	GL 20c
Column 2 – inside	7-12	550x550	GL 20c
Column 3 – inside	13-18	450x450	GL 20c
Core – CLT wall c24	All	200	CLT C24

	C20	C22	C24	C27	C30	C35	C40
	Value	Value	Value	Value	Value	Value	Value
m	505268,6	508199,6	511130,53	514061,51	522854,43	525785,41	528716,39
m_e	28070,48	28233,31	28396,14	28558,97	29047,47	29210,30	29373,13
$n_{1,x}$	0,989	1,011	1,03	1,037	1,041	1,058	1,074
δa	0,0101	0,0098	0,0095	0,0094	0,0092	0,0090	0,0088
δ	0,0701	0,0698	0,0695	0,0694	0,0692	0,0690	0,0688
f_L	9,1964	9,4009	9,5776	9,6427	9,6799	9,8380	9,9867
$S_L(zs)$	0,0317	0,0313	0,0309	0,0308	0,0307	0,0304	0,0301
η_h	15,0470	15,3817	15,6708	15,7773	15,8382	16,0968	16,3402
η_b	6,3532	6,4945	6,6166	6,6615	6,6872	6,7964	6,8992
R_h	0,0642	0,0629	0,0618	0,0614	0,0611	0,0602	0,0593
R_b	0,1450	0,1421	0,1397	0,1388	0,1384	0,1363	0,1344
R^2	0,0208	0,0198	0,0189	0,0186	0,0185	0,0178	0,0172
R	0,1443	0,1406	0,1376	0,1365	0,1360	0,1335	0,1311
v	0,9890	1,0110	1,0300	1,0370	1,0410	1,0580	1,0740

kp(zs)	3,7416	3,7475	3,7525	3,7543	3,7553	3,7596	3,7636
σa(z)	0,0091	0,0089	0,0086	0,0085	0,0083	0,0081	0,0079
$a_{1,x}$(z)	0,0342	0,0332	0,0323	0,0319	0,0313	0,0305	0,0299

Model	Grade – glulam	Average mass	Mode stiffness	Frequency	Peak acceleration
	C20	505268,6	73,00	0,989	0,0342
	C22	508199,6	73,00	1,011	0,0332
	C24	511130,53	72,99	1,03	0,0323
	C26	514061,51	72,99	1,037	0,0319
	C28	522854,43	73,01	1,041	0,0313
	C30	525785,41	73,00	1,058	0,0305
	C32	528716,39	71,99	1,074	0,0299

8.1.1.9 Diagrid – 1,015 Hz

Diagrid			
Glulam member for the building	Story	Length [mm]	Size [mm]
Column 1 – Outer tube long side	1-2	6642,5	325x325
Column 1 – Outer tube short side	1-2	6685,1	200x200
Column 1 – straight	1-2	3000	325x325
Column – inside	1-2	3000	575x575
Column 2 – Outer tube long side	3-4	6642,5	325x325
Column 2 – Outer tube short side	3-4	6685,1	200x200
Column 2 – straight	3-4	3000	325x325
Column – inside	3-4	3000	525x525
Column 3 – Outer tube long side	5-6	6642,5	325x325
Column 3 – Outer tube short side	5-6	6685,1	200x200
Column 3 – straight	5-6	3000	325x325
Column – inside	5-6	3000	475x475
Column 1 – Outer tube long side	7-8	6642,5	250x250
Column 1 – Outer tube short side	7-8	6685,1	200x200
Column 1 – straight	7-8	3000	250x250
Column – inside	7-8	3000	425x425
Column 1 – Outer tube long side	9-10	6642,5	250x250
Column 1 – Outer tube short side	9-10	6685,1	200x200
Column 1 – straight	9-10	3000	250x250
Column – inside	9-10	3000	325x325
Column 1 – Outer tube long side	11-12	6642,5	250x250

Column 1 – Outer tube short side	11-12	6685,1	200x200
Column 1 – straight	11-12	3000	250x250
Column – inside	11-12	3000	275x275
Column 2 – Outer tube long side	13-14	6642,5	200x200
Column 2 – Outer tube short side	13-14	6685,1	200x200
Column 2 – straight	13-14	3000	200x200
Column – inside	13-14	3000	250x250
Column 1 – Outer tube long side	15-16	6642,5	200x200
Column 1 – Outer tube short side	15-16	6685,1	200x200
Column 1 – straight	15-16	3000	200x200
Column – inside	15-16	3000	225x225
Column 1 – Outer tube long side	17-18	6642,5	200x200
Column 1 – Outer tube short side	17-18	6685,1	200x200
Column 1 – straight	17-18	3000	200x200
Column – inside	17-18	3000	200x200
Beam	All		225x225
Core – CLT wall c24	All		200

	C20	C22	C24	C26	C28	C30	C32
	Value	Value	Value	Value	Value	Value	Value
m	202601,2	202601,2	204308,64	207723,47	207723,47	209430,89	211138,31
m_e	11255,62	11255,62	11350,48	11540,19	11540,19	11635,05	11729,91
$n_{1,x}$	1,015	1,015	1,039	1,077	1,0957	1,114	1,132
δa	0,0244	0,0244	0,0237	0,0225	0,0221	0,0215	0,0210
δ	0,0844	0,0844	0,0837	0,0825	0,0821	0,0815	0,0810
f_L	9,4381	9,4381	9,6613	10,0146	10,1885	10,3587	10,5261
$S_L(zs)$	0,0312	0,0312	0,0307	0,0300	0,0297	0,0294	0,0291
η_h	15,4426	15,4426	15,8077	16,3859	16,6704	16,9488	17,2227
η_b	6,5202	6,5202	6,6744	6,9185	7,0386	7,1562	7,2718
R_h	0,0627	0,0627	0,0613	0,0592	0,0582	0,0573	0,0564
R_b	0,1416	0,1416	0,1386	0,1341	0,1320	0,1300	0,1281
R^2	0,0162	0,0162	0,0154	0,0143	0,0137	0,0132	0,0128
R	0,1272	0,1272	0,1240	0,1194	0,1171	0,1150	0,1130
v	1,0150	1,0150	1,0390	1,0770	1,0957	1,1140	1,1320
kp(zs)	3,7486	3,7486	3,7548	3,7643	3,7689	3,7733	3,7775
$\sigma a(z)$	0,0201	0,0201	0,0194	0,0184	0,0180	0,0176	0,0171
$a_{1,x}(z)$	0,0753	0,0753	0,0729	0,0692	0,0679	0,0663	0,0647

Model	Grade – glulam	Average mass	Mode stiffness	Frequency	Peak acceleration

	C20	202601,2	72,00	1,015	0,0753
	C22	202601,2	72,00	1,015	0,0753
	C24	204308,64	71,99	1,039	0,0729
	C26	207723,47	71,99	1,077	0,0692
	C28	207723,47	72,01	1,0957	0,0679
	C30	209430,89	72,00	1,114	0,0663
	C32	211138,31	71,99	1,132	0,0647

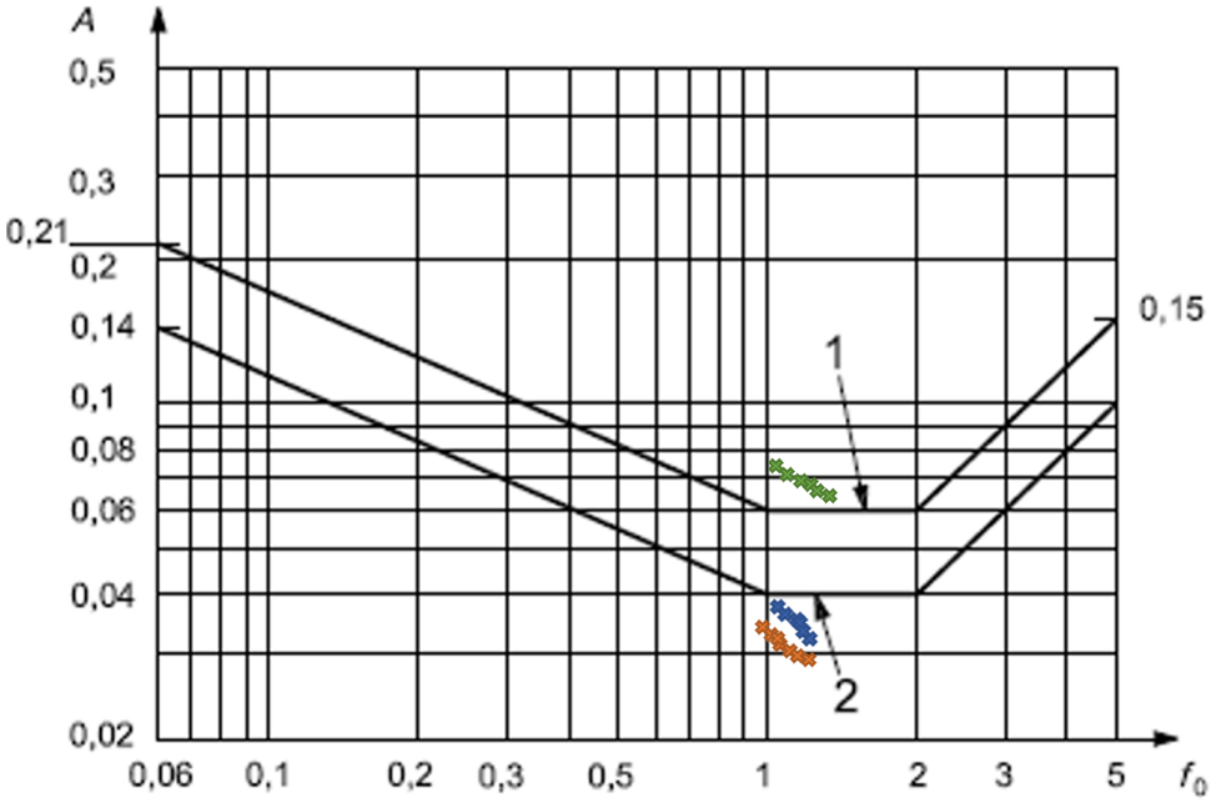

8.1.1.10 Diagrid – 1,62 Hz

Diagrid			
Glulam member for the building	Story	Length [mm]	Size [mm]
Column 1 – Outer tube long side	1-2	6642,5	575x575
Column 1 – Outer tube short side	1-2	6685,1	575x575
Column 1 – straight	1-2	3000	575x575
Column – inside	1-2	3000	575x575

Column 2 – Outer tube long side	3-4	6642,5	525x525
Column 2 – Outer tube short side	3-4	6685,1	525x525
Column 2 – straight	3-4	3000	525x525
Column – inside	3-4	3000	525x525
Column 3 – Outer tube long side	5-6	6642,5	475x475
Column 3 – Outer tube short side	5-6	6685,1	475x475
Column 3 – straight	5-6	3000	475x475
Column – inside	5-6	3000	475x475
Column 1 – Outer tube long side	7-8	6642,5	425x425
Column 1 – Outer tube short side	7-8	6685,1	425x425
Column 1 – straight	7-8	3000	425x425
Column – inside	7-8	3000	425x425
Column 1 – Outer tube long side	9-10	6642,5	325x325
Column 1 – Outer tube short side	9-10	6685,1	325x325
Column 1 – straight	9-10	3000	325x325
Column – inside	9-10	3000	325x325
Column 1 – Outer tube long side	11-12	6642,5	275x275
Column 1 – Outer tube short side	11-12	6685,1	275x275
Column 1 – straight	11-12	3000	275x275
Column – inside	11-12	3000	275x275
Column 2 – Outer tube long side	13-14	6642,5	250x250
Column 2 – Outer tube short side	13-14	6685,1	250x250
Column 2 – straight	13-14	3000	250x250
Column – inside	13-14	3000	250x250
Column 1 – Outer tube long side	15-16	6642,5	225x225
Column 1 – Outer tube short side	15-16	6685,1	225x225
Column 1 – straight	15-16	3000	225x225
Column – inside	15-16	3000	225x225
Column 1 – Outer tube long side	17-18	6642,5	200x200
Column 1 – Outer tube short side	17-18	6685,1	200x200
Column 1 – straight	17-18	3000	200x200
Column – inside	17-18	3000	200x200
Beam	All		225x225
Core – CLT wall c30	All		300

	C20	C22	C24	C26	C28	C30	C32
	Value	Value	Value	Value	Value	Value	Value
m	267917,2	267917,2	269156,06	271633,84	271633,84	272872,73	274111,62
m_e	14884,29	14884,29	14953,11	15090,77	15090,77	15159,60	15228,42

$n_{1,x}$	1,62	1,62	1,663	1,732	1,766	1,798	1,831
δa	0,0116	0,0116	0,0112	0,0107	0,0105	0,0102	0,0100
δ	0,0716	0,0716	0,0712	0,0707	0,0705	0,0702	0,0700
f_L	15,0638	15,0638	15,4636	16,1052	16,4214	16,7190	17,0258
$S_L(zs)$	0,0230	0,0230	0,0226	0,0220	0,0217	0,0215	0,0212
η_h	24,6473	24,6473	25,3015	26,3513	26,8686	27,3555	27,8575
η_b	10,4066	10,4066	10,6829	11,1261	11,3445	11,5501	11,7621
R_h	0,0397	0,0397	0,0387	0,0372	0,0365	0,0359	0,0353
R_b	0,0915	0,0915	0,0892	0,0858	0,0843	0,0828	0,0814
R^2	0,0058	0,0058	0,0054	0,0049	0,0047	0,0045	0,0043
R	0,0759	0,0759	0,0736	0,0701	0,0684	0,0670	0,0655
v	1,6200	1,6200	1,6630	1,7320	1,7660	1,7980	1,8310
kp(zs)	3,8710	3,8710	3,8778	3,8882	3,8932	3,8978	3,9025
$\sigma a(z)$	0,0091	0,0091	0,0087	0,0083	0,0081	0,0078	0,0076
$a_{1,x}(z)$	0,0351	0,0351	0,0339	0,0321	0,0314	0,0306	0,0298

Model	Grade – glulam	Average mass	Mode stiffness	Frequency	Peak acceleration
	C20	267917,2	62	1,62	0,0351
	C22	267917,2	62	1,62	0,0351
	C24	269156,06	62	1,663	0,0339
	C26	271633,84	62	1,732	0,0321
	C28	271633,84	61,99	1,766	0,0314
	C30	272872,73	62	1,798	0,0306
	C32	274111,62	62	1,831	0,0298

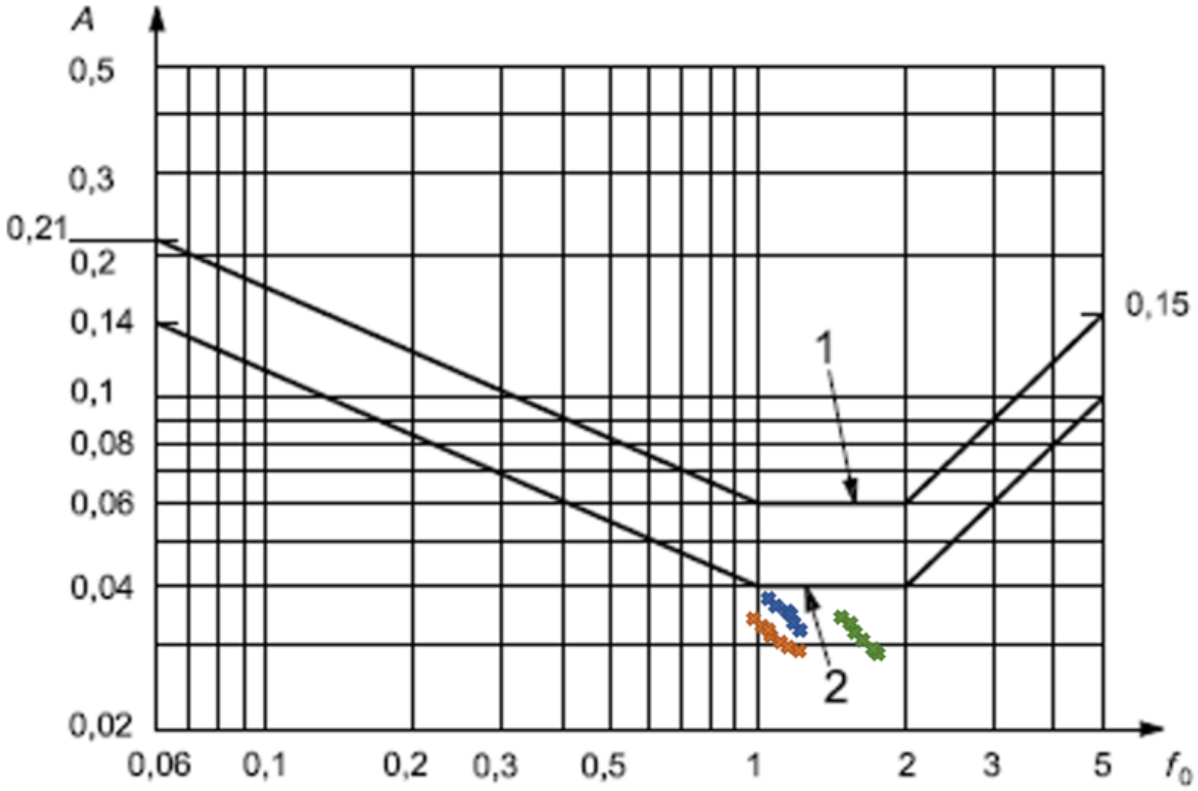
A
0,5
0,3
0,21
0,2
0,14
0,1
0,08
0,06
0,04
0,02
0,15
1
2
0,06
0,1
0,2
0,3
0,5
1
2
3
5
f_0

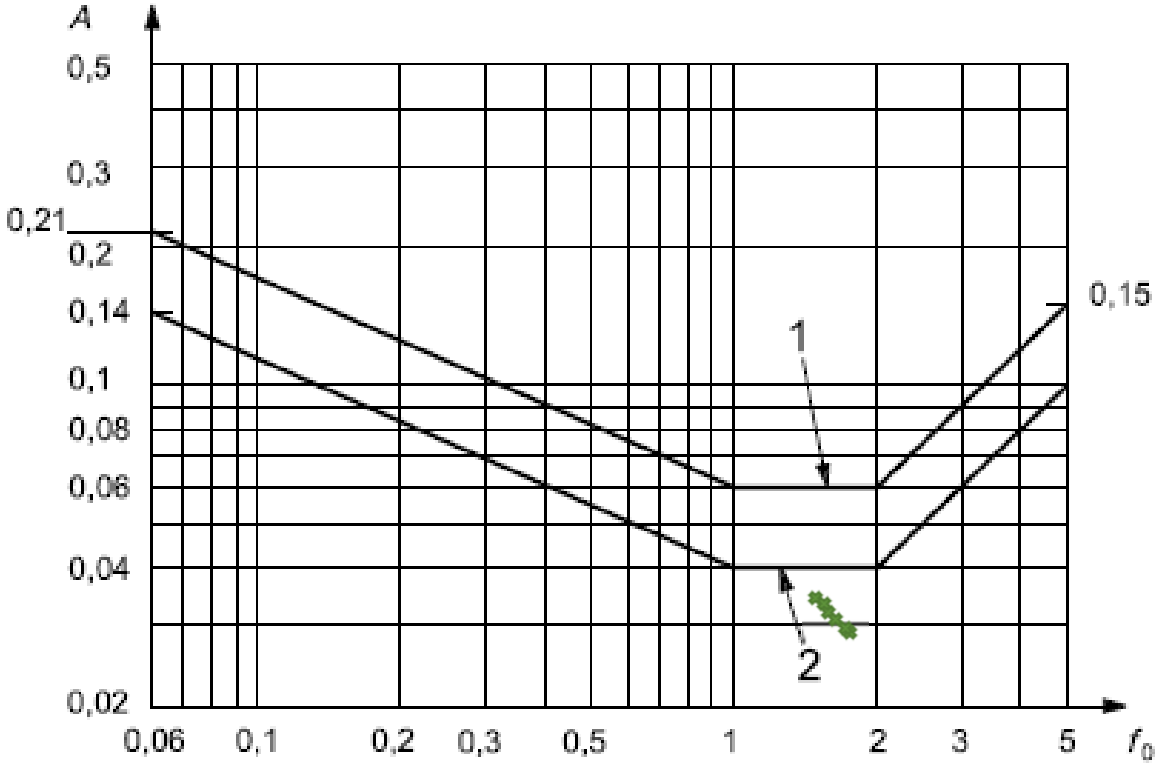
A
0,5
0,3
0,21
0,2
0,14
0,1
0,08
0,06
0,04
0,02
0,15
1
2
0,06
0,1
0,2
0,3
0,5
1
2
3
5
f_0

Norges miljø- og biovitenskapelige universitet
Noregs miljø- og biovitskapelege universitet
Norwegian University of Life Sciences

Postboks 5003
NO-1432 Ås
Norway